VIIS – VEHICLE INFRASTRUCTURE INTERACTION SIMULATION ON "REAL" ROADS

DI Peter Saleh
DI Rainer Stütz
Mag. Stefan Deix
DI (FH) Stephan Kunz
Priv.-Doz. DI Dr. Peter Maurer
arsenal research – Österreichisches Forschungs- und Prüfzentrum Arsenal Ges.m.b.H.
Austria
Paper Number 09-0031

ABSTRACT

The project VIIS (Vehicle Infrastructure Interaction Simulation), an actual research project which was started in January 2008 has the aim to build up on the MARVin (Model for Assessing Risks of Road Infrastructure; Paper of the 20th ESV) outcomes. The idea is to develop a combined simulation system, including all kinds of RoadSTAR data (Road Surface Tester of arsenal research; road condition and trace geometry) to verify crash causal combinations.
The MARVin software tool has been upgraded with traffic density data to get some more comparable and significant results. The crash causations regarding to poor surface characteristics or in-harmonic road geometry can be identified with a higher probability.

The main work is to integrate all relevant RoadSTAR parameters in a simulation software tool. In a beginning procedure a integration in the software PC Crash shows some positive results. The challenge will be to bring the skid resistance values as DXF data in a high density on the virtual route.

Virtual road sections can be designed with real measured data. Crash reconstructions and crash causal combinations (MARVin) are feasible. All kinds of vehicle dynamic data, which can be also logged in the CAN bus system, can be simulated and recalculated. The vehicle infrastructure interaction (road/tyre, suspension/tyre) in a crash situation leads to possible accident compensation measures like new in-vehicle sensors, innovative active safety systems, real time accident risk assessment, interactive road condition maps, etc..

The key point for the future of traffic safety issues are to verify MARVin results with vehicle-infrastructure simulations and to derive preventative measures either on the construction side or in the in-vehicle safety applications.

Visions are to combine theoretical accidentology with practical preventative solutions. Policy, vehicle manufacturer, road operators and map providers can have a benefit resulting from this research.

INTRODUCTION

As a step beyond "accident black spot" identification in road transport and traffic safety arsenal research developed a tool called *Model for Assessing Risks of Road Infrastructure* (*MARVin)*. The general objective is to link road infrastructure parameters with accident statistic data. Furthermore is MARVin a tool to assess and correlate road infrastructure parameters with road accidents (See Figure 1). More precisely, arsenal research uses the very detailed road database of the Austrian road network measured with the RoadSTAR (Road Surface Tester of Arsenal Research [1]). This database is associated with an accident data base, via the position of the accidents. In the accident database about 580.000 accidents are registered (1994 – 2007). As a result, the conjunction between the road database (approx. 24.500 km), with all relevant road infrastructure parameters (curvature, crossfall, skid resistance, texture, etc.) and the accident database was established. Any analysis with MARVin uses this combined database.

Figure 1. One of MARVin's results projected on the real road: skid resistance vs. accident spots

SIMILARITY SEARCH USING DYNAMIC TIME WARPING

One of the most important developments and tools in MARVin is called similarity search, a patented method for the valuation of similar road segments. With this innovative technique the road safety

analyst is able to identify similar road sections in the road network. This is, however, not an easy task, as searching similar sections is not only finding an identical road stretch, but more looking for all parts that are like the sample. The task to identify similar road sections was solved by applying a computer-aided method which was originally developed for automatic speech recognition. The so called Dynamic Time Warping (DTW) [2, 3, 4 and 5] is a method which allows finding an optimal match between two given (multivariate) sequences (e.g. time series) with certain restrictions. In this case DTW yields a nonlinear similarity measure of different parameters with a given road section, the template.

With this development it is possible to analyse even a "virtual", not yet built road section.
A road in the design stage with a specific trace geometry and road condition-parameters can be analyzed by comparing it to already existing road sections (See Figure 2). This is a very important step to test planned and designed roads on their safety characteristics. Applying this method in the design phase will support the accident prevention significantly by identifying potential hazardous road risks before they are built.

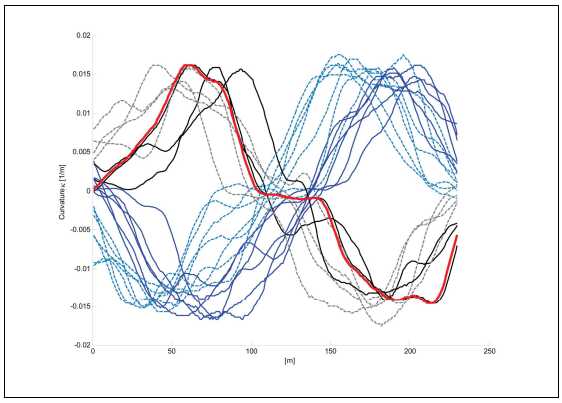

Figure 2. Graph showing result of the similarity search – example for curvature; red line shows the template

Another approach of MARVin is to consider all accidents as objective as possible ("unbiased"). This is conceivable as the parameters of every accident are considered as discrete coordinates in a high-dimensional space. Correlations are perceived by different densities of the points (accidents) in this multi-dimensional space. Based on this approach, methods are developed to analyse the enormous amount of data. Computer-assisted solutions using statistical methods and/or data mining methods are proper tools for this task. Although the processing power to handle both accident database and road database in requires remarkable computing power which should not be underestimated.

PRACTICAL WORK

The first practical work with MARVin was a road safety check of a typical motorcycle route in Austria, to analyse correlations between the number of accidents on specific sites and the road infrastructure parameters. The interesting, but not surprising result was, that although the infrastructure quality of this road was very good (high skid resistance, perfect radii relations and curvature, etc.) the accident rate was rather high. The significant facts for the high risk potential of this road are the number of motorcyclists each day (especially at weekends) and the driven speed. Speed enforcement and awareness campaigns may lead to an accident reduction in this case. Moreover, MARVin was useful to support the development of a national directive for motorcycle safety within a national framework. A detailed check of motorcycle accident events on rural roads and their correlation with curve radii revealed interesting results.

Specifically runoff accidents mostly occur in small radii between 50 and 150 meters; the maximum ratio of runoff accidents in curves is exactly for radii of 100m, followed by 110m and 200m. A detailed analysis on the relations between curve radii, curvature and changing crossfall and their influence on powered two wheelers (PTW) accidents is necessary. The "Similarity Search", which identifies similar accident events on similar road sections, will also be helpful for this task and within further research projects.

VEHICLE INFRASTRUCTURE INTERACTION SIMULATION – VIIS

The main objective of a new research project: *Vehicle Infrastructure Interaction Simulation (VIIS)* is to model the interaction between vehicles and road infrastructure. In this sense the simulation will describe the effects and consequences of road parameters on vehicles in various driving situations. With this approach the simulation will use the findings and results of MARVin to model the respective road sections based on all available road parameters (RoadSTAR Database). It is then possible to simulate and analyse the event of a specific accident. Due to the combination of infrastructure and vehicle models the spectrum of analyses is much wider.

Therefore MARVin has been upgraded with traffic density data to obtain more significant results to be used in *VIIS*. With this approach the crash causations regarding poor surface characteristics or

in-harmonic road geometry will be identified with a higher reliability.

Road segments, to be used for simulation purpose, are designed in virtual reality but using the RoadSTAR DB with real measured data and a high sample rate (See Figure 3). Crash reconstructions and crash causal combination will be highly relevant with this. The vehicle infrastructure interaction (road/tyre, suspension/tyre) in a crash situation (or almost accident) have a major impact on the accident risk. New in-vehicle sensors, active safety systems, real time accident risk assessment, interactive road condition maps, etc. are developments to compensate that risk – and testing those developments in a virtual testing framework under realistic conditions will accelerate the process.

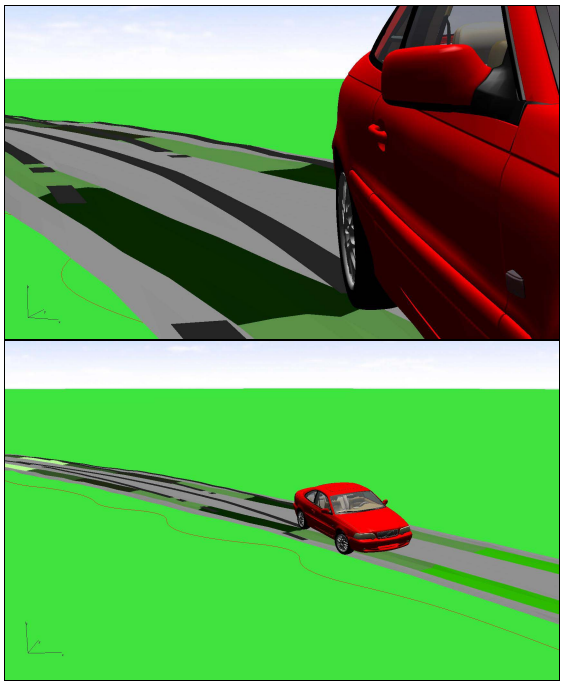

Figure 3. Two snapshot of VIIS results – skid resistance, rut depth and unevenness values used in virtual reality – causing a critical driving situation

VISIONS AND FUTURE

A vision for the future evolution of the proposed approaches and project results is to combine theoretical accident research with practical preventative solutions. It is most likely that policy, road operators, vehicle manufacturers, map providers and most of all the road users have a recognisable benefit resulting from this research.

The next step towards that vision is to verify MARVin results with an innovative vehicle-infrastructure simulation and to derive preventative measures either on the road construction side or in in-vehicle safety applications.

CONCLUSIONS

With the research project MARVin it is possible to identify significant correlations between road accident events and the quality of the road infrastructure. Various road parameters highly relevant for transport safety and an accident database are combined in this analysis. The road parameters are measured with the high-tech measurement vehicle the RoadSTAR on the Austrian road network. The research and development has already been useful to solve practical problems and analyses. Especially the development of the “Similarity Search” opens up new paths in crash-causes-research. The verification of crash-causal-combinations with an innovative simulation framework is an objective to improve the understanding of infrastructure-vehicle interaction during an accident. With this understanding a wide range of preventive measures to reduce accident risks are conceivable.

REFERENCES

[1] P. Maurer, J. Gruber et al (2002), „Straßenzustandserfassung mit dem RoadSTAR“, Messsystem und Genauigkeit, ÖFZ Arsenal Ges.m.b.H., Wien

[2] E. Keogh (2002), “Exact indexing of dynamic time warping”, Proceedings of 28th International Conference on Very Large Data Bases, Hong Kong, China

[3] T. M. Rath and R. Manmatha (2002), “Lower-Bounding of Dynamic Time Warping Distances for Multivariate Time Series”, Technical Report MM-40, Center for Intelligent Information Retrieval, University of Massachusetts Amherst, USA

[4] A. W. Fu, E. Keogh, L. Y. H. Lau and C. A. Ratanamahatana (2005), “Scaling and Time Warping in Time Series Querying”, Proceedings of 31st International Conference on Very Large Data Bases, Trondheim, Norway

[5] E. Keogh and M. J. Pazzani (2001), “Derivative Dynamic Time Warping”, First SIAM International Conference on Data Mining, Chicago

FUSION OF IN-VEHICLE SENSOR DATA TO DEVELOP INTELLIGENT DRIVER TRAINING SYSTEM (IDTS)

Husnain, Malik
Andry, Rakotonirainy
Gregoire S., Larue
Center Of Accident Research And Road Safety – Queensland
Frederic, Maire
School Of Information Technology
Science And Technology Faculty
Queensland University of Technology
Australia
Paper Number 09–0048

ABSTRACT

The over represented number of novice drivers involved in crashes is alarming. Driver training is one of the interventions aimed at mitigating the number of crashes that involve young drivers. To our knowledge, Advanced Driver Assistance Systems (ADAS) have never been comprehensively used in designing an intelligent driver training system. Currently, there is a need to develop and evaluate ADAS that could assess driving competencies. The aim is to develop an unsupervised system called Intelligent Driver Training System (IDTS) that analyzes crash risks in a given driving situation. In order to design a comprehensive IDTS, data is collected from the Driver, Vehicle and Environment (DVE), synchronized and analyzed. The first implementation phase of this intelligent driver training system deals with synchronizing multiple variables acquired from DVE. RTMaps is used to collect and synchronize data like GPS, vehicle dynamics and driver head movement. After the data synchronization, maneuvers are segmented out as right turn, left turn and overtake. Each maneuver is composed of several individual tasks that are necessary to be performed in a sequential manner. This paper focuses on turn maneuvers. Some of the tasks required in the analysis of 'turn' maneuver are: detect the start and end of the turn, detect the indicator status change, check if the indicator was turned on within a safe distance and check the lane keeping during the turn maneuver. This paper proposes a fusion and analysis of heterogeneous data, mainly involved in driving, to determine the risk factor of particular maneuvers within the drive. It also explains the segmentation and risk analysis of the turn maneuver in a drive.

INTRODUCTION

Automobiles have greatly improved the transportation of goods and people around the globe. This factor in-return has enabled us to advance in many other areas. Crashes have been the most prominent danger associated with automobiles. These often result in serious injuries or loss of human life. Over 10 million people are injured yearly worldwide in road accidents. These include two to three million severely injured and 400,000 fatalities [1].

It is well known that drivers are at a greater risk during the early years of driving. About 95 per cent of all accidents are attributed to the human factor [2], whether it is driving too fast, lack of experience or simply misjudging a dangerous situation. Research indicates that young drivers are over represented in crashes because of a lack of experience, poor hazard perception, and a tendency to take risks [3,4]. Research suggests that the best learning environment for the inexperienced driver is the real road system under the supervision of an experienced driver or instructor [3,4].

Driver perception and learning of a particular driving hazard remains a key factor impacting road safety. In-order to comprehensively tackle road safety issues, a complete and integrated framework need to be developed that would include and examine all the parameters that influence driving (i.e. cues related to road, vehicle and driver). This requires the need for a system that can assess multiple maneuvers in a driving scenario as high risk or low risk based on the parameters acquired from DVE. This paper focuses on decomposing and analyzing turn maneuvers.

Figure 1 illustrates three sensors, namely FaceLab (eye tracking system), MobileEye (lane and obstacle detection system) and Vigil System (GPS and vehicle dynamics data logger) to gather data from the driver, environment and vehicle respectively. RTMaps is used to synchronize data from all the above mentioned sensors.

The primary driving tasks are divided into three broad categories: navigation and routing, guidance and maneuvers, and control [5].

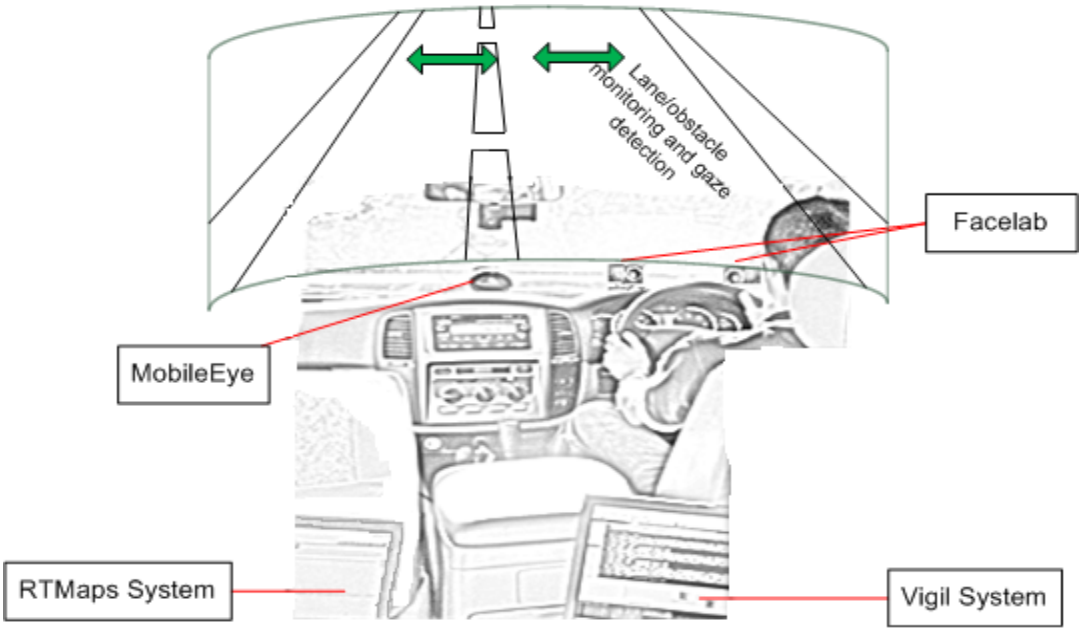

Figure 1. Multi-sensor system structure for Intelligent Driver Training System (IDTS)

The rest of the paper is organized as follows: the next section will briefly mention the related research work in the field of modeling an integrated driving scenario. The following section will comprehensively present our approach for developing the Intelligent Driver Training System (IDTS). This will be followed by mapping of the drive and future work section. Discussion and conclusion will be presented in the final section.

BACKGROUND RESEARCH

Assessing Primary Driving Tasks

It is well known that drivers are at a greater risk during the early years of driving. Researchers in [5] have defined the primary driving tasks as functions that are central to driving and without which moving a vehicle to a destination safely would not be possible.

Many intelligent systems have focused on warning the driver by predicting the trajectory of an oncoming obstacle [7], [6]. Only a few of these systems evaluate the overall driving situation and need to make the driver aware of relevant contextual knowledge extracted from sensors [8].

Execution of all these tasks is necessary for the driver in order to drive effectively.

Responding to critical events during driving requires timely response. A point reiterated in literature critical of driver training is that more in-depth analysis of the driving task and traffic situations is required. This analysis should take into account the cognitive skill aspect such as hazard and risk perception, decision-making, self-monitoring processes, learning styles, and risky attitudes to improve training [9, 7].

Sensors And Data Synchronization

Sensor fusion combines several sensor measurements in order to enhance the knowledge about the state of an object under observation. To increase the safety and efficiency for transportation systems, applications need to combine and comprehensively evaluate the data acquired from multiple sensors. Over the years, different type of sensors like radars, Global Positioning System (GPS), accelerometers, gyroscopic sensors and cameras have been used extensively in Advanced Driving Assistance Systems [6,7,8].

Various sensors can be used to perform obstacles detection: laser scanner, radar range, sonar range, vision (monocular or binocular). Similarly a number of sensors have been developed to measure vehicle dynamics as well. Researchers are now using in vehicle mounted sensors to measure different aspects of driving experience i.e. fatigue, monotony, body movements etc. Researches [15,16] have emphasized the usefulness of capturing driver gaze behaviour in creating a robust driving model.

Driving is a complex task. A single sensor alone is not enough to analyze such a task in a reliable manner. For example, GPS data has limited ability to describe or explain a driving situation. Furthermore a sensor can fail and produce erroneous data. In-order to model a complex driving scenario, multiple sensors data has to be merged to give a good representation of driving activity. Another hurdle in modeling a driving activity is that driving maneuvers can be performed with multiple styles. For example, indicator might not always be used just to signal lane change, or an overtake maneuver could involve a burst of speed but could also be performed by not accelerating hard at all [14]. Therefore it is necessary to view the multisensory data as a whole system to comprehensively model the driving activity.

A successful solution has to combine the benefits of multiple sensors such as GPS, radar, lidar and cameras. In order to obtain a precise synchronization, a sufficiently accurate global time for all sensors and fusion system is necessary. Therefore, to obtain a time consistent state for all sensors, the measurements have to be integrated in the order they were received. IDTS addresses these tasks by combining GPS, cameras and vehicle dynamics data using RTMaps.

METHODOLOGY

Architecture Of IDTS

To model a complex driving scenario in a comprehensive way, it is necessary to fuse several sensors data. Our test vehicle is equipped with vision systems, and sensors to monitor the vehicle dynamics as described in Figure 1.

Currently the test vehicle for this project includes the following sensors.

- Mobile Eye: It is a forward collision warning system that uses a single camera mounted on the windscreen of a vehicle. It also calculates variables such as distance from right/left lane and time to impact [10].

- FaceLab: It is a flexible and mobile tracking device that tracks head pose, eyelid movement and gaze direction in real-time, under real-world conditions unobtrusively. This data can then further be used to monitor driver attentiveness, fatigue e.t.c [11].

- Vigil System: This visual-based management software program analyzes several areas of driving performance. Using GPS, accelerometers and cameras it measures speeds, accelerations, braking, cornering, following distances. The GPS input from this system is used to accurately view the vehicle's trajectory [12].

- RTMaps: It is the software that allows real time multiple data acquisition, data fusion and processing, at a high rate. The acquired data can also be stored for future replay. In this system, RTMaps is responsible for gathering data from the above mentioned systems (i.e. MobileEye, Facelab and vigil system), assigning a timestamp to it, synchronize it and storing the data. [13]

Sensor data fusion and the layered architecture of IDTS are shown in Figure 2. By fusing in multisensory data input, the precision and certainty of calculated estimates is increased e.g. the speed of the vehicle acquired from the odometer can be checked against the speed calculated from the GPS to remove any uncertainty. In this system's architecture, there is a bottom up stream of information acquired from multiple sensors.

As we can see in Figure 2 that the fusion layer is separate from the application layer (i.e. interpretation and assessment layer). This low coupled layered architecture is useful because the application layer does not require any interfacing with individual sensors. This scalable design helps in having multiple application layers while just having one sensor fusion layer (this is the only layer that has to have some knowledge of the sensor's characteristics).

As already mentioned, in this project the task of fusing sensory data input is handled by RTMaps [15]. It timestamps and synchronizes the sensor inputs from MobileEye, Facelab and VigilSystem during the drive. It then stores this drive data for future real-time replay. Processing of Facelab data is currently in progress.

The application layer (i.e. Interpretation + Assessment) described in Figure 2 handles the risk assessment of the maneuvers in the recorded drive. Currently, the interpretation layer detects the start, end and centroid of the turns from the drive (see 'Vehicle Turn Angle Estimation for a Turn Maneuver' section for more information). It then resolves the position where and if the indicator was turned on. It also removes the GPS

uncertainty by calculating the error variance (see 'Estimation of GPS uncertainty' section for more detail). After the classification of the turn, interpreted data is transferred to risk assessment layer where the distance between the start of the turn and start of the indicator is calculated. The distance of the vehicle from the right and left lane along with the speed is also considered to identify the risk involved.

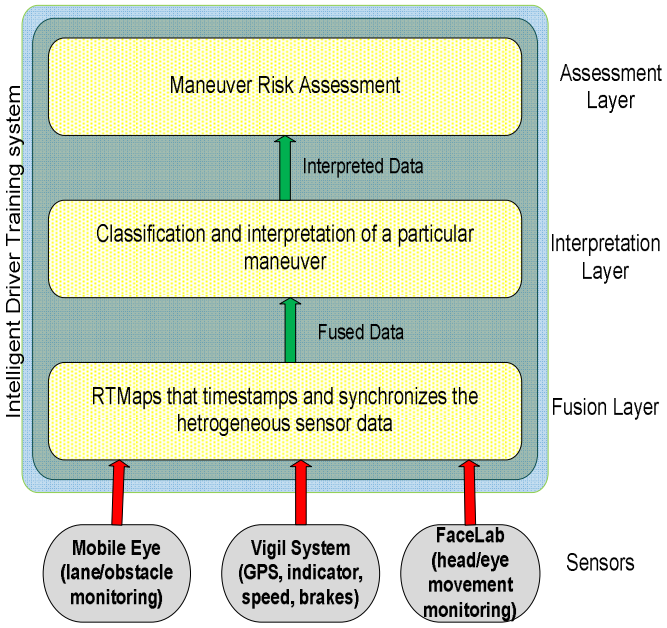

Figure 2: IDTS architecture and processing layers

Risk Assessment Criteria

There are a number of events that frequently occur during driving. A typical driving scenario would comprise of a certain set of driving events and patterns that are repeated over time.

Driver instructors typically assess a certain set of skills to assess drivers during a driver training session. They use various types of standard check lists to assess driving performance. For example, the analysis of a right-hand turn consists of observing a substantial number of sub events. The breakdown of this particular behaviour as stated in a sample driver training manuals is shown in Figure 3.

In the context of a driver training system, this list of driving events will be assessed automatically through the combined information gathered from the in-vehicle recording devices featuring multiple sensors and algorithms used to analyse video data.

Assessment such as the one described in Figure 3 will be used to develop a safe performance protocol model that can be used to assess automatically risk associated with a particular driving maneuver. In-order to achieve a less risky driving situation, a driver would have to perform these tasks properly in a sequential and timely manner. The model will be used as a formal framework to evaluate the perceptual and cognitive skills of the driver.

(Example of) DRIVER EDUCATION PERFORMANCE

Right Turn Assessment

1) Checks mirrors
2) Positions car properly in lane
3) Signals right
4) Reduces speed and keeps wheels straight
5) Checks traffic thoroughly, yielding to pedestrians
6) Starts turn when front wheels are opposite point where curb begins to curve
7) Uses proper steering when going into turn
8) Turns into proper lane
9) Straightens the wheels by using hand-over-hand, or methods maintaining secure control of steering
10) Adjusts speed to traffic flow

Source: Michigan Department of Education (1997, p35)

Figure 3: Driver Education Performance

Using such a system, an accurate measurement of the interaction between the driver, environment and the vehicle will be calculated. Table 1, identifies the sensors or technologies that output data to monitor each sub-event featured in a turn maneuver. For example, by using Facelab's estimates of driver's eye and head movements, tasks like check mirrors and check traffic are verified.

Table 1:

Driving Subtasks and monitoring sensors/technologies

Turn Sub-Events	Sensors/Technology
• Checks mirrors	FaceLab
• Positions car properly in lane	Mobile Eye
• Signals right	Mobile Eye
• Reduces speed and keeps wheel straight	Vigil System, MobileEye
• Checks traffic thoroughly	FaceLab
• Starts turn	Turn analysis algorithms
• Turns into proper lane	MobileEye
• Straightens wheel while maintaining secure control	Vigil System
• Adjusts speed to traffic flow	GPS , MobileEye

Vehicle Turn Angle Estimation For A Turn Maneuver

In-order to effectively model a turn maneuver, it is necessary to determine the complete demographics of a turn. IDTS calculates when the vehicle's turn started, when it finished and determines the centroid and the angle of the turn (i.e. was it a 90 degree turn or 45 degree turn e.t.c.).

Estimation of GPS Uncertainty – Evaluation and management of sensor uncertainty is important in a multisensory environment. GPS uncertainty has to be measured to accurately map the trajectory of test vehicle.

GPS provides the coordinates of a location with certain accuracy depending on its quality. When mapping the trajectory of a moving vehicle, it is important to be able to detect that given two GPS points, whether the second consecutive GPS coordinates represents a new position of the vehicle. Such an issue can be handled through the computation of the experimental variability of the GPS equipment used.

The GPS was placed at a point and multiple recording (frequency 1Hz) were taken to obtain the numerical error variance of the GPS. Errors along the horizontal and vertical axis are independent and equal. So errors along one axis are normally distributed around zero with variance σ^2.Equation 1, was used to compute the variance along each axis separately. Then the maximum value is set as the variance σ^2.

$$\sigma = \sqrt{\frac{1}{N} * \sum_{i=1}^{N} [calcDist(gps(i), meanGPS)]^2} \quad (1).$$

where N is the number of GPS points. And *calcDist* is the function that calculates distance between two GPS points. Implementation of the function '*calcDist*' which is using Haversine [10] formula to calculate distance between two GPS points is given below.

$$\Delta lat = lat2 - lat1$$

$$\Delta long = long2 - long1$$

$$a = \sin^2\left(\frac{\Delta lat}{2}\right) + \cos(lat1).\cos(lat2).\sin^2\left(\frac{\Delta long}{2}\right)$$

$$c = 2.a \tan 2\left(\sqrt{a}, \sqrt{1-a}\right)$$

$$dist = R.c$$

where *lat1* and *lat2* are the latitudes for first and second GPS points respectively. *long1* and *long2* are the longitudes for the first and second GPS points respectively. *R* is the radius of the earth and dist is the calculated distance between the two GPS points.

Errors being normally distributed means 95% of the coordinates obtained by the GPS are distributed within two standard deviations σ around the true position (see Figure 4) [18]. Given a GPS set of coordinates, a 95% confidence interval for the true location can be obtained from the variance as follows:

$$calcDist(GPS.coordinates, TRUE.location) \le 2\sigma \quad (2).$$

See implementation of '*calcDist*'

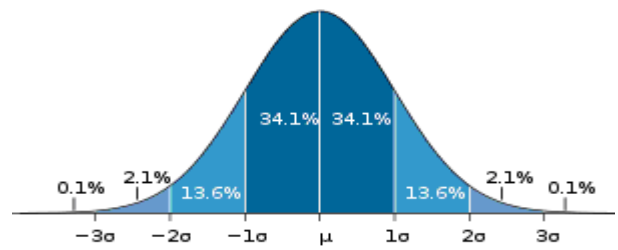

Figure 4. Gaussian distribution density function with mean μ and the variance σ

Numerically, we obtain $\sigma^2 = 0.0272m^2$, which corresponds to a true location inside a circle of radius 32.9cm. In other words two consecutive GPS points closer than 32.9cm cannot be considered as different.

Another issue related to the variability of GPS coordinates is that the direction of the moving vehicle given two consecutive GPS points can be insufficiently accurate for trajectory estimation (particularly in order to determine whether the vehicle is turning or not). In the worst case scenario the inaccuracy on the location estimation can lead to a difference in direction estimation by an angle θ as shown in Figure 5. Let A and B be the two absolute consecutive locations for a moving vehicle. In the worst case scenario, $A^{\sim}$ and $B^{\sim}$ represent the points obtained after the GPS error variance (of 2σ) in A and B respectively. So we can say that inaccuracy of vehicle heading estimation is θ.

For further analysis we require this angle to be small, and we take $\theta = 10°$ as a threshold.

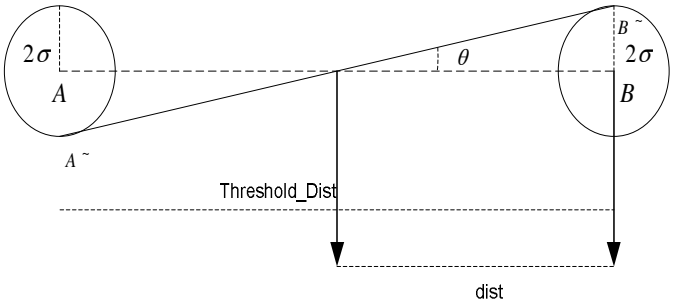

Figure 5. Calculation of Vehicle heading estimation θ

The threshold distance $threshold_dist$ is derived as follows:

$$threshold_dist = 2 * dist \qquad (3).$$

From Figure 5, we can calculate that the distance (dist) is:

$$dist = 2\sigma / \tan\theta \qquad (4).$$

Using Equation 3 and 4, we get:

$$threshold_dist = 4\sigma / \tan\theta \qquad (5).$$

Numerically, we get $threshold_dist = 3.7m$. It means, two consecutive GPS points will be considered the same (i.e. the vehicle is stopped) if their distance is smaller than 3.7m. This threshold distance in useful in calculating the turn angle, as discussed in the following section.

Turn Detection Algorithm

Once the GPS error variance has been calculated, we compute an angle for every GPS point, in-order to determine the vehicle's turn angle. The algorithm for computing an angle for each GPS point (except for the first and last GPS point) is given below:

For all GPS points
Initialize t as 2
Store three points in array Y for time T-1, T and T+1
*Compute the **distance** between GPS points at time T-1 and T+1*

*While **distance** is less than threshold distance*
Add GPS points in Y array for time T-t and T+t, if only points exist for time T-t and T+t
Increase t by 1
*Compute **distance** between GPS points at time T-t and T+t*

*If **distance** is greater than or equal to threshold distance*
*Compute the **tangent angle** θ for GPS point at time T given T-t and T+t*

With the above mentioned algorithm, every GPS point will have a tangent angle based on the points before and after it.

Once the angle for every GPS point is calculated, the derivative of the angle with respect to the distance travelled ($\frac{\Delta\alpha}{\Delta s}$) is computed. $\Delta\alpha$ is the change in angle and Δs is change in distance. This derivative is useful in eliminating those GPS points during which the car didn't move a specified threshold distance. The method for computing the derivative $\frac{\Delta\alpha}{\Delta s}$ at each GPS point is very similar to the method for computing angle θ for every GPS point. For the algorithm below, assume every GPS point now has an assigned angle as well (calculated using the above mentioned algorithm).

For all GPS points
Initialize t as 2
Store three GPS points in array Y for time T-1, T and T+1
*Compute the **distance** between GPS points at time T-1 and T+1*

*While **distance** is less than threshold distance*
Add GPS points in Y array for time T-t and T+t, if only GPS points exist for time T-t and T+t
Increase t by 1
*Compute **distance** between GPS points at time T-t and T+t*

*If **distance** is greater than threshold distance*
Compute the angle difference $\Delta\alpha$ between GPS points at time T-t and T+t
Compute the distance Δs between GPS points at time T-t and T+t
*Compute the **derivative** $\frac{\Delta\alpha}{\Delta s}$ for the GPS point T*

Figure 6 presents the vehicle trajectory in blue, while the red line represents the derivative $\frac{\Delta\alpha}{\Delta s}$ for the respective GPS points. Based on these derivative values, the start, peak and end of the turn are segmented out. The start and end of the turn are crucial in finding out the centroid of the turn. This centroid is then used to calculate the 'safe' distance to switch on the indicator.

Centroid Calculation For The Turn

As already mentioned above the centroid calculation of the turns would be useful in identifying the 'safe' distance at which the driver switches the indicator before the turn. Usually, the exact start and exact end of the turn is debatable i.e. where do we decide that the car started to turn (e.g. when the driver started to turn the steering or when the car turned some significant angle). Therefore, after the derivatives $\frac{\Delta\alpha}{\Delta s}$ for the whole drive have been calculated, the turn is segmented out based on the start and end turn using heuristics. Once the turn has been segmented out from the drive, its centroid is calculated. Even if the exact start of the turn is ambiguous, the centroid of the turn would be always accurate.

The centroid of an area is similar to the center of mass of a body [19]. The centroid of the turn is calculated between the start and end of the turn (i.e. the turn area) using derivative $\frac{\Delta\alpha}{\Delta s}$ as a weight function A_N (see equation 6). Calculating the centroid involves only the geometrical shape of the area. So the area is divided into multiple rectangles and using Equation 6 below, the centroid of the area is calculated.

$$C = \frac{\sum A_N C_N}{\sum A_N} \qquad (6).$$

where C_N is the index of the Nth GPS point in the turn area and C is the centroid of the turn.

Figure 6, illustrates the turn's centroid for both turns in DRIVE 1. Other information, like indicator start, indicator end and turn start/end are helpful in accurately modeling these turns.

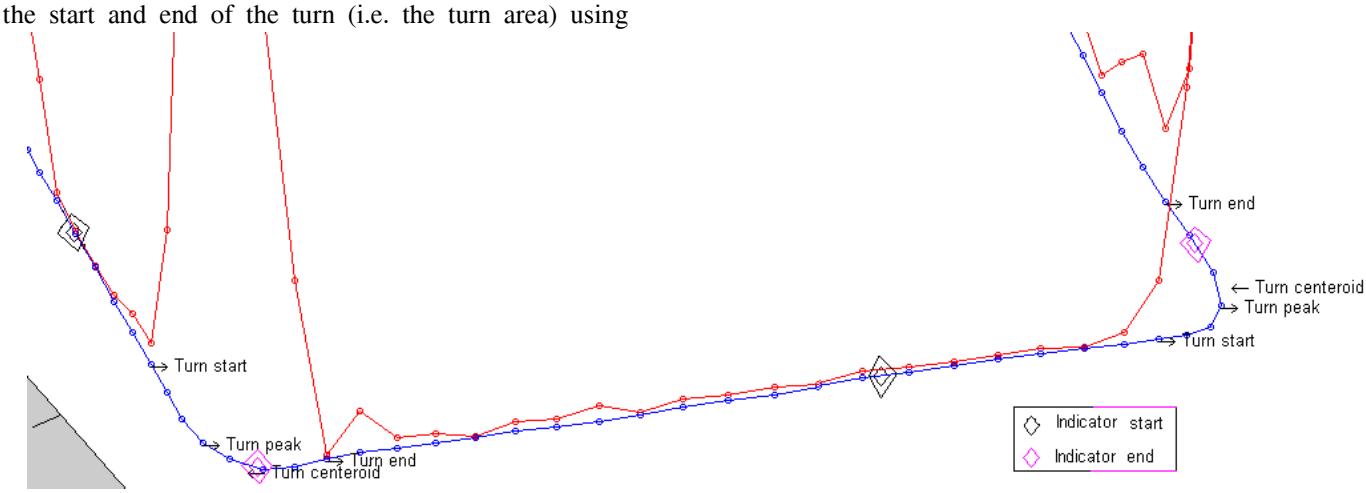

Figure 6. DRIVE1 – Representation of vehicle's GPS trajectory with two left turns (in blue) and the derivative values $\frac{\Delta\alpha}{\Delta s}$ plot for the corresponding GPS points (in red)

Figure 7, presents the turns involved in DRIVE 2. It consisted of three turns, first was a left turn followed by a right and finally a left turn. The derivate $\frac{\Delta\alpha}{\Delta s}$ values are plotted along Y axis and the number of GPS points around X axis. It is evident from the graph that using derivatives, the exact nature of the turn can be deduced e.g. whether it was a left or a right turn (based on the sign of derivative). This data can also be used to compute the vehicle turn angle. From the graph, we can see that the turns can be segmented out from the rest of the drive using heuristics based on the derivative values. All this information coupled with indicator, gaze and lane keeping data effectively model the turn scenario.

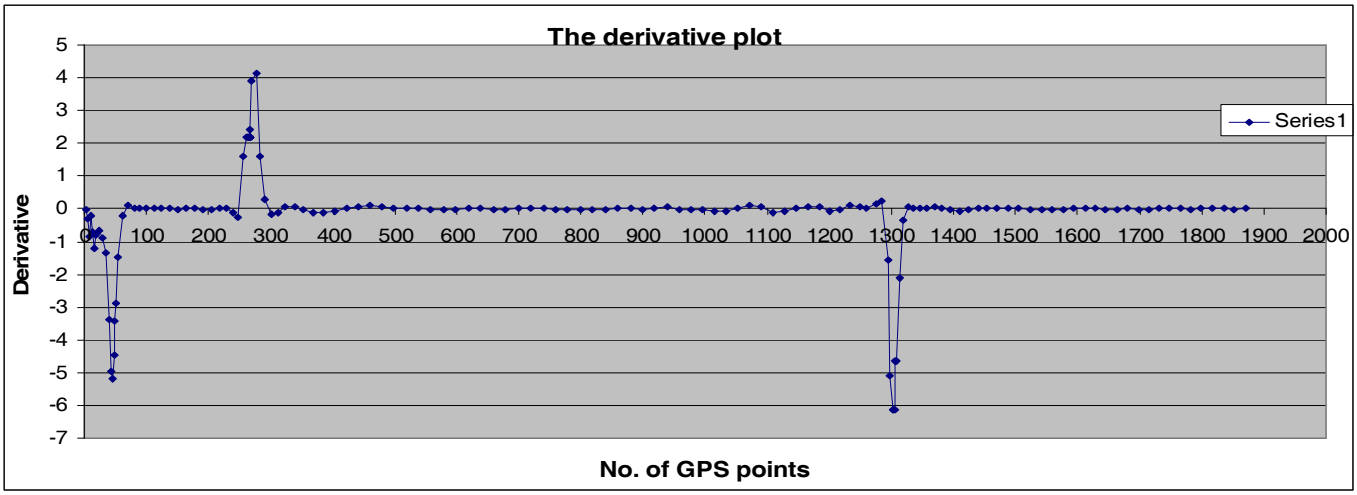

Figure 7. DRIVE 2 – Represents the derivative values $\frac{\Delta\alpha}{\Delta s}$ along Y axis and No. of GPS points on X axis.

MAPPING

Visualization of the drive is an integral part of this project. Since its end users are driver trainers, it is necessary that all drive data and risky situations are represented in a way that is easy to comprehend. Hence, it will be easy for the driver trainers to explain some specific situation to the driver.

Figure 8, presents an example of the vehicle trajectory and drive data for Drive 1. This interactive user interface would help drivers and their trainers to assess certain maneuvers in a drive by combining the multidimensional data acquired from DVE. By combining the numerical information from the graph in Figure 6, this interactive map (Figure 8) is able to show distance between indicator switch on and the turn start/turn centroid. It is also able to show if during a maneuver, driver followed the lane keeping procedure.

Figure 8. DRIVE1 – Representation on map where indicator on (yellow) and indicator off (pink) were performed.

FUTURE RESEARCH

In-order to effectively model a turn maneuver, driver's gaze direction should be tracked as well. Different eye tracking systems together with head tracking algorithm are suggested based on near infra-red or visible light using different hardware architectures.

These systems, by calculating the gaze and head direction in 3D allow calculating the coordinates where the gaze intersects with the world (a virtual plane in-front of the driver). Using perspective projection techniques, we plan to calculate the approximate depth of a drivers' gaze in a real world. Furthermore, this gaze information would be presented on an interactive map. This approximate depth calculation would be very helpful in determining the difference of gaze pattern in experienced and novice drivers.

Along with this, it is necessary to comprehensively model all tasks required for a less risky turn. Further work would be required to model other maneuvers like overtake, roundabout e.t.c.

CONCLUSION

This paper presented a framework for analyzing a turn maneuver. The prototype (IDTS) currently, integrates information related to vehicle dynamics and road

information. Next step is to model driver's gaze data and integrate it in this turn maneuver. The information gathered from DVE will help to contextualize, observe and better assess a range of driving maneuvers. This prototype is the building block to evaluate driver's competency. It acts as a assisting tool for the driver trainers.

Eventually both drivers and driver trainers would be able to assess the drive using IDTS. As already mentioned, a major percentage of road crashes are attributable to driving error. Thus, driver training remains an important road safety intervention to improve driving performance and abilities, particularly amongst young people.

REFERENCES

[1] National Transportation Safety Board, Special Investigation Report - Highway Vehicle- and Infrastructure-based Technology For the Prevention of Rear-end Collisions. NTSB Number SIR-01/01, May 2001

[2] "BMW Driver Training Gears Up for Safer Australian Drivers", http://www.autoweb.com.au/cms/A_108783/title_BMW-Driver-Training-Gears-Up-for-Safer-Australian-Drivers/newsarticle.html

[3] Mayhew, D. R. & Simpson, H.M. (1996). "The Effectiveness and Role of Driver Education and training in a Graduated Licensing System". Ottawa, Ontario: Traffic Injury Research Foundation.

[4] Engström, I., Gregersen, N.P., Hernetkoski, K., Keskinen, E. and Nyberg, A. (2003). Young novice driver education and training: Literature review. VTI-rapport 491A. Linköping.: Swedish National Road and Transport Research Institute.

[5] "Task analysis of ATIS/CVO Functions, Development of human factor guidelines for advanced traveler information system and commercial vehicle operations", Publ. No. FHWA-RD-95-176.

[6] Massimo, Alberto, and Alessandra, "Vision-based intelligent vehicles: State of the art and perspectives," Robotics and Autonomous Systems, vol. 32, pp. 1-16, 2000.

[7] Massimo, Alberto, and Alessandra, "Vision-based intelligent vehicles: State of the art and perspectives," Robotics and Autonomous Systems, vol. 32, pp. 1-16, 2000.

[8] T. M. Manubhai, G. Tarak, and M. Joel, "Looking-In and Looking- Out of a Vehicle: Computer-Vision-Based Enhanced Vehicle Safety", ITS IEEE Transactions, vol. 8, pp. 108-120, 2007.

[9] E. Andreas, P. Jochen, G. Fredrik, and E. Jonas, "Toward Autonomous Collision Avoidance by Steering", ITS, IEEE Transactions on, vol. 8, pp. 84-94, 2007.

[10] Erez Dagan, Ofer Mano, Gideon P. Stein, Amnon Shashua, "Forward Collision Warning with a Single Camera", Intelligent Vehicles Symposium, 2004 IEEE.

[11] Facelab.http://www.seeingmachines.com/facelab.htm

[12] Vigil Vanguard System, http://www.vigilsystems.com/13.0.html

[13] RTMaps: a software for new technologies, real-time and multisensor: www.intempora.com/ENG/maps/index.php?nav1=maps&nav2concept

[14] Arati Gerders, "Automatic maneuver recognition in the Automobile: the fusion of uncertain sensor values using Bayesian models", 3rd international workshop of intelligent transportation, WIT 2006.

[15] D.D. Salvucci, "Inferring driver intent: A case study in Lane-Change Detection", 48th Annual meeting of human factors and ergonomics society, USA 2004.

[16] K. Torkolla, S. Venkatesan, H. Liu, "Sensor sequence modeling for driving", 18th international FLAIRS conference , Florida, USA 2005.

[17] Nico Kaempchen, Klaus Dietmayer, "Data Synchronization Strategies For Multi-Sensor Fusion", Proceedings of 10th World Congress on Intelligent Transport Systems (ITS 2003), Madrid, Spain, 2003

[18] Gaussian Distribution, www.cs.princeton.edu/introcs/11gaussian/

[19] Centroid detection, Centroid Of An Area, http://www.efunda.com/math/areas/Centroid.cfm

[20] Haversine formula, Calculate distance between two Latitude/longitude points http://www.movable-type.co.uk/scripts/latlong.html

COOPERATIVE SENSOR TECHNOLOGY FOR PREVENTIVE VULNERABLE ROAD USER PROTECTION

Ralph H. Rasshofer, Daniel Schwarz
BMW Forschung und Technik GmbH, Haunauer Str. 46, D-80778 Munich
Germany
Christian Morhart, Erwin Biebl
Technische Universität München, Fachgebiet Höchstfrequenztechnik, D-80333 Munich
Germany
Paper Number 09-0136

ABSTRACT

In the proposed cooperative sensor system, pedestrians carry a reactive transceiver which is interrogated by a localization and tracking unit in the car. The prototype system applies Round-Trip Time-of-Flight (RTOF) techniques for the determination of the distance between the transponder and the demonstrator vehicle. A smart antenna array integrated into the car is used to determine the Direction-of-Arrival (DoA) of the transponder's response signal. Knowing the distance and azimuth angle relative to the car, the pedestrian's position and movement are calculated. These data are used as input for a highly reliable collision warning and collision mitigation system.

The sensor system is capable of addressing a huge number of communication partners within each measurement cycle. Additionally, secure burst identification is ensured for a robust localization and the suppression of unwanted co-channel interference. This is achieved by using pseudo random coded signals with a Time Division Multiple Access (TDMA) method. The distance accuracy was improved by introducing a new mirror technique in combination with an interpolation algorithm. The prototype localization system set up at 2.4 GHz covers a range up to 200 m in free field condition. With the current system a distance resolution with centimeter accuracy and an angular measurement accuracy of about 1 degree have been achieved.

Based on this low-cost transponder-based localization system, a preventive vulnerable road user (VRU) protection system has been designed and integrated in a test vehicle. The system is capable to provide a warning to the driver if a crash is likely and to autonomously brake the vehicle if the crash is unavoidable.

INTRODUCTION

Protection of vulnerable road users (VRU) is subject to intense research [1] [2]. Generally speaking, VRU protection systems can be divided into two different groups as shown in Figure 1.

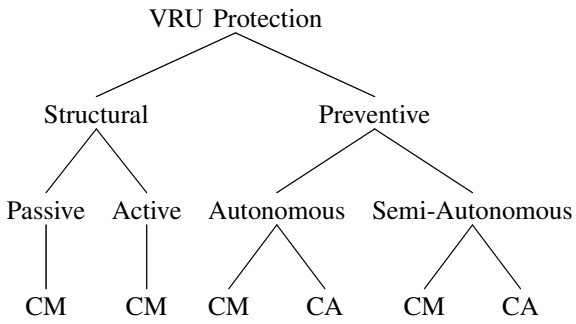

Figure 1: Classes of VRU Protection Systems.
CM: Collision Mitigation Systems
CA: Collision Avoidance Systems

Up to now, mainly re-active protections systems based on structural measures have found their way to the market. In these systems, passive measures like special construction of crash bumpers or active measures like active hoods are taken to minimize the risk of injury or fatality for the VRU after a crash. Common to all re-active systems is, that action only takes place *after* the VRU gets in contact with the vehicle. As a consequence, collision avoidance (CA) is impossible with re-active protection systems and a finite risk of injury and fatality will always be present. As derived recently from accident studies [3], structural measures of pedestrian protection feature only poor effectiveness. To overcome the drawbacks of the structural, re-active approach, preventive protection systems have been proposed [3] [4]. In these systems, protective measures are taken *before* the contact between vehicle and VRU takes place [5]. Protective measures range form fully autonomous emergency braking to preconditioning of the brake system and to warning of the driver, paving the way for both highly effective collision mitigation (CM) systems and for collision avoidance. Although impressive progress has been made, still a large percentage of pedestrian accidents cannot be covered by state-

of-the-art preventive VRU protection systems. This is due to the fact that in these systems, VRU detection, classification and behavioral prediction requires a non-occluded line-of-sight contact between vehicle and VRU [6]. However - as German accident studies have shown [7] - more than 40% of all killed pedestrians were fully or partially hidden until shortly before the impact upon the vehicle and could thus not be protected by current preventive safety systems.
As known from electromagnetic theory, communication to optically hidden partners is possible when using appropriate wavelenghts. To establish a useful communication channel, the wavelength has to be comparable to the size of the objects occluding the line-of-sight contact [8] [9]. Based on this principle, a cooperative sensor system is proposed to detect, localize and track VRUs, predict their behavior and activate protective measures when appropriate [10]. In our approach, a VRU carries a miniature transponder acting as an intelligent radar reflector interrogated by the vehicle. The coded response of the transponder clearly identifies the pedestrian as VRU; the delay of the return signal allows for range determination while its direction-of-arrival indicates the azimuth angle between vehicle and VRU. Careful choice of the system's operation frequency along with intelligent tracking techniques and novel VRU behavior modeling allows for the detection and localization of VRUs even if occluded to the driver. In the Bavarian research project AMULETT, a prototype pedestrian protection system based on 2.5 GHz cooperative sensor technology [11] has be realized an tested. Details on this system along with test results are presented in this work.

COOPERATIVE SENSOR TECHNOLOGY

Distance Measurement

Autonomous distance measurement between two objects mostly uses the Round-Trip Time-of-Flight (RTOF) principle. For the focused application, this corresponds to the time for the signal from the car to the pedestrian and vice versa. Additionally, a fixed waiting time T_w is added on the side of the pedestrian to eliminate the influence of passive reflections and to distinguish the answers from different pedestrian sensors. The distance Δs can then be computed by the totally elapsed time T_p:

$$\Delta s = \frac{T_p - T_w}{2} c_0. \quad (1)$$

Δs is the distance, T_p the elapsed time, T_w the waiting time and c_0 the speed of light.
A variation of the waiting time T_w makes it possible to address different pedestrians [12]. We used a time slot order in which each pedestrian sensor answers in a multiple of a fixed waiting time $n \cdot T_w$ (Figure 2).

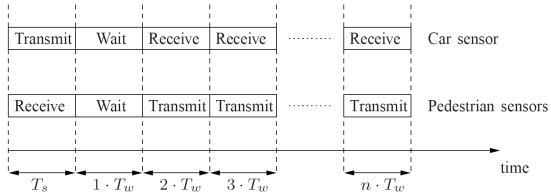

Figure 2: Time slot order in one transmission cycle.

The car sensor starts a measurement cycle by transmitting a data burst with length T_s. All of the pedestrian sensors listen to that burst and answer after an individual waiting time $n \cdot T_w$.
The measurement procedure is carried out by employing a signal correlation technique. The data bursts are encoded with pseudo random codes which are known on each sensor. By correlating the received input signal with the random code the exact time of arrival ΔT can be determined (Figure 3).

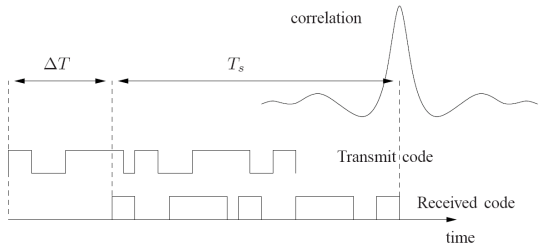

Figure 3: Schematic of a signal transmission between two sensors.

By interpolating the digital correlation result, an even higher distance resolution in a range of a few centimeters has been achieved.
The advantage of this method is a simple modulation and demodulation hardware. In fact, it can be carried out on almost every available transceiver chip providing sufficient bandwidth. Another advantage is the low latency of the measurement procedure. In dependence on the bandwidth, only a few microseconds are necessary to get an adequate correlation result. The downside of this method is an increasing need for processing power, but this can be easily applied in a Field Programmable Gate Array (FPGA) or a Digital Signal Processor (DSP).

Direction-of-Arrival (DoA) Estimation

If the correlation unit of the distance measurement identifies a received signal as valid response

of a transponder, a trigger is given to the DoA measurement device. The incident electromagnetic wave is sampled spatially at six antennas of the antenna array installed behind the windshield of the test vehicle. Therefore, distance and angle estimation perform their calculations within one communication cycle. Phases and amplitudes of the incident signal are used to determine the DoA using the Multiple Signal Classification (MUSIC) algorithm. This subspace-based method is based on the eigenvector decomposition of the covariance matrix

$$R_{uu} = E[u(k)^H u(k)], \tag{2}$$

where $u(k)$ is the received signal at the antenna array. By splitting the eigenvector space into signal space and noise space the MUSIC spectrum is obtained [13]. This MUSIC spectrum is evaluated for incident angles from 0 to 180 degree, whereas peaks in the spectrum indicate the DoA of the transponder signal (see Figure 4). In the localization unit the MUSIC algorithm estimates all incident signals including the multipath. For each hypothesis a quality value is determined, based on the evaluation of the MUSIC spectrum in combination with the power of the received signal.

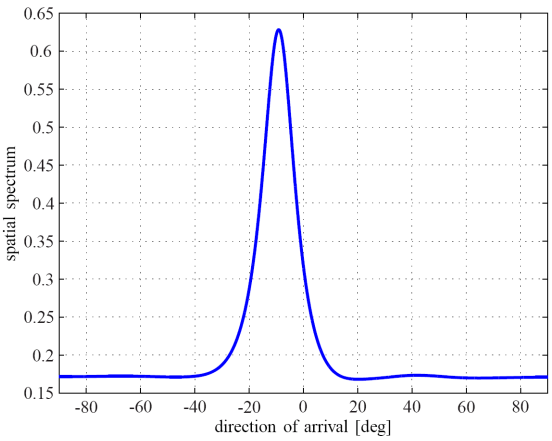

Figure 4: MUSIC spectrum for a transponder located at -9 degree azimuth.

The MUSIC spectrum as well as the correlation results of the distance measurement are used for an adaptive tracking of pedestrian positions.

Object Tracking

An extended KALMAN-FILTER is used to track the obtained transponder positions. Unlike the standard KALMAN-FILTER [14] state transition and observation models don't necessarily have to be linear functions of the state. In the transponder tracking system the observation model h which maps the state variables in cartesian coordinates to the measurement variables in polar coordinates is defined as:

$$z_k = h(x_k) \tag{3}$$

where z_k is the measurement vector

$$z_k = \begin{pmatrix} r \\ \phi \end{pmatrix} \tag{4}$$

and x_k is the state vector.

$$x_k = \begin{pmatrix} x \\ y \\ v_x \\ v_y \end{pmatrix} \tag{5}$$

As function h can't been applied directly to the KALMAN-FILTER equations the partial derivative, the JACOBIAN matrix, needs to be computed [15]. The resulting observation matrix H and the state transition matrix F using a constant velocity model are applied for the tracking of the pedestrian. F is stated as

$$F = \begin{pmatrix} 1 & 0 & T & 0 \\ 0 & 1 & 0 & T \\ 0 & 0 & 1 & 0 \\ 0 & 0 & 0 & 1 \end{pmatrix} \tag{6}$$

where T is the sample time of the system. Taking ego motion parameters of the vehicle like velocity and yaw rate into account, an estimation for movement of the pedestrian in a global coordinate system can be given and used as input for a collision assessment algorithm.

Signal Preprocessing

The principles of the distance measurement as well as the angle measurement allow for a calculation of several hypotheses. In case of multipath propagation under non-LoS conditions the main maximum in the correlation result or in the MUSIC-spectrum might represent a reflected signal arriving from a different direction than direct transponder signal [16]. In these cases positioning based on these maximium values is insufficient. Therefore the secondary maxima are taken into account.

Based on the lastest tracking results the current distance and angle measurements are investigated to determine the correct distance and azimuth information as input for the next tracking cycle. Fig. 5 shows two possible DoAs derived from the MUSIC spectrum, where the smaller peak indicates the azimuth angle of the transponder.

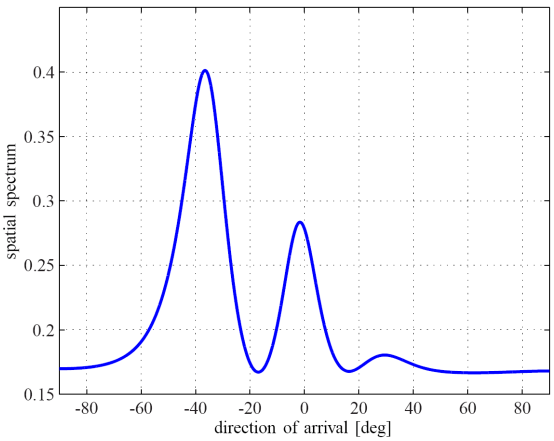

Figure 5: MUSIC spectrum for transponder at -1.4 degree and multipath signal impinging at -37 degree

MEASURED PERFORMANCE OF COOPERATIVE LOCALIZATION SYSTEM

Quality of Distance Measurement

For the characterization of the RTOF sensor a test scenario with a moving car and a fixed pedestrian position was used. The car moved with an approximate speed of 12 km/h straight in the direction of the pedestrian. The measurement started at a distance of 180 m to a distance of 2 m directly in front of the car. As reference a differential GPS (DGPS) system [17] with an accuracy down to 2 cm was used. Fig. 6 shows an extract of the distance values of both systems.

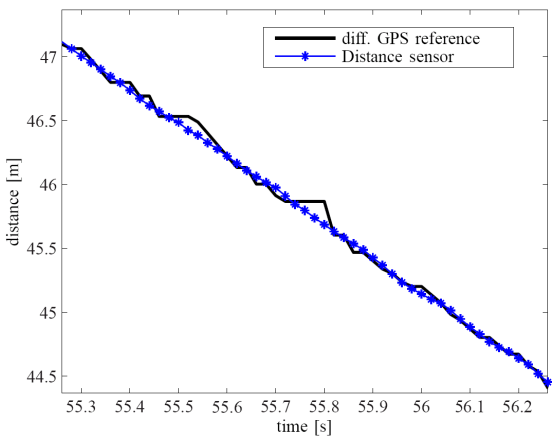

Figure 6: Distance values in the sector from 47 m to 43 m

It became obvious during the measurement campaign, that a DGPS system with a accuracy of 2 cm is no longer sufficient to characterize the system completely.

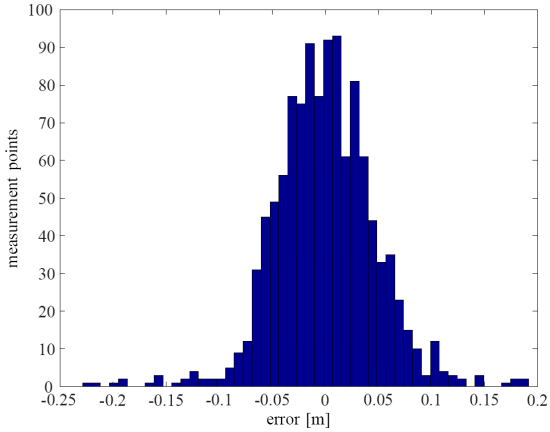

Figure 7: Histogram of the distance error in reference to a DGPS System

As a matter of fact the standard deviation of 4.7 cm is partly caused by the DGPS System inaccuracy. The difference values between both systems are shown in Figure 7.

Quality of Direction-of-Arrival Estimation

To evaluate the performance of the DoA estimation several measurement setups have been chosen. Fig. 8 shows results of a measurement where a pedestrian moved circular in front of the test vehicle carrying the transponder and a differential GPS system as reference.

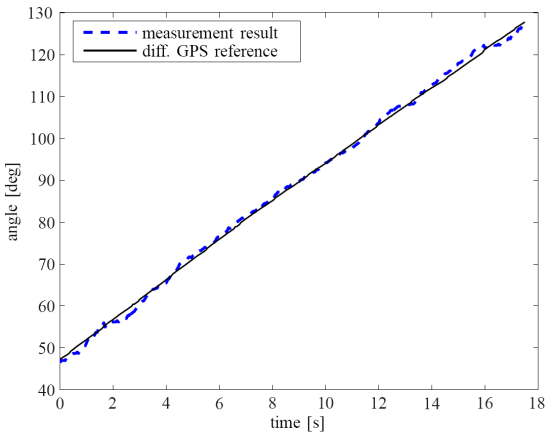

Figure 8: DoA values in the sector from 50 to 130 degree

The distance was kept constant at 15 m in this measurement. This procedure allows for an exact evaluation of the variance and the absolute deviance in dynamic scenarios covering proposed sensor range.

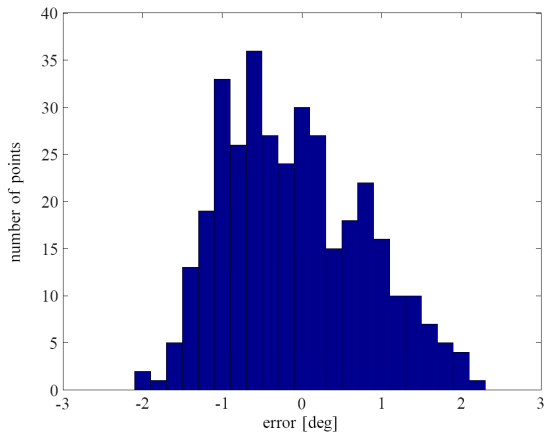

Figure 9: Histogram of DoA values in the sector from 50 to 130 degree

The measurements were repeated several times in different distances and recorded. They showed reproducible results. The standard deviation was determined to be betwen 0.7 and 0.9 degree in all measurements. The differences between the measured angles and the reference for a distance of 15 m are printed in Figure 9. The standard deviation in this example is 0.85 degree.

Performance in Non-Line-of Sight (non-LoS) scenarios

A measurement campaign has been conducted to determine the localization accuracy in a typical urban scenario under non-LoS conditions. While the car drives on the street a pedestrian is standing beside the road occluded by parked cars (Figure 10). Starting at a distance of 20 m the sampled output of the tracking system is compared to the reference system for a transponder height of about 85 cm.

As expected the distance and azimuth angle accuracy decrease compared to the LoS scenario. The distance information shows a mean difference of 0.7 m and a standard deviation of 0.3 m. For the estimated angle a mean difference of 2 deg and a standard deviation of 2.1 deg were calculated. Altogether these results affirm the usability of the cooperative sensor system for pedestrian protection.

Figures 12 and 11 show results of the cooperative sensor system. The tracking output and the reference data are displayed in polar coordinates for a separate evaluation of the two measurement principles.

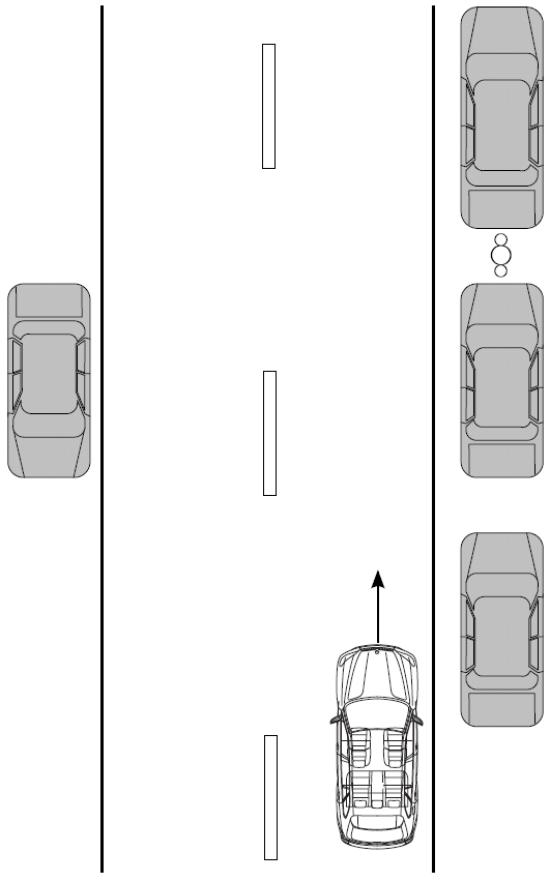

Figure 10: Urban non-LoS scenario with pedestrian occluded by parked cars

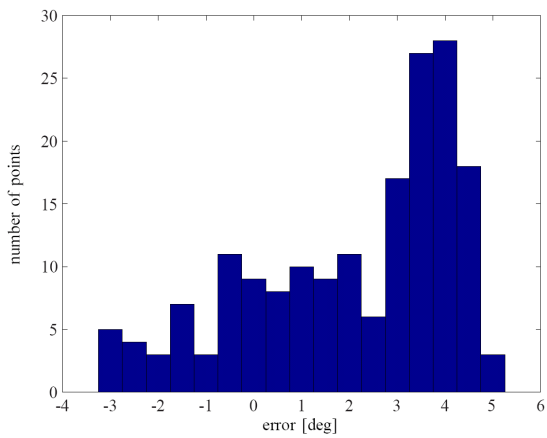

Figure 11: Histogram of error of tracked DoA data in non-LoS scenario

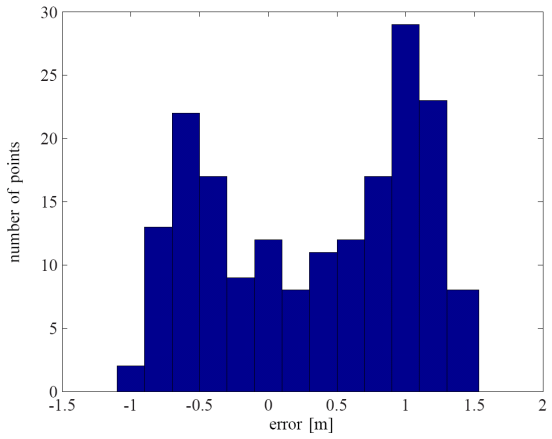

Figure 12: Histogram of error of tracked distance data in non-LoS scenario

CONCLUSION

A cooperative sensor approach for pedestrian protection has been presented. The implemented localization principles have proven to provide contact even without Line-of-Sight (LoS) between communication partners. Positioning accuracy has shown to be sufficient as basis for a highly reliable pedestrian protection system. Even in worst case multipath scenarios without LoS the localization unit has shown to provide adequate results. The clear identification of pedestrians, the positioning accuracy and the sensor range offer the potential to cover a wide range of accident scenarios which cannot be covered with state-of-the-art sensors.

REFERENCES

[1] T. Gandhi and M. Trivedi, "Pedestrian protection systems: Issues, survey, and challenges," *IEEE Trans. Intell. Transp. Syst.*, vol. 8, no. 3, pp. 413–430, 2007.

[2] R. Fröming, "Assessment of integrated pedestrian protection systems," PhD Thesis, TU Berlin, 2008.

[3] D. Wisselmann, K. Gresser, M. Hopstock, and W. Huber, "Präventiver statt passiver Fußgängerschutz," in *Beiträge zum 10. Braunschweiger Symposium für Automatisierungssysteme, Assistenzsysteme und eingebettete Systeme, AAET 2009*, Feb. 2009, pp. 60–76.

[4] Franz Roth, Johann Stoll, André Zander, Stefan Schramm, and Kilian von Neumann-Cosel, "Methodik zur Funktionsentwicklung des vorausschauenden Fußgängerschutzes," *24. VDI/VW-Gemeinschaftstagung Integrierte Sicherheit und Fahrerassistenzsysteme*, 2008.

[5] L. Walchshäusl, R. Lindl, K. Vogel, and T. Tatschke, "Detection of road users in fused sensor data streams for collision mitigation," in *Proc. Advanced Microsystems for Automotive Applications AMAA 2006*, Berlin, Germany, 2006, pp. 53–65.

[6] K. C. Fürstenberg, D. T. Linzmeier, and K. Dietmayer, "Pedestrian recognition and tracking of vehicles using a vehicle based multilayer laserscanner," in *Proc. of ITS 2003 10th World Congress on Intelligent Transport Systems*, Madrid, Spain, 2003.

[7] R. Rasshofer, D. Schwarz, E. Biebl, C. Morhart, O. Scherf, S. Zecha, R. Grünert, and H. Frühauf, "Pedestrian Protection Systems using Cooperative Sensor Technology," *Proceedings of the 11th International Forum on Advanced Microsystems for Automotive Applications (AMAA'07)*, pp. 135–145, 2007.

[8] A. Fackelmeier, C. Morhart, and E. Biebl, "Evaluation of diffraction effects for identifying hidden targets," in *Proceedings of the German Microwave Conference*, Hamburg, Germany, Mar. 2008, pp. 291–294.

[9] ——, "Dual frequency methods for identifying hidden targets in road traffic," in *12th International Forum on Advanced Microsystems for Automotive Applications AMAA 2008*, Berlin, Germany, Mar. 2008, pp. 11–15.

[10] R. Rasshofer, D. Schwarz, K. Gresser, and E. Biebl, "Fußgängerschutz mittels kooperativer Sensorik," in *Proceedings of the 5th Workshop on Driver Assistance Systems, Walting*, 2008, pp. 159–167.

[11] C. Morhart, E. Biebl, D. Schwarz, and R. Rasshofer, "Cooperative multi-user detection and localization for pedestrian protection," in *Proceedings of the German Microwave Conference (to be published)*, Munich, Germany, Mar. 2009.

[12] C. Morhart and E. Biebl, "Ein kooperatives, code-basiertes Abstandsmesssystem für eine große Anzahl simultaner Nutzer," *Frequenz - Journal of RF-Engineering and Telecommunications*, vol. 62, pp. 175–179, Jul. 2008.

[13] R. Schmidt, "Multiple emitter location and signal parameter estimation," *IEEE Trans. Antennas Propag.*, vol. 34, no. 3, pp. 276–280, 1986.

[14] R. Kalman, "A new approach to linear filtering," *Jounal of Basis Engineering*, vol. 82, no. 1, pp. 35–45, 1960.

[15] B. Ristic and S. Arulampalam, *Beyond the Kalman Filter: Particle Filters for Tracking Applications*. Artech House, 2004.

[16] D. Schwarz, R. Rasshofer, and E. Biebl, "Optimized tracking for cooperative sensor systems in multipath environments," *Advances in Radio Science ARS2007 / Kleinheubacher Berichte der U.R.S.I.*, pp. 71–75, 2008.

[17] K. Vogel, "High-Accuracy Reference Data Acquisition for Evaluation of Active Safety Systems by means of a RTK-GNSS-Surveying System," *Proceedings of the 6th European Congress and Exhibition on ITS*, 2007.

USING THE OBJECTIVE RATING METHOD (ORM) AS A QUALITY ASSESSMENT TOOL FOR PHYSICAL TESTS, TEST METHODS, AND MATHEMATICAL MODELS

Linda Eriksson
Håkan Sundmark
Autoliv Sverige AB, Vårgårda
Sweden
Harald Zellmer
Autoliv B.V. & Co. KG, Elmshorn
Germany
Kurt Fograscher
Bernhard Drexl
Autoliv B.V. & Co. KG, Dachau
Germany
Marc Van Slagmaat
Autoliv France, Gournay-en-Bray
France

Paper Number 09-0163

ABSTRACT

There is a daily need to assess the quality of our work. On the crash track, the tests should be repeatable, the chosen test method should fulfil the test purpose and every result should have an explanation. The tests performed may also be used to validate mathematical models, the accuracy of which must then be assessed, or, to show whether a new design or method influences the performance or not. Regardless of which, there is a need of a quality assessment tool. By applying the Objective Rating Method on performed rear-end sled tests, Autoliv has previously shown that the BioRID II dummy allows for both repeatable and reproducible testing. Here, the ORM has been evaluated on frontal, side impact and component tests and the corresponding models.

For frontal impacts, test repeatability has been assessed, and correlation between physical tests and mathematical models are shown. For side impacts, the test repeatability, test method predictability and mathematical model predictability have been assessed. The repeatability of frontal sled tests is comparable with that presented for rear-end sled tests, while the side impact sled test repeatability is generally somewhat lower.

Although the ORM has to be used with care and knowledge, it is a useful tool, especially for assessments regarding test repeatability and reproducibility. The ORM allows for agreement, in advance, on a quality level for tests and mathematical models. Beneficial is that the ORM not only compares peak values but also curve shapes. Furthermore, the ORM compares two tests; many methods require several tests and that is normally not available in daily work.

INTRODUCTION

There are several methods to assess the repeatability or reproducibility of duplicated tests, or the predictability of simulation models or test methods. One common method in daily work is to visually compare results for two tests and decide if they are sufficiently similar or not. This method is often fast to carry out, but the decision may differ depending on personal experience and opinion. Therefore, this kind of method is not solitary suitable as a quality assessment tool for scientific or professional purposes. A useful correlation quality assessment tool must be suitable for many types of inputs; for test and simulations issues it should be possible to compare scalars such as criteria and peak values, and curve shapes. Also, the rating from poor to good correlation must be obvious. Further, the result must be independent of the user and it should be easy to evaluate and understand. Preferable, the tool should be easy and fast to use.

Autoliv has used several test quality assessment tools during the years. In a recent study ([1]), the repeatability and reproducibility of rear-end impact tests with the BioRID II were assessed by using the ORM ([2]). For that purpose, the ORM was found to be a good tool. Therefore, this paper will continue the evaluation of the ORM; this time applied on conducted frontal impact, side impact, and airbag module component tests and corresponding simulations from four Autoliv sites in Europe. Also, the ORM was used to evaluate the correlation between test methods. Thresholds for good and poor correlation for a few types of comparisons will be proposed along with a method to define which signals to included in a comparison.

METHOD

The ORM

The Objective Rating Method, ORM, assesses the correlation between duplicated tests (repeatability or reproducibility) or between a test and a simulation (predictability). The ORM enables comparison between scalars, such as criteria, minimum and maximum peak values, and their occurrence times, and between curve shapes.

The ORM scalar correlations are calculated according to Equation 1. This expression is called the Factor Method and calculates the correlation between the reference test and the comparison test. The results range from 0 to 100%, where 100% represents a perfect match. The curve shape correlation is calculated according to Equation 2. This expression is called the Weighted Integrated Factor Method and is a combination of the Factor Method and the Root Mean Square Addition Method. This means that the correlation in each time step contributes to the total correlation just as the function value would contribute to the total area underneath the curve. The δ is very small and used to avoid division by zero. *r* and *c* are used as abbreviations for *reference* and *comparison*, respectively.

$$ORM_{scalar} = \frac{\max(0, reference \cdot comparison)}{\max(reference^2, comparison^2)} \quad \textbf{(1)}$$

$$ORM_{shape} = 1 - \sqrt{\frac{\int \left(\max(|r(t)|,|c(t)|) \cdot \left(1 - \frac{\max(0, r(t) \cdot c(t))}{\max(\delta, r(t)^2, c(t)^2)} \right)^2 \right) dt}{\int \max(|r(t)|,|c(t)|) dt}} \quad \textbf{(2)}$$

ORM values are calculated not only for the scalars and the curve shapes, but also for groups of scalars and curve shapes. The contribution of each ORM value in its group is defined by a weight factor, W. Equation 3 is used to calculate the ORM value for each group. Further, the groups are arranged into one single ORM value that is the correlation for the complete system. The contribution of the group ORM values to the complete ORM value is defined by weight factors, W. Equation 4 is used to calculate the ORM value for the complete system.

$$ORM_{group} = 1 - \sqrt{\frac{\sum \left(W_{scalar\ or\ shape} \cdot (1 - ORM_{scalar\ or\ shape})^2 \right)}{\sum W_{scalar\ or\ shape}}} \quad \textbf{(3)}$$

$$ORM_{complete} = 1 - \sqrt{\frac{\sum \left(W_{group} \cdot (1 - ORM_{group})^2 \right)}{\sum W_{group}}} \quad \textbf{(4)}$$

A study was conducted in order to better understand the correlation of the ORM values to engineering judgements and to identify possible weaknesses of the ORM. A typical acceleration curve was used (Figure 1) as the reference curve, and an identical curve was used as the comparison curved but shifted or scaled in several steps in X (e.g. along the time axis) and Y (e.g. along the amplitude axis), or inverted. The curves were evaluated in the time range 0.01 to 0.12 s. Furthermore, another curve (Figure 2) was used to assess the correlation between a filtered (CFC60) and an unfiltered curve. For each comparison, the correlation of the maximum peak, its occurrence time, and the curve shape were calculated. Also, the group ORM value for these three components were calculated, all with equal weight. The group ORM values were then presented along with correlations assessed by engineering judgement in order to propose thresholds in ORM for correlation assessments. The engineers used a four-level scale: OK/acceptable/NOK/–. OK means okay, NOK means not okay, and the dash (–) shows that the curves are very dissimilar.

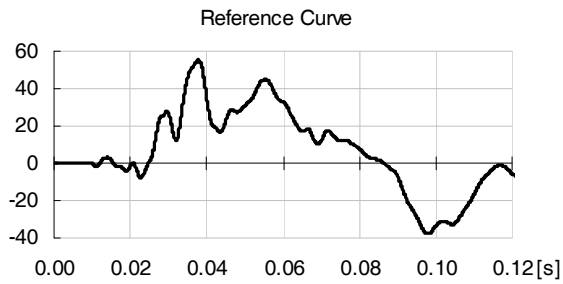

Figure 1. The acceleration curve used as the reference curve in the ORM evaluation.

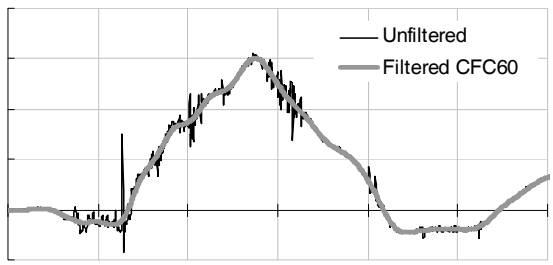

Figure 2. The curves compared to assess ORM values for a filtered versus an unfiltered curve.

Frontal impacts

<u>Series 1 – Evaluation of Included Signals</u> In order to evaluate how the selection of included signals influences on the complete ORM values one pair of USNCAP driver side sled tests were analyzed. Seven different sets of signals were composed.

- Set 1 contained the criteria HIC36 and Chest3ms, and these were equally weighted to compose the complete ORM value.
- Set 2 contained one group (weight 1/2) with head, chest, and pelvis accelerations, lumbar spine, femur, and belt loads, and chest deflection; and one group (weight 1/2) with only sled x-acceleration. Mainly peak values of the signals were compared, and a few of their occurrence times were added with half weight. The belt force

peaks were given half weight as well. No curve correlations were included in this set.

- Set 3 contained one group (weight 1/11) with head and neck signals, one group (weight 2/11) with chest signals, one group (weight 1/11) with lumbar spine signals, one group (weight 2/11) with pelvis signals, one group (weight 1/11) with femur signals, one group (weight 2/11) with belt signals, and one group (weight 2/11) with sled x-accelerations. For all signals, all available components were included, and in the chest, lumbar spine, and pelvis groups the signals acting in the dummy sagittal plane were given double weight.
- Set 4 contained one group (weight 4/14) with sled x-acceleration, belt signals and dummy placement signals, and five groups with most of the measured dummy signals: head (weight 3/14), upper neck (weight 1/14), chest (weight 3/14), lumbar spine (weight 1/14), and pelvis and femur (weight 2/14). For the head and chest the main peaks and the curve shapes were included. For the other included signals, only the main peaks were included.
- Set 5 contained one group (weight 2/12) with sled x-accelerations, one group (weight 2/12) with belt signals, and six groups with most of the measured dummy signals: head (weight 2/12), upper neck (weight 1/12), chest (weight 2/12), lumbar spine (weight 1/12), pelvis (weight 1/12) and femur (weight 1/12). All available components were included. Dummy signals acting in the dummy sagittal plane were given higher weights. Curve shapes were given higher weights than peaks and their occurrence times.
- Set 6 contained one group (weight 3/22) with sled x-accelerations, one group (weight 3/22) with belt signals, and six groups with most of the measured dummy signals: head (weight 3/22), upper neck (weight 1/22), chest (weight 3/22), lumbar spine (weight 3/22), pelvis (weight 3/22) and femur (weight 3/22). For almost all signals, the main peaks, their occurrence times, and the curve shapes were included, with the exceptions of the upper neck and sled for which only the curve shapes were included.
- Set 7 contained one group (weight 4/5) with dummy signals: head, chest, and pelvis x- and z-accelerations, upper neck loads, chest deflection, and femur z-forces, and one group (weight 1/5) with belt signals. For almost all signals one third of the components were significant peaks, one third their occurrence times, and one third curve shapes. The sled pulse curve shape correlations were evaluated separately and not included in the complete ORM value.

The two compared tests were analysed visually by engineers in order to rate the frontal sled test repeatability on a five-level-scale: dissimilar, nearly dissimilar, fairly similar, similar, and almost identical.

Series 2 – Correlations between Sled Tests Sled test repeatability was assessed for tests with a belted Hybrid III 50 %-ile seated on a padded R16 seat. Two tests with the EuroNCAP pulse and three tests with the USNCAP pulse were compared; in total were four comparisons performed. The signals included in the comparisons were selected with the same method as used in Set 7: head, chest and pelvis x-and z-accelerations, upper neck and lumbar spine F_x, F_z, and M_y, chest deflection, torso displacement, femur z-forces, belt forces, and belt displacement. For all signals the curve shapes correlations during 200 ms, the minimum or maximum peak value and occurrence time were included; for five signals both minimum and maximum peaks and occurrence times were included. All signals were contributing with the same weight to the complete ORM value. The sled pulse correlation was not included in the complete ORM value, but checked separately. The four pairs of compared tests were analysed visually by test engineers in order to rate their overall repeatability on a five-level-scale: dissimilar, nearly dissimilar, fairly similar, similar, and almost identical.

Series 3 – Correlations between Sled Tests Five USNCAP sled tests were included in Series 3. Sled tests #1 to #3 were conducted with the Hybrid III 50%-ile and sled tests #4 and #5 with the Hybrid III 5%-ile. The ORM correlations were assessed for #1 versus #2, #1 versus #3, #2 versus #3, and #4 versus #5. The signals included in the ORM analyses were selected according to the method used in Set 7. The five pairs of compared tests were analysed visually by test engineers in order to rate their repeatability on a five-level-scale: dissimilar, nearly dissimilar, fairly similar, similar, and almost identical.

Series 2 – Correlations between Simulations and Sled Tests The tests conducted in Series 2 were aimed as verification tests for Madymo models of belt systems. The models of the belt systems were built up of validated belt component models and tuned to mimic the chosen load limiter levels and test conditions. The sled test predictability of the final Madymo system models were assessed by the ORM. A similar signal set were used as those used to correlate the tests in Series 2, the main differences were that the lumbar spine loads and the torso displacement were omitted, and the time interval differed. Due to the aim of verifying the Madymo belt system models predictability in normal crash conditions, the correlations were assessed during the first 85 ms of the USNCAP simulations and during the first 110 ms of the EuroNCAP simulations. After that the dummy chest hit its legs and that should not be mimicked by the Madymo models. The usefulness of the Madymo models was assessed by simulation engineers.

Series 3 – Correlations between Simulations and Sled Tests Sled tests #2 and #3 conducted in Series 3 were used as verification tests to a Madymo system simulation. The sled test predictabilities of the final Madymo model were assessed by the ORM. A similar signal set as used to correlate the tests in Series 3 were used. The usefulness of the Madymo model was assessed by simulation engineers.

Side Impacts

The ORM was used to guide in an EuroNCAP side impact project, from component development to full scale crash tests. On component level, the ORM was used to assess that sufficiently predictability levels were reached. Later, the predictability of the complete systems mathematical models were assessed by the ORM. The project included sled tests and full scale crash tests for the MDB and the pole load cases. In order to assess the predictability of the sled tests to the full scale crash test the ORM was used. Also, ORM was used to confirm that changes of the safety components did influence the dummy performance. All steps and correlations will not be covered in this study. In all cases the ORM was applied the repeatability or predictability was also rated by engineering judgement.

Mathematical models of side impact airbags were built up in LS-Dyna and tuned to four component tests: static deployments for airbags with no vent holes and equipped with ordinary vent holes and dynamic tests with an impactor at 7 m/s and a total weight of 12 kg for the pelvis and thorax parts and with an impactor at 4 m/s and a total weight of 20 kg for the pelvis and thorax parts. Two static tests of each type, and three dynamic tests of each type were conducted and the repeatability level were assessed by the ORM. For all tests, signals in the pelvis part and the thorax part were collected. For the static tests, the two bag pressures were compared from 10 to 60 ms. For each pressure signal, the peak, its occurrence time, and the curve shape correlation were given equal weight and repeatabilities were assessed by the ORM. For the dynamic tests, the two bag pressures and the displacement, velocity, and acceleration of the impactors were compared from 10 to 60 ms or to strike through. For the accelerations and pressures, peak values, their occurrence times, and the curve shapes were included with equal weight and for the displacement and velocities only the curve shapes were included and these were given the same weight as all other components. One side impact airbag mathematical model was compared by the ORM to all conducted tests, and the same signals sets were used as in the repeatability assessments.

Mathematical models of the side impact safety components were fitted into mathematical models of full scale crash tests and the components were optimized to perform well in the EuroNCAP MDB and pole tests. Sled tests were then conducted, and these aimed to mimic the mathematical models of full scale crash tests. The repeatability of the sled tests were assessed by the ORM. Then, one full scale MDB crash test and one full scale pole crash test were conducted and the sled test predictabilities of the full scale crash tests were assessed by the ORM. The sled test set-ups were then improved to better mimic the full scale crash tests and these improvements were assessed by the ORM. The repeatabilities were assessed by the ORM for these sled tests as well. The mathematical models were updated and used to improve the EuroNCAP performance further, and sled tests were conducted to assess these improvements. The predictability and the repeatability of the sled tests were assessed by the ORM, and the ORM was also used to assess if the changes of the safety component resulted in significant changes of the dummy readings in the sled tests. Finally full scale crash tests were performed and the sled test predictabilities of these were assessed by the ORM. The ORM sets used in the side impact project where selected according to the method used in Set 7 in this study. In this paper, only the ORM values for the MDB tests and simulations will be presented.

RESULTS

The ORM

ORM values for an extensive set-up of curves were compared with the correlations assessed by engineering judgements. The filtered versus the unfiltered curve were compared, and the ORM value was 97% for the maximum peak correlation, 99% for the occurrence time correlation, and 89% for the curve shape correlation. The group ORM value was 93% and the curves were judged to have okay correlation (OK). For the normal versus the inverted curve, the ORM value for the peak occurrence time correlation was 100%, but the other two correlations were zero, resulting in a group ORM value of 18%. These curves were rated as very dissimilar (–). The ORM values for the comparisons in which one of the two curves was shifted or scaled are given in Table 1 along with the engineering judgements. As can be seen in all groups with increasing shifting or scaling, the scalar, the curve shape and the group ORM values are continuously decreasing which is fundamental for a consistent correlation assessment tool.

Frontal impacts

Series 1 – Evaluation of Included Signals The complete ORM value was 96% for Set 1 and Set 2, 84% for Set 3, Set 4, and set 6, 73% for Set 5, and 88% for Set 7. It can be concluded that the choice of signals and components included in the ORM analysis largely influence on the complete ORM values. The sled tests were judged as almost identical by several test engineers.

Table 1.
ORM values in percent for the comparisons in which one of the curves was adjusted, along with the correlations assessed by engineering judgements. OK means okay, Acc. means acceptable, and NOK means not okay. – means that there is no correlation due to very dissimilar curves.

Adjustment of the comparison curve	Peak ORM value	Peak time ORM value	Curve shape ORM value	Group ORM value	Engineering judgement
Shift Y + 1	98	100	91	95	OK
Shift Y + 5	92	100	72	83	OK
Shift Y + 10	85	100	57	74	Acc.
Shift Y + 20	73	100	39	62	NOK
Shift Y + 40	58	100	23	49	–
Shift Y + 80	41	100	14	37	–
Scale Y*1.1	91	100	91	93	OK
Scale Y*1.2	83	100	83	87	OK
Scale Y*1.3	77	100	77	81	OK
Scale Y*1.4	71	100	71	77	Acc.
Scale Y*1.5	67	100	67	73	Acc.
Scale Y*1.8	56	100	56	64	NOK
Shift X+ 0.001	100	97	79	80	OK
Shift X+ 0.005	100	88	50	70	Acc.
Shift X+ 0.01	100	79	35	61	NOK
Shift X+ 0.02	100	65	21	50	–
Shift X+ 0.04	100	49	6	38	–
Shift X+ 0.08	100	32	1	31	–
Scale X*1.1	100	91	44	67	NOK
Scale X*1.2	100	83	31	59	NOK
Scale X*1.3	100	77	29	57	NOK
Scale X*1.4	100	71	26	54	–
Scale X*1.5	100	67	23	51	–
Scale X*1.8	100	56	16	45	–
Scale X*1.1 & Y*1.1	91	91	43	66	NOK
Scale X*1.5 & Y*1.5	67	67	21	48	–
Scale Y*1.1 & X*1.5	91	67	22	45	–
Shift X + 0.005 & Y + 5	92	88	47	68	NOK
Shift X + 0.03 & Y + 30	65	56	20	44	–
Shift X + 0.005 & Y + 30	65	88	27	53	–

Series 2 – Correlations between Sled Tests First, the two EuroNCAP tests were compared. The sled pulse curve shape correlation was very high, 93%. The complete ORM value was 87%. The ORM value was 86% for the group of dummy signals, and 91% for the group of belt signals. For all included signals, the average peak value correlation was 93%, the average peak value occurrence time correlation was 95%, and the average curve shape correlation was 85%. Then, three USNCAP tests were compared in pairs. The sled pulse curve shape correlations were all very high, these ranged from 94 to 96%. The complete ORM values were 81, 85, and 86%. The ORM values were 79, 84, and 84% for the groups of dummy signals, and 90, 90, and 96% for the groups of belt signals. For all included signals in each comparison, the average peak value correlations were 91, 94, and 94%, the average peak value occurrence time correlation was 97, 98, and 98%, and the average curve shape correlation was 77, 81, and 82%. The EuroNCAP sled tests were judged as almost identical, and the USNCAP sled tests as similar by several test engineers.

Series 3 – Correlations between Sled Tests The crash pulse in sled test #1 differed significantly from those in sled tests #2 and #3: the amplitude differed about 4g and the pulse ended about 10 ms later. In ORM values the crash pulse curve shape correlation was 70 and 71% for the pairs including sled test #1, and 95% for sled test #2 versus #3. The crash pulse curve correlation was 93% for #4 versus #5. The complete ORM values were 76% for sled test #1 versus #2, 77% for #1 versus #3, 86% for #2 versus #3, and 81% for sled test 4# versus #5. The comparisons including sled test #1 were rated as nearly dissimilar, test #2 versus #3 as similar, and #4 versus #5 as fairly similar.

Series 2 – Correlations between Simulations and Sled Tests The Madymo model of the EuroNCAP system predicted the three EuroNCAP tests in Series 2 with 75, 76 and 78% in terms of complete ORM values. For the groups of dummy signals the predictabilities were 73, 73, and 74%, and the predictabilities were 86, 86, and 87% for the group of belt signals. The Madymo model of the USNCAP system predicted both USNCAP tests in Series 2 with 75% in terms of complete ORM values. For the groups of dummy signals the predictabilities were 72 and 73%, and the predictabilities were 87 and 88% for the group of belt signals. The Madymo models were judged as useful by simulation engineers.

Series 3 – Correlations between Simulations and Sled Tests The complete ORM values for the predictabilities were 68 and 69% to sled test #2 and #3, respectively. The average peak value predictions were 81% for both comparisons, the average peak value occurrence time predictions were 81% for both comparisons, and the curve shape correlations were 60 and 61%, respectively. The Madymo models were judged as useful by simulation engineers.

Side Impacts

The ORM was used to assess the repeatability of static and dynamic airbag component tests and the mathematical model predictabilities of these tests. Two static tests with no vent hole were conducted and reached 93% in complete ORM value. These tests were rated as similar by engineers. For the static tests with ordinary vent holes, the complete ORM values was 80% and the test repeatability rated as poor by engineers since the pressure curves in the pelvis part were unlike from 15 to 30 ms due to a squeezed tube; the pelvis pressure curve shape correlation was 68%. Three dynamic tests were conducted at 7 m/s. The complete ORM values were 86 and 89% for the tests judged as fairly similar and 91% for the test judged as similar. Three dynamic tests were conducted at 4 m/s. Two pairs of tests were judged as fairly similar due to different pelvis accelerations. The complete ORM values for these were 85 and 86%. One pair of tests were judged as almost

identical and reached a complete ORM value of 95%. The mathematical model predictabilities were 87 and 90% for the static tests with no vent holes, and 86% for the static test with ordinary vent whole. No predictability ORM value was calculated for the test with the squeezed tube. The predictabilities of the dynamic tests at 7 m/s were 82 to 85%, and the predictabilities of the tests at 4 m/s were 71 to 76%. Overall, the mathematical model was judged to predict the tests sufficiently well.

Sled tests were conducted with settings estimated by mathematical modelling. The sled test repeatability was 85% and judged as similar for almost all included signals. The sled crash pulse shape repeatability was 87% and the door crash pulse shape repeatability was 89%. The mathematical models predicted both sled tests with only 46% in terms of complete ORM values. However, the most important signals resulted in higher ORM values: the predictabilities of the abdomen were both 60% and the predictabilities of the rib deflections were 74 and 78%. The sled tests predicted the full scale crash test with 55 and 56% in terms of complete ORM values. For the mathematical models, the predictability of the full scale crash test was 50% for the abdomen and 57% for the rib deflections. The predictability of the full scale crash test was judged as insufficient for both the sled tests and the mathematical models. Hence, a new loop of tests and simulations were performed.

The repeatability of the next pair of sled tests was 71% and these tests were judged as nearly dissimilar. The sled and the door crash pulse shape correlations were 82% and 79%, respectively. It was possible to assess which of the two that was more accurate than the other, and that test will be used in the coming comparisons. The sled tests predicted the full scale crash tests with 62%; the predictability of the abdomen was 60% and the predictability of the rib deflections was 80%. The corresponding number for the mathematical model predictability was 51% for the abdomen and 56% for the rib deflections. Two pairs of sled tests with improved safety components were then conducted. The repeatabilities within these pairs were 77 and 80%. The correlations between the pairs were 73 and 64%, indicating that the changes of the safety components resulted in changes of the dummy readings. The final safety components were then used in a full scale crash test. The sled test predictability of this full scale crash test was only 51%: the rib deflections predictabilities were 75% and 76%, and the abdomen predictabilities were 27 and 28%. The very low values of the abdomen predictability were due to that the front and middle forces measured in the sled tests were around or just below zero and a bit above zero in the full scale crash test which resulted in ORM values close to zero. The correlation between the abdominal rear forces, which were the important signals, was 96%.

DISCUSSION

The ORM

The Objective Rating Method, ORM, was published in 2005 by [2] as a tool for assessing the predictability of Madymo simulation models to mechanical tests. [2] stated that high correlation is 65% or above for mechanical test repeatability. This statement was based on component tests with one Hybrid III 50%-ile without arms and lower legs. Ten different tests were repeated ten times, and in each test thirty signals were recorded. All signals of the repeated tests were then compared to the first test in each test series. However, which signals compared or weight factors used, are not specified. According to the authors, special attention was given to positioning the dummy before each test to ensure good repeatability, and a well-defined environment was used in the tests. A couple of previous studies, [1] and [3], have shown that an ORM value of 65% most likely is a too low threshold to correctly rate two tests as highly repeatable, although the threshold is depending on which signals and components that are included. This study shows that correlations above 65% can be judged as poor, indicating that a higher threshold should be more proposed. Furthermore, there should preferably be different requirements on scalar and curve shape correlations.

In an earlier study ([1]) the ORM was applied to twenty-six pairs of rear-end sled tests in order to assess the BioRID II repeatability and reproducibility. The tests were conducted at two crash test sites. Four BioRID II dummies, five different seats, and three crash pulses were used. Both criteria and dummy readings were compared. The BioRID II repeatability, in terms of complete ORM values, ranged from 83 to 90%, and the reproducibility ranged from 74 to 78%. In this study, other types of tests were included, as well as mathematical models. For those of the comparisons conducted in this study that were conducted with the same set-up selection methodology as used in [1], i.e. Set 7, the complete ORM values for frontal sled test repeatability ranged from 81 to 88%, and the mathematical system model predictability ranged from 68 to 78%. Hence, the sled test repeatability is in the same range for rear-end and frontal impacts. In the BioRID II repeatability ORM values a few criteria are included, that may be one reason why the rear-end tests have slightly higher complete ORM values than the frontal impacts. The reproducibility ORM values for the rear-end sled tests are somewhat higher than the predictability ORM values for the frontal simulation models. That was expected, since two physical dummies in duplicated sled tests should mirror each other fairly well, while simplified mathematical models of the dummy and the sled test environment hardly can mirror its mechanical counterpart exactly. Nevertheless, the predictabilities of the mathematical

models are fairly good, and the models are judge as useful by engineers. For the side impact tests conducted in this study, the sled test repeatability ranged from 77 to 85% for the MDB sled tests that were properly conducted. For the pole sled tests conducted in the same side impact project, the repeatability ranged from 72 to 80%. Side impact tests are more complex than most of the rear-end and frontal impact tests, and therefore it might be more difficult to reach good repeatability in side impacts sled test. Additional studies to this one are needed to define thresholds for good correlation in terms of ORM values for several types of tests, simulations and purposes within the car safety area.

The ORM evaluation in this study, with shifted and scaled curves, showed a perfect match between ORM values and engineering judgement if the values for okay correlations are above 80%, acceptable correlations between 70 and 80%, not okay correlations between 55 and 70%, and for ORM values below 55% there are no correlations at all due to very dissimilar curves. Although the ORM values match the engineering judgement perfectly for these evaluations, it might be possible that these levels do not correlate for ORM values and engineering judgement for other types of curves and more realistic differences between curves than those formulated in this evaluation. The comparison in which one of the curves was shifted 0.001 s in X resulted in a curve shape ORM value of 79% (Table 1) although these curves are almost identical from an engineers point of view. This ORM value is a result of the curve shape correlation being calculated as a relative error in each time step (Equation 2), and consequently the ORM value will decrease for curves with steep slopes and for curves oscillating around zero in amplitude.

One application of a correlation rating method is to develop an automatic tuning tool that uses the calculated objective correlations as optimization targets for tuning mathematical models to mimic performed tests. Automatic tuning tools have been evaluated on module level for several types of airbags. The ranges of the tuning parameters were predefined to avoid unrealistic values. The models were tuned toward airbag pressure and impactor deceleration measured in several linear impactor or drop tests at different loading configurations. In some cases, also bag pressures measured in static tests have been used for model tuning. Not only the maximum peak correlation, its occurrence time correlation and the curve shape correlation from ORM have been evaluated, but also the Absolute Error Integral Criteria, the Error Integral Criteria, and the Curve Slope Criteria. Different weights on the six criteria have been evaluated in order to find a set of signals that result in models which with high accuracy are rated equally by the correlation tool and experienced engineers. Studies have been conducted to find appropriate weights to the criteria in order to achieve a proper performance of the models during the full test period. Up to date, no weight set-up has been found that works properly for all kind of airbag tests. However, for impactor tests it appears as criteria measuring the curve shape correlation should be more heavily weighted. Investigations of cutting off sections of signals that are known to be inaccurate measured or modelled, such as the deployment peak in an airbag pressure curve, and long sections of signals that are very low in amplitude compared to the peak values, have been made. Both these cuttings have been found beneficial, however these make the automatic tuning tool more complicated to use and require engineering experience. Applying these cuttings and extra weights on the curve correlation criteria, 80% have been identified as an appropriate threshold for good correlation for airbag model to impactor tests. Values between 70 and 80% are acceptable. For some airbag models values above 80% were not reached, likely due to deficiencies in physical representation of relevant parameters in the mathematical models or insufficient information of the test set-up or test repeatability. A prerequisite for automatic tuning is that the criteria used in the optimization must accurately rate the status of models the whole way from poor to good correlation, otherwise the correlation values cannot be used as optimization targets since the inaccuracy for poor and less good correlations may reduce the possibility for the optimization method to find the optimum. Further, in some cases, models have reached the same correlation values, although some were judged as sufficiently good and some were judged as insufficiently good by engineers. This indicates that both the ORM and the ORM with additional criteria need further development for the automatic tuning application. The correlation method needs to be further evaluated on a broad number of test cases in terms of correlation criteria included, weights used, time ranges used, signals and components included, and correlation criteria thresholds. Also, tuning parameters and optimization method for multiple loading conditions must be further evaluated.

Frontal Impacts

Series 1 – Evaluation of Included Signals Not only USNCAP sled test repeatability was evaluated in this part; one pair of USNCAP BiW driver tests and five pairs of EuroNCAP BiW driver and passenger tests were also analysed. For the BiW tests, the set-up of the sets were slightly different from those sets used for the USNCAP sled tests due to different requirements and measured signals. However, the methods of selecting the signals were similar. Hence, the complete ORM values from the different types of tests can be compared. Since the repeatabilities of

these tests also were rated by engineering judgement on the five-level-scale, a reliable set for ORM comparisons of duplicated frontal tests can be recommended. The complete ORM values from the different types of tests are given in Table 2 along with the engineering judgement of the test repeat-ability. These data are also plotted in Figure 3 to Figure 9, along with the linear trend lines and their R^2 values. The R^2 values show the quality of the line fits; the higher the R^2 value is, the better is the fit. Among the seven sets evaluated in this study, Set 7 had the highest R^2 value, 88%. The other sets had R^2 values between 27 and 78%. Hence, the set-up used in Set 7 is the set-up that most likely results in an ORM value that correlates to the engineering judgement. The method of selecting signals, components, and groups, and their weights according to Set 7 is further explained in the Recommendations section.

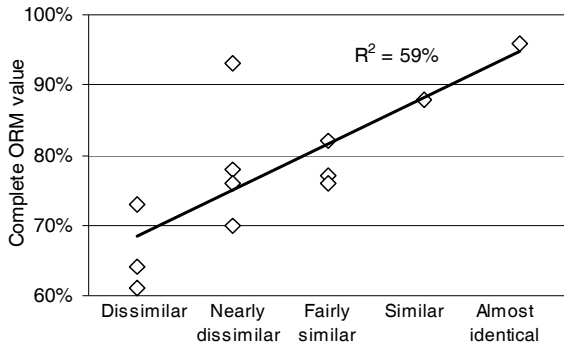

Figure 3. Complete ORM values calculated with signal Set 1 for the twelve compared pairs of tests in Series 1 versus the engineering judgement of the repeatability of each pair. The linear regression shows the trend, and the R^2 value shows how good the fit is.

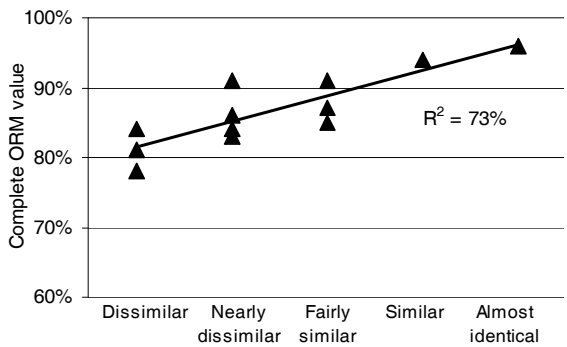

Figure 4. Complete ORM values calculated with signal Set 2 for the twelve compared pairs of tests in Series 1 versus the engineering judgement of the repeatability of each pair. The linear regression shows the trend, and the R^2 value shows how good the fit is.

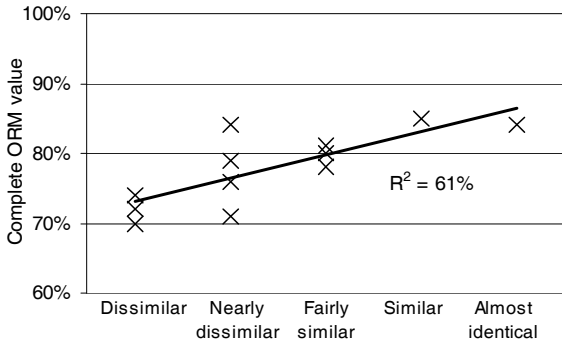

Figure 5. Complete ORM values calculated with signal Set 3 for the twelve compared pairs of tests in Series 1 versus the engineering judgement of the repeatability of each pair. The linear regression shows the trend, and the R^2 value shows how good the fit is.

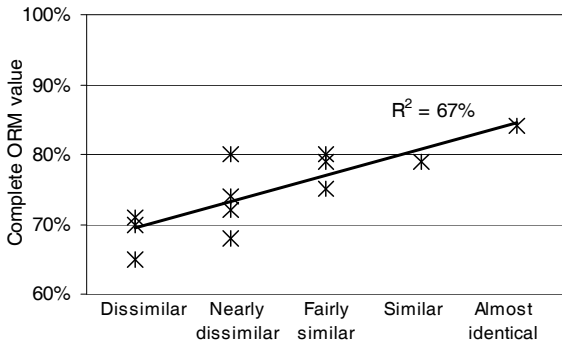

Figure 6. Complete ORM values calculated with signal Set 4 for the twelve compared pairs of tests in Series 1 versus the engineering judgement of the repeatability of each pair. The linear regression shows the trend, and the R^2 value shows how good the fit is.

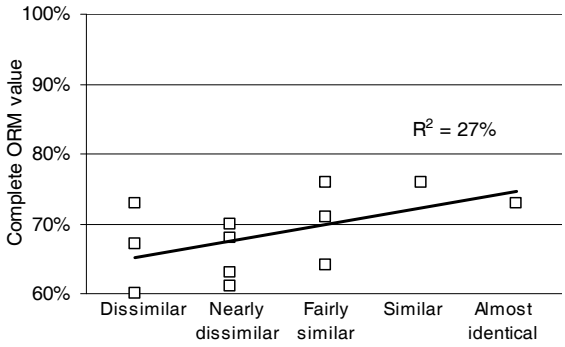

Figure 7. Complete ORM values calculated with signal Set 5 for the twelve compared pairs of tests in Series 1 versus the engineering judgement of the repeatability of each pair. The linear regression shows the trend, and the R^2 value shows how good the fit is.

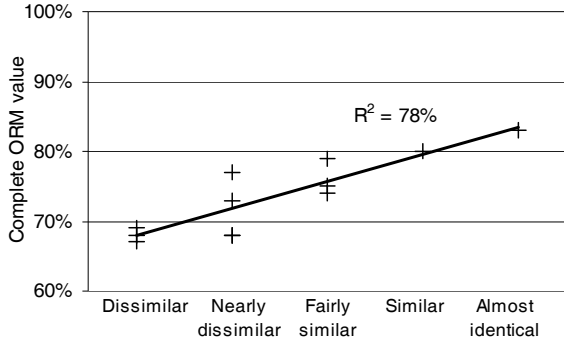

Figure 8. Complete ORM values calculated with signal Set 6 for the twelve compared pairs of tests in Series 1 versus the engineering judgement of the repeatability of each pair. The linear regression shows the trend, and the R^2 value shows how good the fit is.

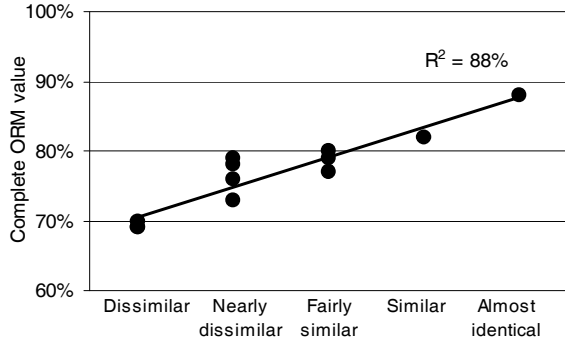

Figure 9. Complete ORM values calculated with signal Set 7 for the twelve compared pairs of tests in Series 1 versus the engineering judgement of the repeatability of each pair. The linear regression shows the trend, and the R^2 value shows how good the fit is

Table 2.
Complete ORM values in percent and engineering judgement for the comparisons in Series 1.

Test / Set-up	USNCAP Sled Tests	USNCAP BiW Tests	EuroNCAP BiW Tests D1	EuroNCAP BiW Tests D2	EuroNCAP BiW Tests D3	EuroNCAP BiW Tests D4	EuroNCAP BiW Tests D5	EuroNCAP BiW Tests P1	EuroNCAP BiW Tests P2	EuroNCAP BiW Tests P3	EuroNCAP BiW Tests P4	EuroNCAP BiW Tests P5
Set 1	96	93	78	73	64	76	77	61	82	70	76	88
Set 2	96	91	86	84	78	83	85	81	91	84	87	94
Set 3	84	71	76	70	74	79	80	72	78	84	81	85
Set 4	84	72	80	71	70	74	80	65	79	68	75	79
Set 5	73	63	68	73	67	70	71	60	64	61	76	76
Set 6	83	68	77	68	69	73	79	67	74	68	75	80
Set 7	88	78	79	69	70	76	79	69	80	73	77	82
Eng. judge.	Almost identical	Nearly dissimilar	Nearly dissimilar	Dissimilar	Dissimilar	Nearly dissimilar	Fairly similar	Dissimilar	Fairly similar	Nearly dissimilar	Fairly similar	Similar

<u>Series 2 – Correlations between Sled Tests</u> On the whole, the repeatability ORM values were high for the comparisons conducted for the tests in Series 2. Visual inspections of the tests by experienced test engineers assessed that the EuroNCAP sled tests were almost identical and the USNCAP sled tests were similar. Further, all signal correlations were rated visually in three grades: good/either/poor. Based on these grades, thresholds for ORM values for good and poor correlation can be recommended. Peak value correlations that were judged as good mostly had ORM values above 90%, and those judged as poor mostly had ORM values below 80%. Values between 80 and 90% were either good or poor, and it is recommended to assess these individually. For peak value occurrence time correlations ORM values above 90% are almost always good; values below 90% should be assessed individually. There are two not too rare reasons to low peak value occurrence time ORM values besides the case when the peaks occur with a long time apart. First, ORM values can be confusing for times early in the crash event since the ORM value is a ratio between the first and the last of the two compared times. Second, low peak time occurrence ORM values can be a result of double peaks with almost equal amplitudes, but the maximum peak in opposite order; this indicates a poor correlation by engineering judgement only if the peak occurrence time is critical. The curve shape correlations generally results in lower ORM values than scalar correlations. Curve shape correlation ORM values above 75% were almost always judged as good, while values below 60% were judged as poor. Curve correlations ORM values between 60 and 75% are recommended to be evaluated individually. Consequently, comparisons of sets with significant signals that contain about 30% curve shape correlations and 70% peak value and their occurrence time correlations have good correlations if the complete ORM values are above circa 80%. Independent of the complete ORM value, it is recommended to visually inspect all curves and corresponding component ORM values to uncover confusions. A drawback with the ORM is that the curve correlation (Equation 2) punishes signals with long intervals of amplitudes close to zero and signals that cross through the time axis numerous times unfairly hard. Consequently, the complete ORM value can be a bit too low compared to the grade given by engineering judgement. Further, the

complete ORM value is a weighted mean which may hide a few ORM values that are lower than wanted, an inspection will identify these. The crash pulse should preferable be analysed separately; ORM values above 90% for crash pulse shape corresponds to almost identical curves.

Series 3 – Correlations between Sled Tests The five tests in Series 3 were compared both visually and by aid of the ORM. The visual inspection of tests #1, #2, and #3, which were intended to be identical, showed that #1 versus #2 and #1 versus #3 were nearly dissimilar and the corresponding complete ORM values were 76 and 77%, respectively. The reason for the poor correlations of these tests is most likely that the pulse differed a lot for test #1; the corresponding crash pulse curve shape correlations were only 70 and 71%. Sled tests #2 and #3 were judged as similar; the corresponding complete ORM value was 86% and the pulse shape correlation was 95%. Sled test #4 versus #5 was fairly similar; the corresponding complete ORM value was 81% and the crash pulse shape correlation was 93%. For these four comparisons, the amplitudes of the component ORM values are given in Figure 10 to Figure 13. In each figure, the ORM components are sorted in amplitude, and the three patterns on the bars represent peak ORM values, peak occurrence time ORM values, and curve shape ORM values. Comparing Figure 10 and Figure 11 with Figure 12 and Figure 13, it can be seen that the ORM values in general are higher in the latter two figures than in the former two; as indicated by the complete ORM values and in line with the engineering judgements. Using the thresholds for good (≥90% for scalars and ≥75% for curve shapes) and poor (<80% for scalars and <60% for curve shapes), one can see that the two pairs of tests rated as nearly dissimilar only have 56 and 59% of the scalars rated as good, and only 22 and 28% of the curve shapes rated as good, while the two pairs of tests judged as nearly similar and similar have 75 and 78% of the scalars and 67 and 83% of the curve shapes rated as good. Hence, the tests compared in Figure 12 and Figure 13 have both about the same amount of scalar components rated as good but the latter has less curve shapes rated as good than the former. This partly explains why the complete ORM values and engineering judgement differed for these comparisons. Nevertheless, most component ORM values are good in Figure 13 making these tests sufficiently repeatable for most purposes. By plotting the bars in order, one can easily find out if just a few components cause a low complete ORM value, or if all components are low and therefore aggregate to a low complete ORM value. This kind of plot is also useful in order to find out which signals and components that may need to be further analysed.

In order to get a feeling for the ORM values, Figure 15 to Figure 19 contain the dummy readings from sled test #1 to #3 and the Madymo simulation in Series 3 and the corresponding ORM values.

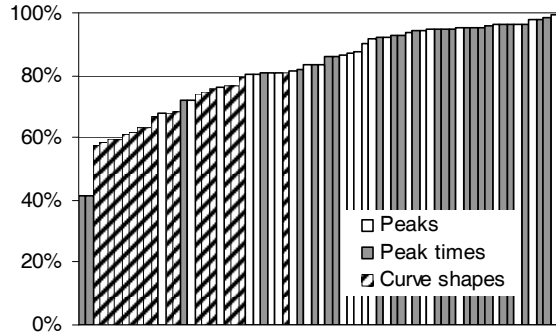

Figure 10. All component ORM values for comparison #1 versus #2 in Series 3. The ORM values are sorted in amplitude and the different patterns show the kind of component compared. The complete ORM value is 76%, and the crash pulse curve shape correlation is 71%.

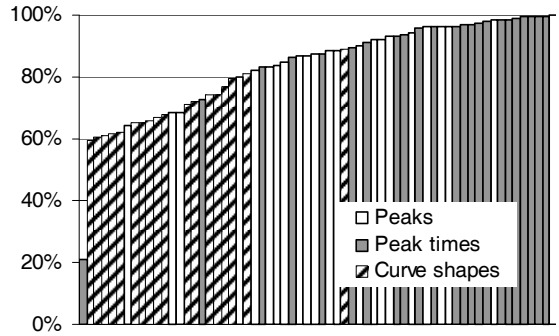

Figure 11. All component ORM values for comparison #1 versus #3 in Series 3. The ORM values are sorted in amplitude and the different patterns show the kind of component compared. The complete ORM value is 77%, and the crash pulse curve shape correlation is 70%.

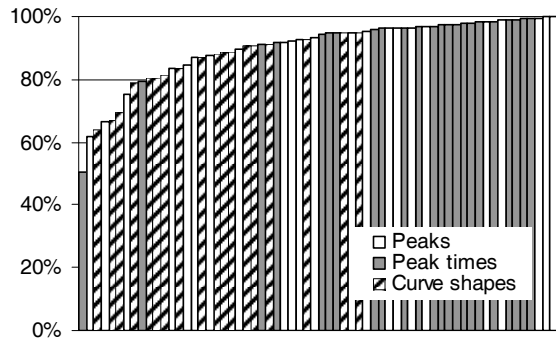

Figure 12. All component ORM values for comparison #2 versus #3 in Series 3. The ORM values are sorted in amplitude and the different patterns show the kind of component compared. The complete ORM value is 86%, and the crash pulse curve shape correlation is 95%.

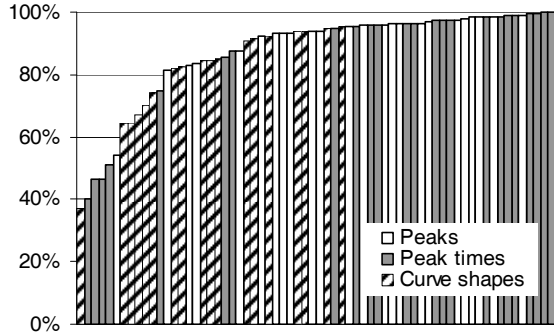

Figure 13. All component ORM values for comparison #4 versus #5 in Series 3. The ORM values are sorted in amplitude and the different patterns show the kind of component compared. The complete ORM value is 81%, and the crash pulse curve shape correlation is 93%.

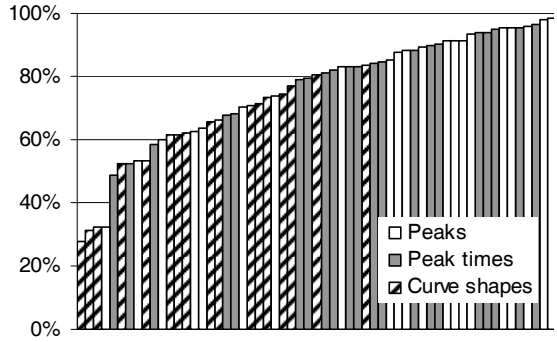

Figure 14. All component ORM values for comparison #3 in Series 3 vs. the Madymo simulation. The ORM values are sorted in amplitude and the different patterns show the kind of component compared. The complete ORM value is 69%, and the crash pulse curve shape correlation is 91%.

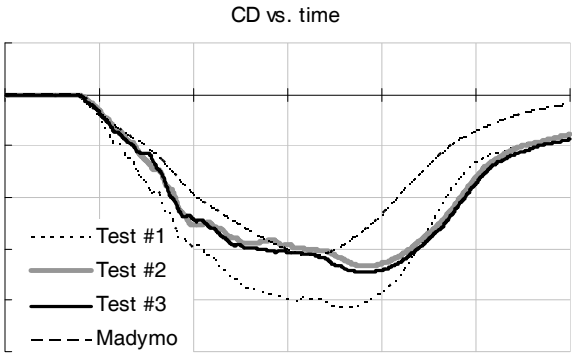

	Max Peak	Max Peak Time	Min Peak	Min Peak Time	Curve Shape
#1 vs. #2	-	-	83	93	81
#2 vs. #3	-	-	96	98	95
Madymo vs. #3	-	-	91	83	66

Figure 15. Chest deflection curves for sled test #1 to #3 and Madymo simulation and ORM values for the comparisons #1 versus #3 (different pulses), #2 versus #3, and Madymo simulation versus #3.

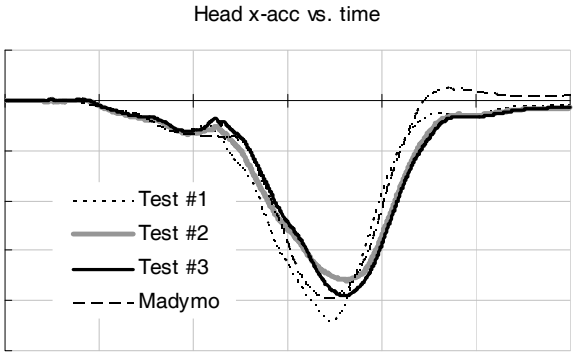

	Max Peak	Max Peak Time	Min Peak	Min Peak Time	Curve Shape
#1 vs. #2	-	-	88	97	72
#2 vs. #3	-	-	92	99	89
Madymo vs. #3	-	-	98	96	66

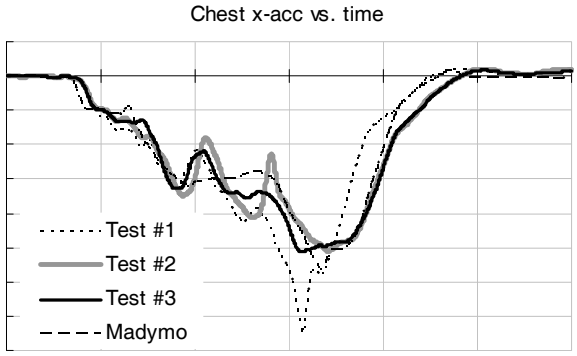

	Max Peak	Max Peak Time	Min Peak	Min Peak Time	Curve Shape
#1 vs. #2	-	-	68	100	71
#2 vs. #3	-	-	99	92	88
Madymo vs. #3	-	-	91	94	77

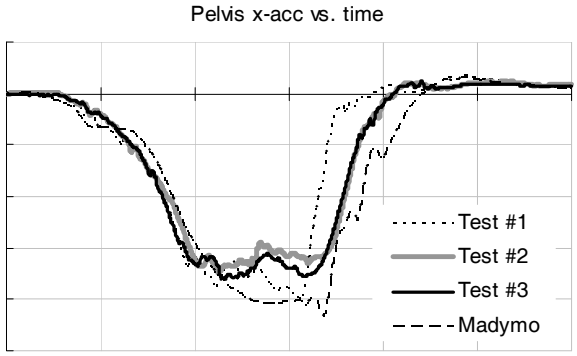

	Max Peak	Max Peak Time	Min Peak	Min Peak Time	Curve Shape
#1 vs. #2	-	-	90	73	68
#2 vs. #3	-	-	96	99	91
Madymo vs. #3	-	-	83	68	71

Figure 16. Head, chest, and pelvis x-acceleration curves for sled test #1 to #3 and Madymo simulation and ORM values for the comparisons #1 versus #3 (different pulses), #2 versus #3, and Madymo simulation versus #3.

Head z-acc vs. time

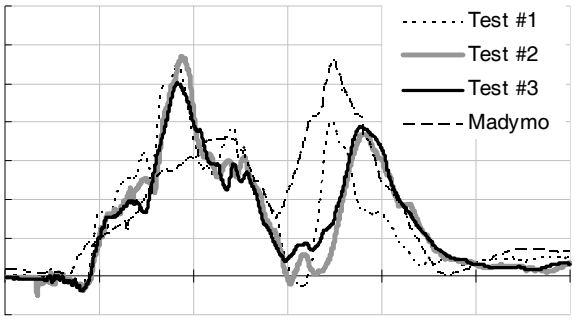

	Max Peak	Max Peak Time	Min Peak	Min Peak Time	Curve Shape
#1 vs. #2	92	99	-	-	61
#2 vs. #3	88	98	-	-	79
Madymo vs. #3	89	52	-	-	53

Chest z-acc vs. time

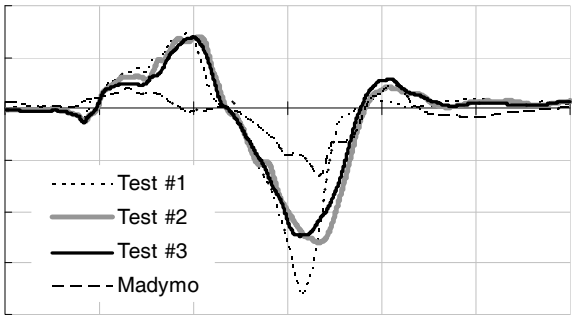

	Max Peak	Max Peak Time	Min Peak	Min Peak Time	Curve Shape
#1 vs. #2	94	97	68	99	61
#2 vs. #3	100	96	95	94	80
Madymo vs. #3	33	49	53	94	31

Pelvis z-acc vs. time

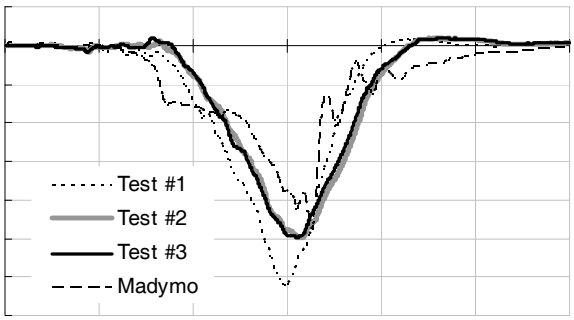

	Max Peak	Max Peak Time	Min Peak	Min Peak Time	Curve Shape
#1 vs. #2	-	-	80	96	65
#2 vs. #3	-	-	100	98	89
Madymo vs. #3	-	-	96	95	52

Figure 17. Head, chest, and pelvis z-acceleration curves for sled test #1 to #3 and Madymo simulation and ORM values for the comparisons #1 versus #3 (different pulses), #2 versus #3, and Madymo simulation versus #3.

Upper Neck Fx vs. time

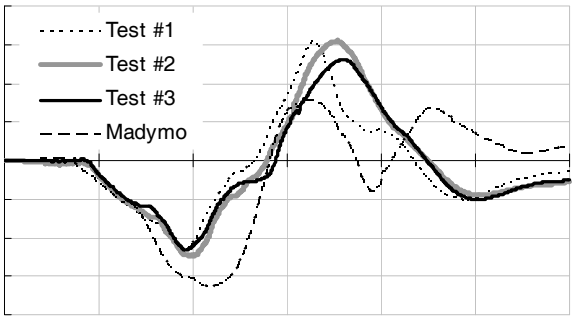

	Max Peak	Max Peak Time	Min Peak	Min Peak Time	Curve Shape
#1 vs. #2	85	91	98	98	60
#2 vs. #3	84	98	93	96	81
Madymo vs. #3	60	90	70	88	32

Upper Neck Fz vs. time

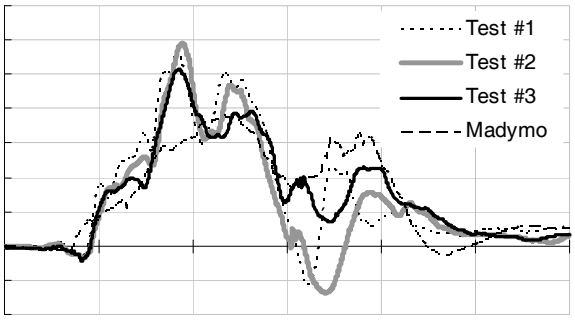

	Max Peak	Max Peak Time	Min Peak	Min Peak Time	Curve Shape
#1 vs. #2	92	100	-	-	61
#2 vs. #3	87	98	-	-	64
Madymo vs. #3	74	79	-	-	62

Upper Neck My vs. time

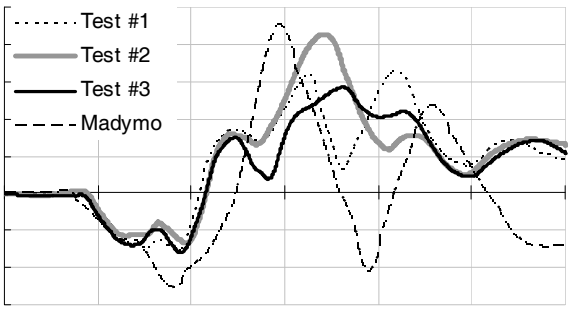

	Max Peak	Max Peak Time	Min Peak	Min Peak Time	Curve Shape
#1 vs. #2	87	86	97	99	65
#2 vs. #3	66	95	83	97	70
Madymo vs. #3	63	81	63	96	28

Figure 18. Upper neck F_x, F_z, and M_y curves for sled test #1 to #3 and Madymo simulation and ORM values for the comparisons #1 versus #3 (different pulses), #2 versus #3, and Madymo simulation versus #3.

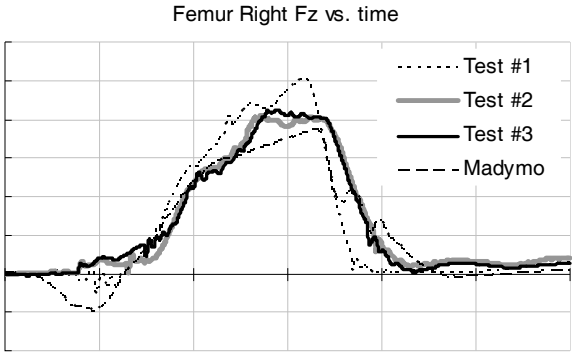

	Max Peak	Max Peak Time	Min Peak	Min Peak Time	Curve Shape
#1 vs. #2	-	-	84	88	62
#2 vs. #3	-	-	97	98	84
Madymo vs. #3	-	-	88	84	61

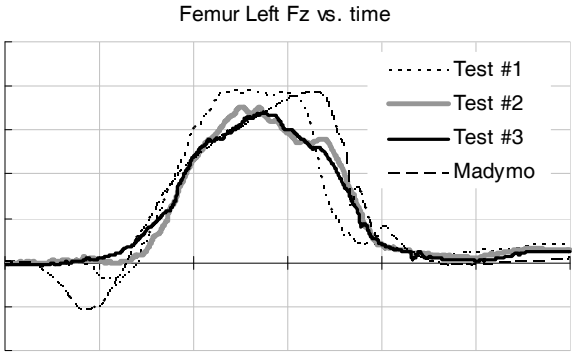

	Max Peak	Max Peak Time	Min Peak	Min Peak Time	Curve Shape
#1 vs. #2	-	-	87	96	67
#2 vs. #3	-	-	96	91	81
Madymo vs. #3	-	-	88	84	62

Figure 19. Femur right left F_z curves for sled test #1 to #3 and Madymo simulation and ORM values for the comparisons #1 versus #3 (different pulses), #2 versus #3, and Madymo simulation versus #3.

Series 2 and 3 – Correlations between Simulations and Sled Tests Although the ORM signal sets differed somewhat between the predictability and the repeatability assessments, these ORM values were compared. In general, and as expected, the Madymo models have lower predictability ORM values than the corresponding sled test repeatability ORM values. Nevertheless, the Madymo models were found to be useful. The Madymo models average peak value prediction ranged from 81 to 88%, the average peak value time occurrence prediction ranged from 81 to 95%, and the average curve shape prediction ranged from 60 to 69%. Corresponding values for the sled test repeatabilities are 91 to 94%, 95 to 98%, and 77 to 85%. The Madymo model of the EuroNCAP system in Series 2 predicts the three EuroNCAP tests with 75 to 78% and the corresponding sled test repeatability ORM values ranged from 81 to 86%. The Madymo model of the USNCAP system predicts both of the two USNCAP tests in Series 2 with 75% and the corresponding sled test repeatability was 87%. The Madymo model of the USNCAP sled tests with the Hybrid III 50%-ile in Series 3 predicts test #2 and #3 with 68 and 69% and the corresponding sled test repeatability was 86%. From a simulation engineering point of view, the Madymo models verified in this study were assessed as useful for product development and evaluation. Hence, Madymo models that reached about 80% or higher of the sled test repeatability ORM values were found to be useful. Nevertheless, higher ORM values are needed to fully predict tests with simulations. Depending on the purpose of the models, additional weight on the curve shapes can result in better understanding if the models predict trends adequately or not in cases when the peak values are poorly predicted. In order to attain useful ORM values of predictability, it is important to include mainly those signals which will be used in coming simulations; otherwise the ORM values will be confused by less predictive and irrelevant signals. Further, the recommended ORM values for models may differ depending on the type of test and system used, but also on modelling technique (MBS or FEM), and the purpose of the simulation.

Side Impacts

The ORM was used to guide in a side impact project. Both sled tests and full scale crash test were performed, and mathematical models were built up to predict the tests and improve the EuroNCAP results. The complete ORM values for the mathematical model predictabilities of the sled tests and the full scale crash tests, as well as the sled test predictabilities of the full scale crash tests, were rather low. Therefore, the dummy signals were divided into subgroups that made it possible to focus on those signals predominantly important for test purpose. Thus, it could be assessed that these signals were sufficiently well predicted. The ORM was also used to show that improvements of the safety components influenced the dummy performance by comparing ORM values from tests with and without the improved system to the repeatability values of truly duplicated tests. By analysing the signals individually, it was possible to find out which of the signals that were highly, moderately and insignificantly influenced by the change in the safety components. Overall, the ORM values assisted in the communication with the customer during this project.

The mathematical models of the airbags used were normally tuned to mimic two configurations of static tests and two configurations of dynamic test, and each configuration were repeated at least once. The mathematical models in the side impact project were tuned manually, and the ORM was applied afterwards to assess their predictabilities. For the airbag presented in the side impact part, the test repeatabilities were in all cases but one very good. Good

test repeatability and representative tests are crucial for tuning a mathematical model into an accurate model of a real airbag. In case of a low test repeatability ORM value, it is important to find out if the low value was caused by a test failure, a result of any ORM shortcomings, or just a spread in the tested components. If the low value was caused by a test failure, the mathematical model can be tuned to mimic just the accurate test. If the low value was caused by a shortcoming in the ORM and the signals correlations are judged better than the ORM value indicates, one may cut off sections of the signals or change the weights to better rate the repeatability. Otherwise, the mathematical model must be tuned to mimic both tests and will most likely return predictability ORM values lower than the repeatability for the corresponding tests.

CONCLUSIONS

ORM is a useful tool, especially for test repeatability and reproducibility assessments, although it should be used with care and knowledge. For all ORM correlations performed, it is recommended to check the included signals and components in order to identify scalar or curves correlations that might have been too low rated due to shortcomings of the ORM. The ORM allows for agreement, in advance, on a quality level for tests and mathematical models. Beneficial is that the ORM not only compares peak values but also curve shapes. Furthermore, the ORM compares two tests; many methods require several tests and that is normally not available in daily work.

This study shows that high ORM values correspond to good correlations, but for a few cases good correlations result in somewhat too low ORM values. For curve correlations rated as poor by ORM, the ORM does not sufficiently discriminate between curves that are poor but useful and poor but useless. This might be a drawback for simulation model predictability assessments, since the correlation level can be rather low although the models fulfil their purposes.

RECOMMENDATIONS

The usefulness of an ORM correlation is highly depending on the set of signals and components used. In this study, the Set 7 correlated to engineering judgement most accurately. The method of selecting signals and components according to Set 7 for a system correlation assessment is in detail described in A. to D. Normally, all signals and components should be compared up to the time when the crash is over. An example of a signal set selected with this method can be found in Table 3.

A. *Crash pulse group* Compare the crash pulse shape separately; it should not be included in the complete system comparison. Hence, set the group weight to zero.
B. *Criteria group* Criteria may be included in the complete ORM value, or analysed separately depending of the aim of the comparison. When the criteria are excluded in the complete ORM value, the comparison will focus more on overall repeatability, reproducibility or predictability. If the criteria group is excluded in the complete ORM value, set the group weight to zero. Otherwise, let the weight of this group be equal to the number of criteria.
C. *Dummy group* Include all kinematics and load cells signals acting in the motion plane, and avoid resultant signals. Signals in other directions than the motion plane are normally much lower and will most likely confuse the findings with less important data if they are included. For all included signals, include both minimum and maximum peaks if these are significant and not enormously different in amplitudes; otherwise include only the highest peak. For all included peaks, also include their occurrence times. Include the curve shape correlation for all included signals. For each included signal, set the total weight of the peak or peaks to 1, set also the total weight of the peak occurrence time or times to 1, and set the curve shape correlation weight to 1. Let the weight of the dummy group be equal to the number of included signals. In order to better focus on different parts of the dummy, the dummy group can be divided into subgroups.
D. *Safety group* Include all signals from the safety equipment that show how these parts perform. For all included signals, include both minimum and maximum peaks if these are significant and not enormously different in amplitudes; otherwise include only the highest peak. For all included peaks, also include their occurrence times. Include the curve shape correlation for all included signals. For each included signal, set the total weight of the peak or peaks to 1, set also the total weight of the peak occurrence time or times to 1, and set the curve shape correlation weight to 1. Let the weight of the safety group be equal to the number of included signals.

On signal level, good correlations are predominately associated with ORM values of 90% or above for peak value and peak value occurrence time correlations, and with ORM values of 75% or above for curve shape correlations. For extremely good curve correlation, as wanted for crash pulses, 90% is a preferable threshold. Peak value correlation ORM values below 80% and curve shape correlation ORM values below 60% are generally associated with poor correlation or no correlation at all.

Using an appropriate set of signals, in which about one third of the components are curve shapes, the proposal of ORM value representing good repeatability for frontal sled tests is 80% or above. Sled

test reproducibility, and more complex frontal tests, such as BiW and full scale crash tests, should be rated as good with a bit lower complete ORM values. The requirement on the predictability ORM values of a mathematical system model should be lower than the corresponding repeatability ORM values.

REFERENCES

[1] Eriksson, L., Zellmer, H. 2007 "Assessing the BioRID II Repeatability and Reproducibility by Applying the Objective Rating Method (ORM) on Rear-End Sled Tests" In proceedings of the 20th International Technical Conference of the Enhanced Safety of Vehicles (June 18-21, Lyon, France) Paper No. 07-0201-O.

[2] Hovenga, P. E., Spit, H. H., Uijldert, M., Dalenoort, A. M. 2005 "Improved Prediction of Hybrid-III Injury Values using Advanced Multibody Techniques and Objective Rating" In proceedings of the SAE 2005 World Congress & Exhibition (April, Detroit, MI, USA) Paper No. 05AE-222.

[3] Eriksson, L. 2008 "Repeatability and reproducibility ORM values for the BioRID II criteria and the dynamic assessment points used in the Euro NCAP rear-end testing protocol" In proceedings of the 2nd International Conference of Whiplash – Neck Pain in Car Crashes (Erding, Germany, Nov. 18-19). TÜV SÜD Akademie, Germany.

Table 3
Signals and weights used for a USNACP frontal sled test according to the selection method proposed in Recommendations section.

Group	W_{group}	Signal	Comp.	$W_{scalar/shape}$
Crash Pulse	0	Sled x-acc	Curve shape	1
Criteria	0	HIC36	Scalar	1
		Chest 3ms	Scalar	1
Dummy	12	Head x-acc	Min peak	1
			Min peak time	1
			Curve shape	1
		Head z-acc	Max peak	1
			Max peak time	1
			Curve shape	1
		Chest x-acc	Min peak	1
			Min peak time	1
			Curve shape	1
		Chest z-acc	Max peak	0.5
			Max peak time	0.5
			Min peak	0.5
			Min peak time	0.5
			Curve shape	1
		Pelvis x-acc	Min peak	1
			Min peak time	1
			Curve shape	1
		Pelvis z-acc	Min peak	1
			Min peak time	1
			Curve shape	1
		Chest defl.	Max peak	1
			Max peak time	1
			Curve shape	1
		Upper Neck F_x	Max peak	0.5
			Max peak time	0.5
			Min peak	0.5
			Min peak time	0.5
			Curve shape	1
		Upper Neck F_z	Max peak	1
			Max peak time	1
			Curve shape	1
		Upper Neck M_y	Max peak	0.5
			Max peak time	0.5
			Min peak	0.5
			Min peak time	0.5
			Curve shape	1
		Femur Left	Max peak	0.5
			Max peak time	0.5
			Min peak	0.5
			Min peak time	0.5
			Curve shape	1
		Femur Right	Max peak	0.5
			Max peak time	0.5
			Min peak	0.5
			Min peak time	0.5
			Curve shape	1
Safety	3	Webbing disp.	Max peak	0.5
			Max peak time	0.5
			Min peak	0.5
			Min peak time	0.5
			Curve shape	1
		Belt Force B3	Max peak	1
			Max peak time	1
			Curve shape	1
		Belt Force B6	Max peak	1
			Max peak time	1
			Curve shape	1

DRIVER BEHAVIOR MODELING USING HYBRID DYNAMIC SYSTEMS FOR 'DRIVER-AWARE' ACTIVE VEHICLE SAFETY

Pinar Boyraz, Amardeep Sathyanarayana, John H.L. Hansen
Erik Jonsson School of Engineering and Computer Science
University of Texas at Dallas
Richardson, TX, USA

ABSTRACT

Modern safety systems are transforming vehicles from human-controlled passive devices into human-centric intelligent/ active systems. There is a wide range of systems from fully autonomous vehicles to human-augmented control devices which have emerged in this field. In current trends, co-operative active systems have the driver in the decision and control processes are favored for their 'human-centric' approach. However, these systems pose a challenge in the design process since obtaining reliable human behavior models are difficult due to the complex nature of driving task in a dynamic traffic environment. From a control theory perspective, driving can be seen as a combination of continuous control segments combined with a discrete decision process. In this study, we will model driver behavior utilizing Hybrid Dynamic Systems (HDS) combining stochastic modeling tools (such as Hidden Markov Models) with control theoretic models. A subset of CAN-Bus and video channels from a demographically balanced UTDrive Corpus containing video (2 channels: driver and road scene), audio, and CAN-Bus signals of realistic driving sessions for 77 drivers are used to verify HDS models of lateral and longitudinal control behaviour. The model is used to suggest 'driver-aware' active safety system capable of assisting the driver in several lateral control tasks; lane-keeping, curve-negotiation and lane changing.

INTRODUCTION

Understanding, analyzing and modeling human driver behaviour in a realistic way is extremely important in enhancing the safety of the vehicles. In a study supported by NHTSA, it was found that driver error was the major contributor in more than 90% of the crashes examined **[1].** Cooperative driver assisting systems (DAS) or human-centric active vehicle safety (AVS) presents an opportunity to prevent/avoid some of these accidents. These promising technologies can be realized with an associated cost in research and implementation trials. The difficulty arises because of the co-operation requirement with human and the human driving behavior is a poorly understood subject. The dynamics of driving come from three sources: driver, vehicle and the environment. Although, several systems exist to improve the vehicle dynamics and handling, the driver behaviour and the role of the environment remained the overlooked components of the safety problem until now. The vehicle component was the first one to be examined and improved thanks to precise non-linear, continuous vehicle models and numerical simulations. The uncertain, non-stationary, highly dynamic, stochastic or discrete event-driven characteristics of driving comes mainly from human driver and traffic context imposing on the driver to react in a certain way. These characteristics of driving are more difficult to model, understand and control and they conceal the underlying cause of most of the accidents. Therefore, future active safety systems need to take driver behaviour and traffic context into account for efficient accident avoidance/ prevention. In other words, AVS or DAS should be 'driver-aware' and 'context-aware'. The context awareness can be achieved by monitoring and analyzing the micro-traffic environment around the host-vehicle. The sub-systems of such a system may include a computer vision system for lane mark, vehicle and pedestrian detection and tracking together with road sign recognition. In recent years, such systems are designed and reported with great prospects of being beneficial **[2, 3].** For an example in context-aware systems, one can refer to **[4].** In this paper, the focus is driver-awareness to be able to design human-

centric AVS and adaptive DAS with particular interest in lateral control.

The paper is organized in the following way. First, a critical survey of driver behaviour modeling approaches is given identifying the need for a hybrid realistic model specifically designed for the use of DAS or AVS development. In this section, also the driver models are categorized to give more insight into the problem of which model is more appropriate for what type of applications. Next the main frame of the proposed driver model is presented together with the theoretical methods and implications from human factors engineering studies. It is extremely important that the model delivers both a theoretical framework which is mathematically tractable and an explanation of physical and cognitive processes involved in control strategy of human driver. The proposed model is divided into lateral and longitudinal parts; however, these two models are coupled and the full model is given next. After construction of the theoretical framework supported with experimental observations from previous studies the model is validated using driving data which is collected in real traffic environment. Finally, the advantages and limitations of the proposed model are presented in the conclusion section.

Critical Survey of Driver Modeling Approaches

Driver models are needed for different purposes from assessing vehicle dynamics to monitoring driver status or just simply to better understand the underlying dynamics in driver behaviour. In addition to several types of need for driver models, each related research field emphasizes a different aspect of the driver (i.e. cognition, perception, processing reaction, control). Driver modeling approaches can be roughly divided into following groups: human factors, control theoretic, stochastic/ non-linear and hybrid models. A schematic of driver modeling approaches is given in Fig.1.

It is noticeable that especially lateral control has been modeled by control theoretic approach due to its continuous characteristics. An example of this type of driver model can be found in [5] employing control theoretic approaches for lateral control behaviour. This model includes driver's delays, feedback in form of lateral position error, and neuro-muscular response taken from an earlier work on flight-pilot modeling studies [6].

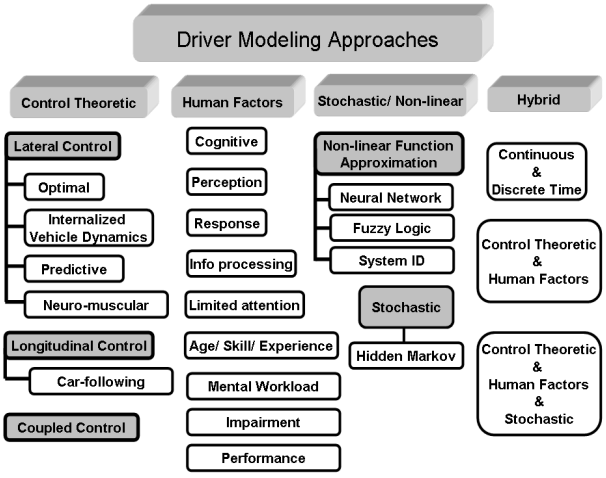

Figure1. A schematic grouping of driver modeling approaches

Other noticeable and widely known control theoretic models for lateral control can be listed as McRuer's model [7] containing anticipatory, compensatory and precognitive control for better representation, and MacAdam's optimal preview control model [8]. The common property of these models is that all of them agree with cross-over model [9] which can explain single loop manual tasks performed by humans. The advantage of control theoretic models is that they give a physical/causal relationship between the input and output variables. In this aspect, the control theoretic models may give insight into driver behaviour. Although some of them ignore the non-linearity, they provide a sound mathematical framework in analyzing driver behaviour in control level. However useful they may be, it should be noted though that most of the control theoretic models are designed to be used in improving vehicle dynamics and handling quality, but not for explaining driver behaviour or design of co-operative systems. These driver models have low fidelity in reproducing driver control commands that have similar characteristics to a real driver in time-domain. The main reason of this infidelity is that these models are designed for tracking the center of the lane or road-median almost perfectly, whereas a real driver would deviate from the median more as demonstrated by [10]. The human driver allows the lateral position error to build up until it reaches a threshold that driver perceives it as a deviation and makes correction. This is known as

complacency, and it is also related to the fact that most of the sensory input that driver uses is not instant measurement of the lateral position but visual cues and vestibular feedback. In order to perceive and process this feedback takes time and it is not instantly used by the driver but delayed. A similar behaviour is observed also in longitudinal control while car-following and was taken into account in Lubashewsky's rational driver model [11]. Since the existing control theoretic models cannot account for complacency, [10] used driver simulator data to identify lateral control model of the driver using system identification tools and ARX models. In [12] driver steering model was identified with particular interest in structured and unstructured model uncertainty. Their work is important as they imply that the structured uncertainty can be used to monitor driver and use adaptive control framework to address the risk from driver performance deterioration whereas the unstructured certainty coming from unmodelled nonlinearity can be addressed by robust control. The non-stationary, uncertain and non-linear nature of driver behaviour was understood by other researchers too. In [13] cascaded Neural Networks (NN) are used with some flexibility employing Extended Kalman Filters (EKF) for update and variable activation in newly added neuron layers. HMM is used to measure the stochastic similarity [14] between the model output and real driver data. This measure is reported to be better than mean square error since the nature of driving is stochastic and we should be looking for main trends in the data not the exact match in numerical sense. In fact, Markov Chains were used to sequence a bank of Kalman Filters for predicting driver actions using preparatory input actions [15]. Hidden Markov Models (HMM) were used to learn human action and transfer human skills for tele-robotics applications [16]. HMMs has later proved to be a very convenient tool in modeling driving control inputs or observed vehicle dynamics and it is widely used to model driver behaviour in several frameworks. In [17] HMM framework is used to recognize different driver maneuvers and [18] used a similar framework for a top to bottom approach in search for 'drivermes', the meaningful smallest unit of driving signals. In our previous studies, HMMs were used to recognize maneuvers and detect the driver distraction or driver faults using a hierarchical approach [19, 20]. Although HMMs are very powerful and can reproduce the driver behaviour with high stochastic fidelity, we lack the capability of explaining the physical/causal meaning of the resulting models.

In addition to mathematical approaches a large group of driver models are derived in human factor engineering. These models consider cognitive, perceptual, and neuro-muscular limitations of human. These models provide very important insight into driver behaviour especially explaining some of the uncertainty, delay and non-linear characteristics. In addition to this, the control theoretic and stochastic models tend to use measured (i.e. observable) data and they often stay in the control level modeling. The tactical and strategic levels in Michon's hierarchical model [21] cannot be modeled with control theoretic or stochastic approaches. [22] proposed ACT-R cognitive model of the driver modeling the information processing and inherent delays of the human cognitive system. As it can be seen, the models derived from human factor engineering are very useful; however, they do not represent a full driver model. Therefore, combined model structures including control aspects, stochastic processes and cognitive capabilities are proposed. These models can be described as 'hybrid' models. This approach is relatively new and very promising for obtaining comprehensive models. For example, [23] described human perception process by a discrete event technique the execution part is modeled by general predictive controllers and the velocity control is represented by a finite state machine to reveal its discontinuous control dynamics. In [24], researchers used a controller switching model for modeling collision avoidance maneuver employing piecewise polynomials. Furthermore [25] used similar approach for modeling vehicle following task dividing the car following control into four different modes. Another model using switching control is used by [26] employing simple control laws and defining the switching rule by a knowledge base.

In this paper, a hybrid driver model combining stochastic, control theoretic and human factor approaches is proposed. The main aim is to obtain a comprehensive driver model including all available knowledge and state-of-art methods in driver modeling for development of human-centric active safety.

Proposed Driver Model

The proposed driver model includes a stochastic longitudinal velocity control model coupled with a realistic control theoretic lateral model based on [5]. Although the lateral model is based on a limited

control theoretic model the complacency phenomena is represented by delaying the position feedback to represent the human limitation. The vehicle model used in Hess model is updated by the velocity supplied by longitudinal model therefore coupling the control strategies. This approach is more realistic than assuming the vehicle longitudinal velocity constant in the lateral model. The main aim of the model is to obtain a driver-adaptable (tunable) and realistic lateral control model coupled with longitudinal dynamics to use in DAS and AVS development. In next sections longitudinal, lateral control strategies are given and finally the full driver model is explained.

Longitudinal Control Strategy

Longitudinal control strategy of driver is inherently discontinuous since the control is achieved by changing between gas and brake at discrete times. In addition to this, the underlying control rule cannot be easily revealed without including the micro-traffic context (i.e. car following, congestion or free driving). For this reason a stochastic modeling approach such as HMM can help us learn the velocity control of driver from observations.

HMM is a naturally suitable tool to model driver behavior for the following reasons:

- HMMs can model the stochastic nature of the driving behavior, providing sufficient statistical smoothing while offering effective temporal modeling,
- The variations in the driving signals across the drivers can be modeled (driver identification) or suppressed (driver-independent route models) according to the requirements of the desired task.

HMMs can be characterised by:

(1) A set of distinct states $S=\{S_i\}$ with q_t denoting a state at time t, with number N

(2) The initial state distribution $\Pi=\{\Pi_i\}$

(3) The state transition probability distribution $A=\{a_{ij}\}$

(4) Each state can produce one of M distinct observation symbols from the set $V=\{V_i\}$

(5)The observation probability distribution function in state j, B_j

Therefore, HMMs can be written in the form of a vector $\lambda=\{N,M,A,B,\Pi\}$. For further information, readers should refer to [27].

In modelling velocity control behaviour of human driver by HMM we used a topology seen in Figure 2. This model represents three states in velocity control: constant, increasing and decreasing. The transitions between any of the two the states out of three are possible and a dynamic variable indicated as *d* can be retrieved as the model stays at one state in certain time. These waiting times can account for certain control strategy in speed control adopted and the state transition probabilities give insight into how several control strategies are switched to obtain a plausible speed control. The emission output of each state is represented by a continuous function to model the speed profile with parameters of a line.

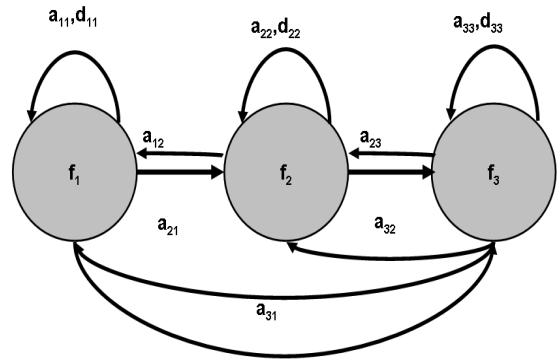

Figure 2. HMM topology for velocity control

Lateral Control Strategy

The lateral control strategy of driver is modeled using a modified control theoretic model based on Hess's work [5]. Two improvements to this model are:

(1) introduction of a dead zone which filters out the lateral position errors below a certain threshold band accounting for complacency of drivers

(2) replacement of the constant velocity LTI model of lateral vehicle dynamics model with LTV model updating the speed and recalculating the model with the inputs from longitudinal velocity model.

The modified lateral driver model and complacency term is shown in Figure 3. Some of the constants seen in the block diagram of lateral driver model are taken from [5], however, the tuning parameters of ω_c (cross over frequency) and time constants T_1, T_2 and T_3 are explored in a range to better fit the model to real driver steering signals. In addition to this, the complacency term dead-zone band changes from one driver to another. Some drivers are more sensitive and correct the errors more often while others let the

lateral position error to accumulate. This band can be related to experience and one's confidence in their driving skills.

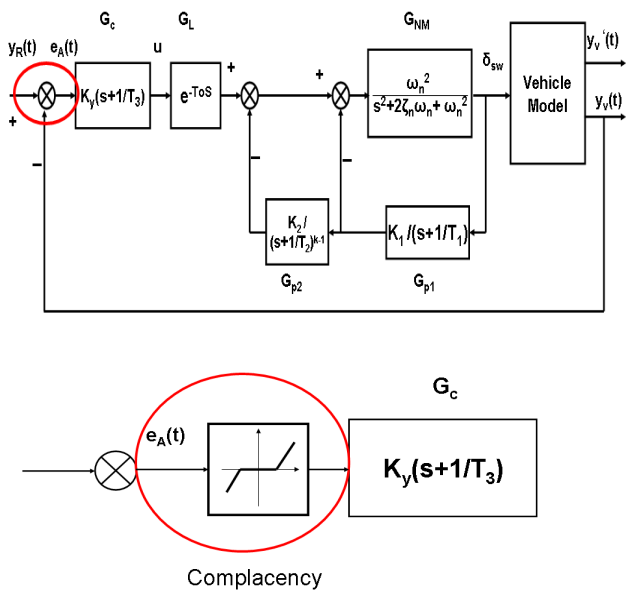

Figure 3. Driver model for lateral control

The vehicle model used is known as 'bicycle model' [28] for calculating the lateral dynamics of the vehicle and linearized at a constant longitudinal velocity. In order to obtain more realistic behaviour from this model, it is updated by changing longitudinal velocity at discrete time steps. Therefore the resulting vehicle model is a hybrid system containing a set of linear-continuous time, time-invariant models of vehicle switched by a discrete update driven by longitudinal speed changes. As a consequence the resultant model is non-linear and closer to realistic vehicle response. The model inputs are steering wheel angle, longitudinal vehicle velocity and outputs are lateral acceleration and side slip angle. The lateral acceleration output of this model is used to calculate the lateral speed and finally lateral position of the vehicle employing numerical integration by trapezoids. The variables of model are given in Table 1.

Table1. Variables of vehicle model

Symbol	Meaning
c_f or c_r	cornering stiffness coefficients for front and back tire
J	Yaw moment of inertia about z-axis passing at CG
m	Mass of the vehicle
r	Yaw rate of vehicle at CG
U	Vehicle speed at CG
y_c	Lateral offset or deviation at CG
τ	Wheel steering angle of the front tyre
α_f or α_r	Slip angle of front or rear tyre
β	Vehicle side slip angle at CG
ρ_{ref}	Reference road curvature
ψ	Yaw/ heading angle
ψ_d	Desired yaw angle
ω	Angular frequency of the vehicle

The equations of motion using the variables given in Table 1 are presented in equations (1-2).

$$\begin{bmatrix} \dot{\beta} \\ r \end{bmatrix} = \begin{bmatrix} a_{11} & a_{12} \\ a_{21} & a_{22} \end{bmatrix} \begin{bmatrix} \beta \\ r \end{bmatrix} + \begin{bmatrix} b_1 \\ b_2 \end{bmatrix} \tau \qquad (1)$$

Where, in a format $\dot{x} = Ax + Bu$,

$$\dot{x} = \begin{bmatrix} \dot{\beta} \\ r \end{bmatrix}, \; A = \begin{bmatrix} a_{11} & a_{12} \\ a_{21} & a_{22} \end{bmatrix}, \; B = \begin{bmatrix} b_1 \\ b_2 \end{bmatrix}, \; u = \tau$$

And in the output format, $y = Cx + Du$

$$\begin{bmatrix} a_s \\ \beta \\ r \end{bmatrix} = \begin{bmatrix} c_{11} & c_{12} \\ 1 & 0 \\ 0 & 1 \end{bmatrix} \begin{bmatrix} \beta \\ r \end{bmatrix} + \begin{bmatrix} d_1 \\ 0 \\ 0 \end{bmatrix} \tau$$

Where, $y = \begin{bmatrix} a_s \\ \beta \\ r \end{bmatrix}, C = \begin{bmatrix} c_{11} & c_{12} \\ 1 & 0 \\ 0 & 1 \end{bmatrix}$ and $D = \begin{bmatrix} d_1 \\ 0 \\ 0 \end{bmatrix}$.

The elements of the matrices are given explicitly here:

$$a_{11} = -(C_f + C_r)/mU,$$
$$a_{12} = -1 + [(h_r C_r - h_f C_f)/mU^2]$$
$$a_{21} = (h_r C_r - h_f C_f)/J, \; a_{22} = -(h_f^2 C_f + h_r^2)/JU$$
$$b_1 = C_f/mU, \; b_2 = h_f C_f/J$$
$$c_{11} = -[(C_f + C_r)/m] + [l_s(h_r C_r - h_f C_f)/J]$$
$$c_{12} = [(h_r C_r - h_f C_f)/mU] - l_s[(h_f^2 C_f + h_r^2 C_r)/JU]$$
$$d_1 = [(C_f/m) + l_s(h_f C_f/J)] \qquad (2)$$

Combined Full Driver Model

As mentioned before, the lateral and longitudinal models are coupled via the update of vehicle model using the velocity outputs of HMM model for driver velocity control. HMM model uses 1-2 sec history of velocity from CAN-Bus to predict the future sequence. Therefore the vehicle model in lateral driver model is updated before the driver input to this model reaches for new calculation of lateral position. The longitudinal and lateral control strategies are closely related in a two-way relationship:

(1) In higher speeds, the driver is expected to correct the steering wheel with smaller magnitudes.
(2) In sharp turns, the driver might prefer to reduce the longitudinal speed and during the lane change towards a faster lane the speed should be increased to avoid interference with the upcoming traffic.

The combined model has non-linear and stochastic properties together and accounts for the complacency of human driver. The next session reports on model verification using real CAN-Bus data.

Selected Model Verification Results

In model verification, CAN-Bus data is used to assess the model in its fidelity to reproduce steering wheel angle and vehicle speed commands. The model was able to reproduce the expected signals with some drawbacks and advantages:

(1) The steering wheel angle contained a high frequency term
(2) The identification ok K and T parameters in lateral control require several iterations. However, once it is set, these parameters can represent driver characteristics or status.

The model is capable of reproducing steering wheel angle commands in lane keeping, curve negotiation and lane change profiles. The application of complacency zone in the model was found very useful since it gives the safety margin of the driver in the lateral control task and it is a driver-specific characteristic. In addition to this internal delay due to processing and the gain of feedback from proprioreceptive system are explored. It was observed that increasing the internal delay from 0.15 (nominal) to 1-15 sec interval representing driver distraction caused the error building in lateral position and the vehicle drifted. It was also observed that increasing the gain from proprioreceptive feedback reduces the errors in lateral position tracking. This is also observed during the experiments; the novice drivers relying on only visual feedback have larger errors while the expert drivers depend on the feedback from neuro-muscular system (i.e. thus their gain is higher in that component) and have less lateral positioning errors. The effect of vestibular/proprioreceptive feedback gain is represented from validation experiments performed in Simulink (Figure 4 and 5).

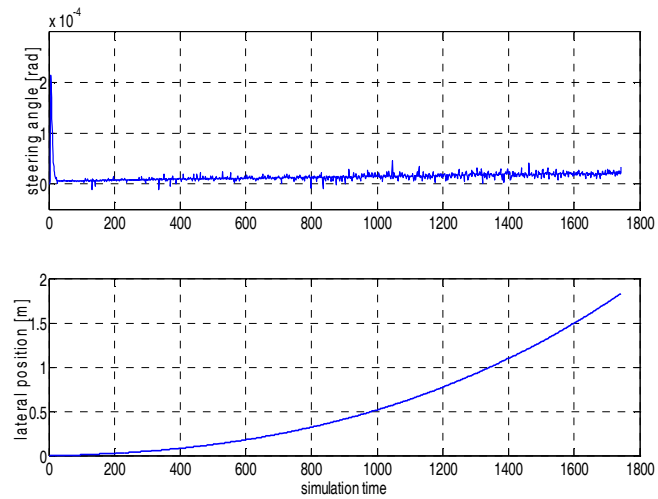

Figure 4. Drift in lane keeping task (max 2 m) with internal delay of 1 sec and proprioreceptive gain of 2.

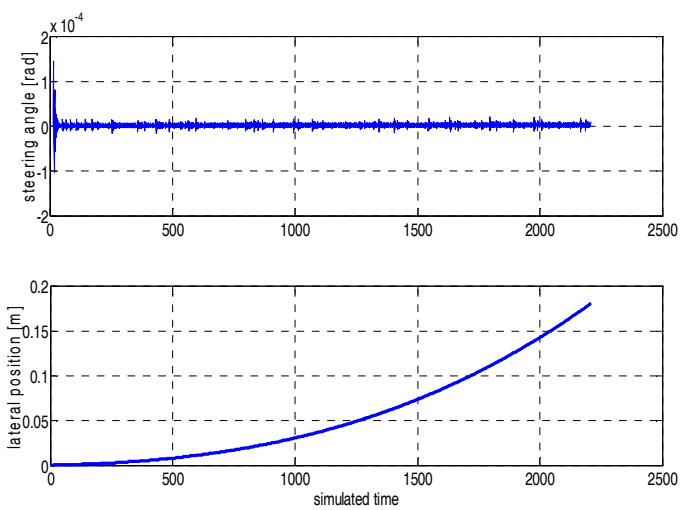

Figure 5. Drift in lane keeping task with an internal delay of 1 sec and proprioreceptive gain of 20.

CONCLUSIONS

In this paper, a hybrid model using a stochastic model for velocity control and a continuous control theoretic model for lateral control are combined. The lateral model is modified in order to represent driver complacency. In addition to that internal processing time is represented by a delay term which can account for distraction since it blocks the processing sources of the driver. Finally the importance of vestibular feedback is shown by observing the drift in using the feedback from this system less (Fig..4) or more (Fig.5). This type of change can represent the difference between novice and expert driver, since the expert driver would trust more on muscle system/learned skills than visual input.

In summary, the proposed driver model can account for human deficiencies or bottlenecks in information processing, complacency. Also, the model can explain the effects of the distraction in a tracking task (i.e. lane keeping) and the experience level (i.e. changing gains in different feedback channels). For these reasons, the model is very convenient to be used in developing human-centric lane assistance/ control systems.

In our future work, the proposed model will be improved and several driver behaviour, performance and characteristics will be linked and added using Hybrid Dynamic Systems and stochastic modeling tools.

REFERENCES

[1] Hendricks, D.L. Fell, J.C., and Freedman, M., 'The relative frequency of unsafe driving acts in serious traffic crashes', Report no: DOT-HS-809-206, Jan 2001.

[2] McCall, J.C., Trivedi, M.M., 'Video-Based Lane Estimation and Tracking for Driver Assistance: Survey, System and Evaluation', *IEEE Transactions on Intelligent Transportation Systems,* vol. 7, no.1, pp. 20-37, March 2006.

[3] Kim, Z., 'Robust Lane Detection and Tracking in Challanging Scenarios', , *IEEE Transactions on Intelligent Transportation Systems,* vol. 9, no.1, pp. 16-26, March 2008.

[4] Rakotonirainy, A., Maire, F., 'Context-Aware Driving Behaviour Model', In *Proceeedings of the 19th International Technical Conference on the Enhanced Safety of Vehicles (ESV'19),*2005.

[5] Hess, R.A., Modjtahedzadeh, 'A Control Theoretic Model of Driver Steering Behavior', *IEEE Control Systems Magazine,*pp.3-8, 1990.

[6] Hess, R.A., 'A model based theory for analyzing human control behavior', in *Advances in Man-Machine System Research,* W.B.House (ed.), vol.2, London, JAI Press, pp. 129-175, 1985.

[7]McRuer, D., Weir, D., 'Theory of manual vehicular control', *Ergonom.,* vol.12, pp.599-633, 1969.

[8] MacAdam, C., 'Application of an optimal preview control for simulation of closed-loop automobile driving', *IEEE Trans. Syst. Man. Cybrn.,* vol. SMC-11, pp.393-399, Sept 1981.

[9]] McRuer, D.T., Krendel, E., 'Mathematical models of human pilot behavior', AGARDograph, No.188. Jan 1974.

[10] Pilutti, T., Ulsoy, A.G., 'Identification of Driver State for Lane Keeping Tasks', *IEEE Trans. on Syst., Man, Cybern., Part A: Syst. And Humans,* vol.29, no.5, Sept 1999.

[11] Lubashevsky, I., Wagner, P., Mahnke, R., 'Bounded rational driver models', *European Physical Journal B,* vol.31, p.243.

[12] Chen, L-K, Ulsoy, A.G., 'Identification of a driver steering model, and model uncertainty from driver simulator data', *Journal of Dynamic Systems, Meausrement and Control,*vol.123, pp. 623-629, 2001.

[13]Nechyba, M.C., Xu, Y., 'Human Control Strategy: Abstraction, Verification and Replication', *IEEE Control Systems Mag.,* pp. 48-61, Oct. 1997.

[14] Nechyba, M.C., Xu, Y., 'On Discontinuous Human Control Strategies',In *Proceedings IEEE Int. Conference on Robotics and Automation,* vol.3.,pp. 2237-2243, 1998.

[15] Petland, A., Liu, A., 'Modeling and Prediction of Human Behavior', *Neural Computation,* vol.11,pp.229-242, 1999.

[16] Yang, J., Xu, Y., Chen, C., 'Human Action Learning via Hidden Markov Model', *IEEE Trans. on Syst. Man Cybern, Part A: Syst. And Humans,*vol.27, no.1, pp. 34-44, 1997.

[17] Mitrovic, D., "Reliable Method for Events Recognition", *IEEE Trans. on Intelligent Transp. Syst.,* vol. 6, no. 2, pp. 198-205, June, 2005.

[18] K. Torkkola, S. Venkatesan, H. Liu, "Sensor Sequence Modeling for Driving", FLAIRS Conference, pp. 721-727, Clearwater Beach, Florida, USA, , 2005. [online source: DBLP, http://dblp.uni-trier.de]

[19]Boyraz, P., Acar, M., Kerr, D., 'Signal Modelling and Hidden Markov Models for Driving Manoeuvre Recognition and Driver Fault Diagnosis in an urban road scenario', In *Proc. of IEEE IVS'07,* pp. 987-992, Istanbul, Turkey, 13-15 June, 2007.

[20] Sathyanarayana, A., Boyraz, P., Hansen, J.H.L, 'Driver Behaviour Analysis and Route Recognition by Hidden Markov Models', 2008 IEEE International Conference on Vehicular Electronics and Safety, 22-24 September 2008, Ohio, USA.

[**21]** Michon, J.A., 'Explanatory pitfalls and rule-based driver models', *Accident Analysis and Prevention,* vol.21, no.4, pp.341-353, 1989.

[22] Salvucci, D. D. Modeling driver behavior in a cognitive architecture. *Human Factors,vol. 48*, 362-380,2006.

[23] Kiencke, U., Majjad, R, Kramer, S, 'Modeling and performance analysis of a hybrid driver model', *Control Engineering Practice,* vol.7, pp. 985-991, 1999.

[24] Kim, J-H, Hayakawa,S, Suzuki, T., Hayashi, K., Okuma, S., Tsuchida, N., Shimizu, M., Kido, S., 'Modeling of Driver's Collision Avoidance Maneuver Based on Controller Switching Model', *IEEE Trans. on Syst. Man Cybern. , Part B: Cybern.,*vol.35, no.6, Dec 2005.

[25] Akita, T., Inagaki, S., Suzuki, T, Hayakawa, S, Tsuchida, N., 'Hybrid System Modeling of Human Driver in the Vehicle Following Task', In *Proceedings of SICE Annual Conference,* Kagawa, Japan, pp. 1122-1127, 2007.

[26] Inata, K., Raksincharoensak, P., Nagai, M., 'Driver Behavior Modeling Based on Database of Personal Mobility Driving Urban Area', In *Proceeding of Int. Conf. On Control Automation and Systems,* pp. 2902-2907, Oct. 14-17, Seoul, Korea.

[27] Rabiner, L.R. "A Tutorial on hidden Markov models and selected applications in speech recognition", *Proc. IEEE,* vol. 77, Issue 2, Feb 1989, pp. 48-61.

[28] You, S-S, Kim, H-S, Lateral dynamics and robust control synthesis for automated car steering, Proc. of IMechE, Part D, Vol. 215, pp. 31-43, 2001.

YAW RATE ERROR – A DYNAMIC MEASURE OF LANE KEEPING CONTROL PERFORMANCE FOR THE RETROSPECTIVE ANALYSIS OF NATURALISTIC DRIVING DATA

Tim Gordon,
Adam Blankespoor,
Michelle Barnes,
Dan Blower,
Paul Green,
Lidia Kostyniuk
University of Michigan Transportation Research Institute
Michigan, USA
Paper Number 09-0326

ABSTRACT

The aim of this work is to define and evaluate a "yaw rate error" (YRE) derived from naturalistic driving data to quantify driver steering performance during lane keeping. This measure of lane keeping performance is based on the predicted kinematic control error at any instance. Scope is limited to the demonstration that such a quantity exists, that can be computed from naturalistic driving data, and that it correlates with instantaneous control performance in real-world driving. The YRE is defined as a measure of conflict: the difference between current vehicle yaw rate and kinematic values required to be consistent with forward lane boundary crossing. A second, well-known measure is computed for comparison: the predicted time to lane crossing (TTLC). All data is obtained from naturalistic driving databases containing detailed information (over 200 signals at 10 Hz.) on driver input and vehicle response as well as aspects of the highway and traffic environment. As a continuously updated measure of the control correction required by an alert driver, it is expected that the YRE will be more informative of driving situations than the simpler kinematic measure TTLC. This latter measure is only loosely related to the closed loop control of vehicle motion. For example a very small TTLC can represent either a critical case where the vehicle is about to depart the lane and requires a large correction, or it could be a case where the vehicle is close to the lane boundary but with small lateral velocity requiring only a small correction. The YRE represents the severity of the possible lane departure in a natural way, accounting for current position, path direction, and path curvature. While no in-depth statistical analysis is conducted for YRE, it is proposed as a new tool for post-hoc analysis of driver steering performance during lane keeping.

INTRODUCTION

Driving is a control task based on visual input; it includes filtering of input for relevance, extracting signals or patterns from that visual information, and hence provides a reference to guide steering and speed control. Control action then involves manual effort by the driver to modulate vehicle motion using further force and acceleration cues [1-3]. Here we focus on the visual reference for lane keeping in terms of a conflict measure or error criterion. In broad terms we seek a simple measure of the control reference for when the driver is concerned with staying in the lane but less concerned with some optimal path within that lane. To this end we introduce and evaluate a suitable measure of "yaw rate correction required" or yaw rate error. Since no preferred path is computed, the YRE is computed for multiple lane boundary points and the most critical of these will represent the overall correction required. This metric has been used previously in driver modeling [4] and applied to collision avoidance [5]

The approach is analogous to longitudinal speed control in traffic, where control action required can be found in terms of the vehicle deceleration required to avoid a collision with the vehicle in front. Again, this contrasts with the predicted time to collision (TTC), based on instantaneous positions and velocities of the vehicles [6]. While in the speed control problem there is essentially a single target point, the more complex lane keeping activity involves multiple conflict points and more complex vehicle kinematics.

We focus on yaw velocity rather than the related variables of path curvature and lateral acceleration because of the focus on visual reference. Yaw velocity is directly available to the driver as the perceived angular rate of distant or peripheral objects across the field of view. Path curvature by contrast

requires a constructive element as the driver "imagines" the path of the vehicle, something that is surely more appropriate to low speed maneuvering Again, vehicle lateral acceleration is not a visual input, but rather a feedback for the lower level manual control of the vehicle. Thus the emphasis on yaw rate as the reference is based on its availability through visual feedback, analogous to what happens in vehicle stability control [7] – vehicle yaw rate is directly measured and compared to a reference – though in this case it is based on anticipated vehicle response to steering at the current speed. In this case path curvature is not directly measurable, and lateral acceleration is subject to disturbances such as body roll; also, the lateral acceleration is dependent on sensor location, unlike the yaw rate, which is only sensitive to sensor orientation.

It is also worth noting that under simple conditions of constant speed, minimal vehicle sideslip (i.e when the vehicle is in a normal stable condition) and negligible body roll angle, the three variables mentioned (path curvature, yaw rate and lateral acceleration) are actually proportional to each other. So under these simple conditions any one of these variables might be used for the present purpose. We now turn to the details of the yaw error criterion.

For any point on the road or lane boundary, we are to determine whether a yaw rate correction is needed to avoid going outside of the lane/road. If so the yaw correction required is a measure of conflict. The maximum magnitude of all such corrections (left or right) is to be our conflict measure, though it is often of interest to analyze "worst right boundary case" and "worst left boundary case" in parallel. Additional information is relevant, namely the distance and polarity (left, right) of any conflict point, as well as the *horizon* distance: the maximum distance or headway for which – under ideal yaw rate – no conflicts occur). The horizon distance is a combined measure of position and direction error, as well as road geometry, and arises naturally out of the YRE analysis.

As mentioned, YRE and these associated measures are related to TTLC, but are expected to incorporate a greater degree of continuity and relevance to the control task. Unlike TTLC, the "angle of attack" of the lane excursion is implicitly included, so it potentially attaches due significance to how severe the predicted lane excursion will be, not just when it will be. For this reason YRE is expected to be a superior combined metric of lane keeping performance analysis than TTLC.

This study was motivated by a more general problem of establishing surrogates for road departure crashes [8,9]. The idea is to find kinematic or other variables that respond to road, traffic and driver conditions in a way that mimics the pattern of crash occurrence. Provided the dependency is based on common cause (for example due to disturbances in the closed loop control of the vehicle), detailed analysis of surrogates and counter-measures is much more feasible than the corresponding analysis of crash occurrence. In this paper we restrict attention to the YRE metric of interest, and leave aside its factorial analysis relative to crash frequencies.

YAW RATE ERROR DEFINITION

In Figure 1 we consider the lateral vehicle control relative to a single "conflict point" *P*. This is presumed to be on the right lane boundary, so the yaw rate (assumed positive in the case shown, with the vehicle curving to the right) should be no more than for the critical case shown; the vehicle point *Q* required to pass to the left of *P*, while here it just intersects with *P*. Using polar coordinates (ϕ, d), ϕ is the azimuth angle and *d* is the distance-to-target, both computed relative to the velocity vector at the reference point *Q*. This in turn is oriented at an angle ϕ_0 relative to the vehicle axes, and if we assume *Q* to be at the outside edge of the front right tire, then ϕ_0 is very roughly equal to the steering angle at the right front wheel.

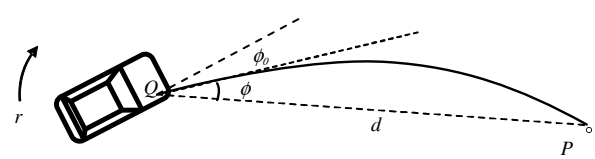

Figure 1. Turning kinematics – critical case where reference point *Q* intersects with boundary edge point *P* during a steady-state turn.

Assuming the vehicle path is in the form of a circular arc, the geometry is represented in Figure 2; we find that the critical case occurs when the turning radius *R* satisfies the equation

$$\sin\phi = \frac{d}{2R} \tag{1}$$

which is equivalent to the yaw rate condition

$$r = \frac{2U \sin \phi}{d} \qquad (2)$$

U being vehicle speed. Thus equation (2) defines the maximum yaw rate of the vehicle to avoid conflict with a right boundary point P

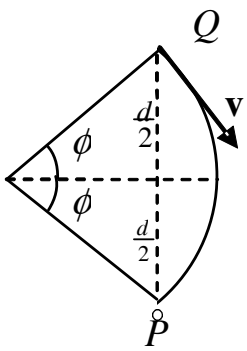

Figure 2. Basic geometry of steady turning motion.

ESTIMATION METHOD

When using driving data, we do not have direct information on all of the variables used in equation (2) – the absolute coordinates of the boundary points are unknown, as are their relative locations to the vehicle; hence they must be inferred from the lane tracker, which estimates of lateral position and lane width. Note that while in principle GPS could be used, it is far from being accurate enough to give useful estimation of the lane keeping performance, so this was not considered.

The idea is to use the vehicle itself, with known speed and yaw rate, to provide a reference for which to estimate the relative position of the lane boundary over time. From the variations in lateral lane position over time, the lane geometry is to be estimated, and variables such as ϕ and d derived.

We also need to estimate the azimuth offset ϕ_0 for the direction of the velocity vector at the front wheel relative to the vehicle longitudinal axis (at low speed this is the steer angle, but in general it depends on the front axle cornering stiffness). In the case where steer angle and cornering stiffness is not available, a simple estimate can be made based on general vehicle dynamics properties

$$\tan \phi_0 = \frac{rL}{U - rc} \qquad (3)$$

where r is the yaw rate, L is the wheelbase, $2c$ is the front track, and U is the instantaneous vehicle speed (this equation is based on the assumption of near-zero slip angle at the rear axle, but is expected to be reasonably accurate). Simple adjustments are to be made to this equation when considering left side boundary points.

Figure 3 shows the modified geometry when boundary point B is offset from the vehicle path. For simplicity assume a fixed preview time T to the boundary point, and an approximately constant curvature for the path of the reference point from Q to P. In the figure, ϕ is the azimuth angle to the boundary point B, while θ is now the critical azimuth angle corresponding to the motion from Q to P. (Again, both angles are defined relative to the velocity vector, not the vehicle longitudinal axis).

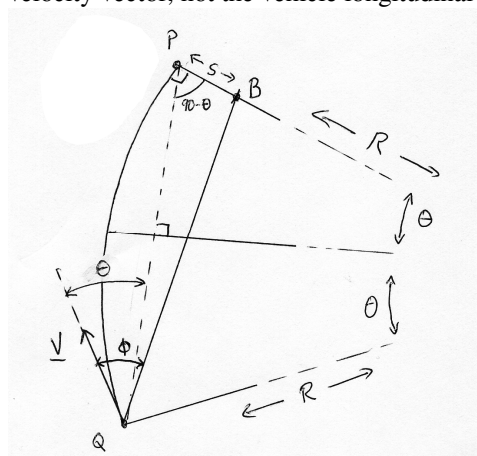

Figure 3. Sketch of turning geometry for an offset boundary point *B*.

During the vehicle motion from Q to P, the heading angle and direction of velocity vector V change by 2θ, so numerically integrating the yaw rate over the time interval T we have

$$\theta = \tfrac{1}{2} \sum_i r(t_i)\, \delta t \qquad (4).$$

The mean radius of turn, R, during the time interval can also be obtained from the yaw rate:

$$\frac{2\theta}{T} = \frac{\overline{U}}{R} \qquad (5)$$

where $\overline{U}$ is the mean vehicle speed during the interval, and both sides of this equation are estimates of the mean yaw rate during time interval T. Then, to determine ϕ, we consider triangle BPQ in Figure 4. Angles at P and Q are known in terms of ϕ and θ, and hence the angle at B is given by

$$\beta = 180 - (90 - \theta + \alpha) = 90 + \theta - \alpha = 90 + 2\theta - \phi$$

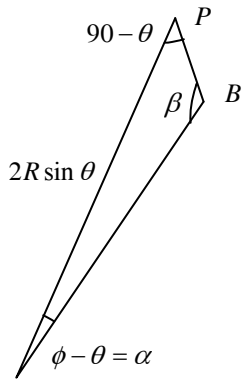

Figure 4. Geometry to determine ϕ

Then from the sine rule

$$\frac{\sin\beta}{2R\sin\theta} = \frac{\sin(\phi-\theta)}{s} \qquad (6)$$

which is a nonlinear implicit equation for ϕ in terms of other known variables. For normal highway driving we expect $\alpha = \phi - \theta$ to be sufficiently small (less than around 5°) to allow the approximation $\sin\alpha \approx \alpha$, $\cos\alpha \approx 1$. In this case

$$\begin{aligned}\sin\beta &= \sin(\theta + (90-\alpha)) \\ &= \sin\theta\cos(90-\alpha) + \cos\theta\sin(90-\alpha) \\ &= \sin\theta\sin\alpha + \cos\theta\cos\alpha \\ &\approx \sin\theta\,\alpha + \cos\theta\end{aligned}$$

Substituting this into equation (6) then gives

$$\frac{\sin\theta\,\alpha + \cos\theta}{2R\sin\theta} = \frac{\alpha}{s}$$

Hence

$$\alpha\left(\frac{1}{s} - \frac{1}{2R}\right) = \frac{1}{2R\tan\theta}$$

giving the approximate expression for ϕ (with all angles in radians)

$$\phi = \theta + \frac{s}{(2R-s)\tan\theta} \qquad (6a).$$

Distance $d = |QB|$ is also found from the geometry of Figure 4:

$$\begin{aligned}d &= |QP|\cos\alpha - |BP|\cos(90-\theta) \\ &\approx 2R\sin\theta - s\sin\theta\end{aligned}$$

and hence

$$d = (2R - s)\sin\theta \qquad (7).$$

Equations (4), (5), (6a) and (7) then determine all the relevant terms in the critical yaw rate expression

$$r_c = \frac{2U\sin\phi}{d} \qquad (8)$$

where U is the instantaneous vehicle speed at Q, and now we use r_c to denote the critical yaw.

Multiple calculations can be performed for point pairs (P,Q) for values of T in a range of say 0.5-2 seconds, and the results referenced on the initial point Q. We are then interested in the minimum value of r_c (Q) and its corresponding distance d from Q. The yaw rate error is then

$$yre(t_Q) = r(t_Q) - r_c{}^*(Q) \qquad (9)$$

where $r(t_Q)$ is the vehicle yaw rate at time t_Q, and $r_c{}^*(Q)$ was the minimum critical yaw rate at Q.

A second yaw rate error for left boundary points also has to be found, making similar calculations with relevant shift of reference point (to the outside of the left front tire) together with relevant sign changes.

The above equations are obtained for computing YRE, but it is worth noting that with a minor adjustment they can be used to determine local road curvature from the on-board vehicle data (assuming lane position, speed and yaw rate are measured) removing the effects of vehicle lateral drift. The method is to estimate the critical yaw rate for a shifted point P that has the same lateral offset as current point Q: thus replace $s = s(P)$ in the above, by $s' = s(P) - s(Q)$. The critical yaw rate r_c' is then the yaw rate that maintains equal lane deviation over time interval T, and hence provides the radius of curvature R_e (referenced at the right lane boundary) we obtain

$$R_e = \frac{\overline{U}}{r_c'} - s' \qquad (10).$$

RESULTS

The estimation method described above was used to determine the YRE for driving events recorded in the Road Departure Crash Warning (RDCW) field operational test database [10], which contains more than 200 data channels recorded at 10 Hz or 20 Hz, depending on the signal; included within these data is a wide range of information on driver input, vehicle response as well as aspects of the highway and traffic environment. As well as objective data from sensors, video images of the forward scene and drivers face were available to establish context. Here we present data from three events which appear quite typical or real-world lane keeping.

Event 1, depicted in Figure 5, was of a driver negotiating an on-ramp which is in the form of a right-hand curve. The left plot shows the location of the left and right front wheels relative to the lane boundaries (note that there is some variation in the lane width, but that most of the variations are in the dashed lines which depict the outside edges of the front tires). This event shows a situation where the driver maintained a position very close to the lane boundary with several excursions beyond the boundary. From video review, it appeared that the driver's attention was switching between reading a map and looking at the road ahead. Clearly the event represents an example of poor lane keeping. Figure 6(a) shows critical and actual yaw rate time histories, as well as lateral distance within the lane boundary (scale by a factor 0.1 so that scales are reasonably consistent).

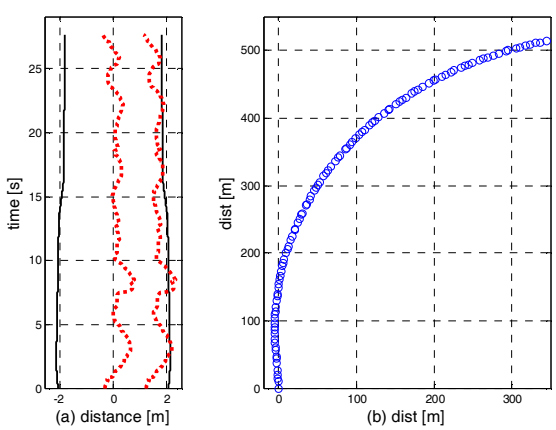

Figure 5. The vehicle path for event 1. (a) The dotted lines represent the left and right edges of the vehicle with respect to the center of the lane markings (solid lines). (b) The X-Y position of the vehicle in space.

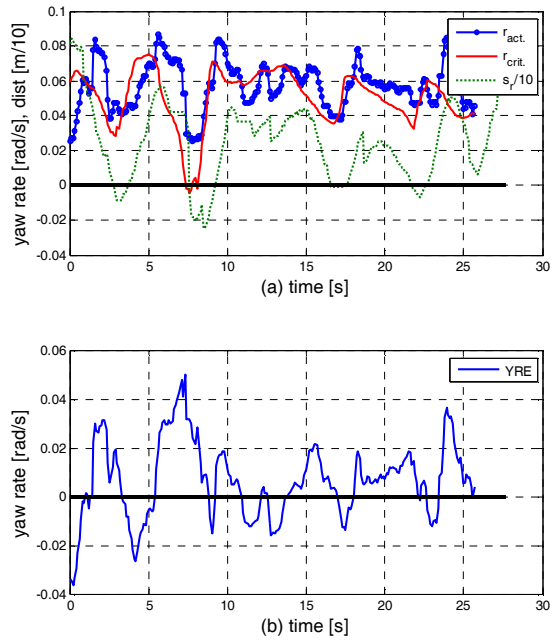

Figure 6. The yaw rate parameters for event 1; (a) the actual yaw rate, critical yaw rate, and distance to the right lane boundary, and (b) the calculated YRE through the curve.

All conflicts for this event appear to be "right side only", so the yaw rate error in Figure 6(b) is positive whenever the current location and path predict at least on lane boundary conflict within the chosen time horizon (0.5 – 2 sec). We see that YRE is always positive at the start of a lane excursion, and actually always becomes positive before a lane excursion occurs. In this sense, as would be expected, it is predictive of each lane excursion.

Figure 7 shows YRE again (lower plot) together with the time to lane crossing (TTLC) in the upper plot and also its reciprocal (inverse TTLC, or ITTLC) in the center plot. ITTLC might be preferred as a conflict metric since large values indicate proximity to a lane excursion, in contrast to TTLC which is large when the vehicle is tracking the lane well. The main features seen in Figure 7 are the great variations and major discontinuities in TTLC and ITTLC, as compared to the much more continuous form of YRE. This suggests that YRE may potentially connect more directly to the continuous steering control behavior of the driver, especially since lane crossing is not generally a catastrophic event and does not generate a panic response from the driver.

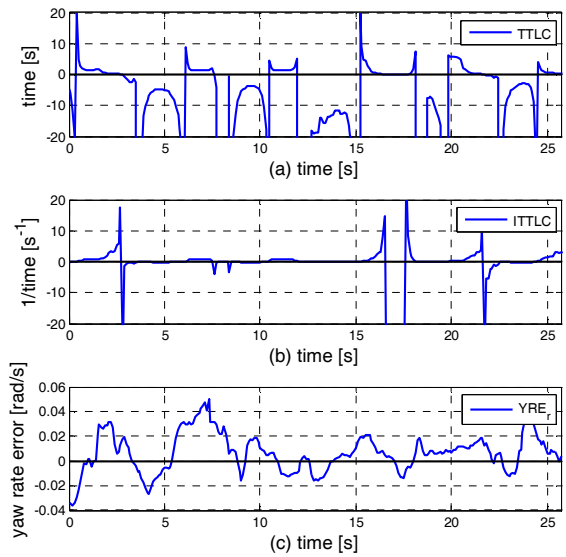

Figure 7. A comparison of the driver risk parameters for event 1; (a) the TTLC, (b) the ITTLC, and (c) the YRE.

In Figure 8 this is tested informally by plotting steer response (upper curve) as well as YRE (lower curve). Each local peak of the YRE curve seems to coincide with a sharp negative slope in the steering, and this is clearly the case at the YRE peaks at around t=2, 7, 16 and 24 seconds – these sharp reactions seem to correlate with corrective actions by the driver in a way that TTLC, ITTLC and even lane crossing in Figure 6(a) do not. The distracted driver in this event is not responding to YRE as it reaches positive values, but arguably when attention to the road coincides with a positive value of YRE.

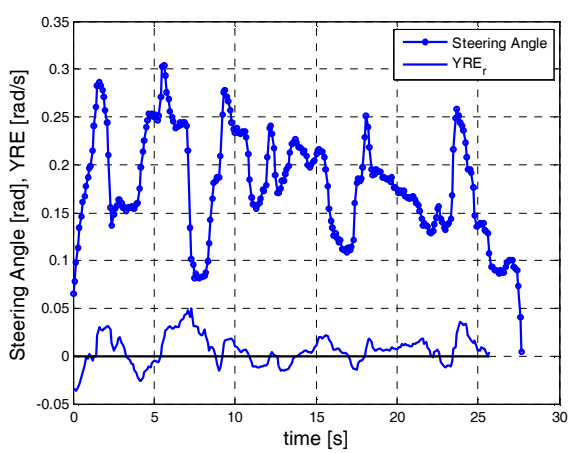

Figure 8. A comparison of the driver controlled steering angle and the calculated YRE for event 1.

The second event from the RDCW data was a single boundary crossing followed by a correction back to the middle of the lane. The vehicle trajectory data can be seen in Figure 9. The event is somewhat simpler than event 1, in that only one major excursion exists. Figure 10 shows the event in terms of yaw rate and critical yaw rate, and it's interesting that the conflict most heavily dominated by variations in the critical yaw rate rather than the actual yaw rate. In the upper plot, the yaw rate exceeds its critical value at around 7 seconds, while the first lane excursion takes place around 1 second later, again showing the predictive nature of YRE. In the lower plot, the YRE undergoes a correction at t=10 seconds and from the previous analysis we would expect to see a sharp negative slope in the steering angle then.

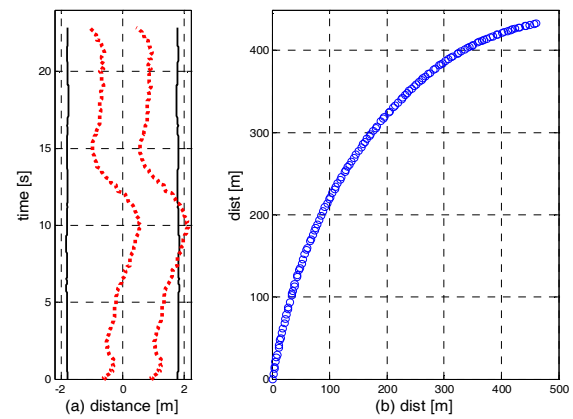

Figure 9. The vehicle path for event 2. (a) The dotted lines represent the left and right edges of the vehicle with respect to the center of the lane markings (solid lines). (b) The X-Y trajectory of the vehicle.

First we note however that in Figure 11, the previous comparisons with TTLC and ITTLC are repeated, the time-based metrics showing large discontinuities, while YRE varies continuously and in a simple way during the event – it grows at a very roughly uniform rate until the correction is presumably applied at t=10 seconds, then decays uniformly until at around 12 seconds it is corrected again in the opposite sense. Turning to Figure 12 a sharp negative slope is seen at t=10, and a positive slope steering correction takes place at t=12, as expected. Of course there are other steering corrections visible in Figure 12, and not all are directly predicted by conflicts with the right lane boundary, but perhaps some involve the right lane boundary. To this end we consider below a modified plot of vehicle yaw rate plotted over the pair of critical boundary cases.

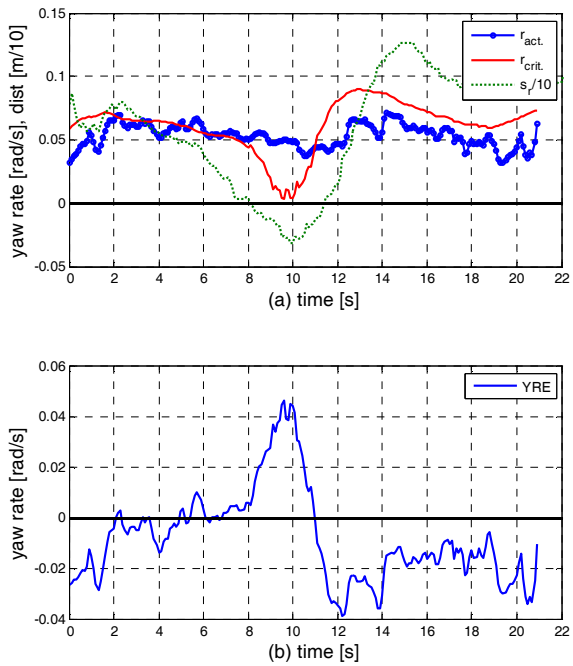

Figure 10. The yaw rate parameters for event 2; (a) the actual yaw rate, critical yaw rate, and distance to the right lane boundary, and (b) the calculated YRE through the curve.

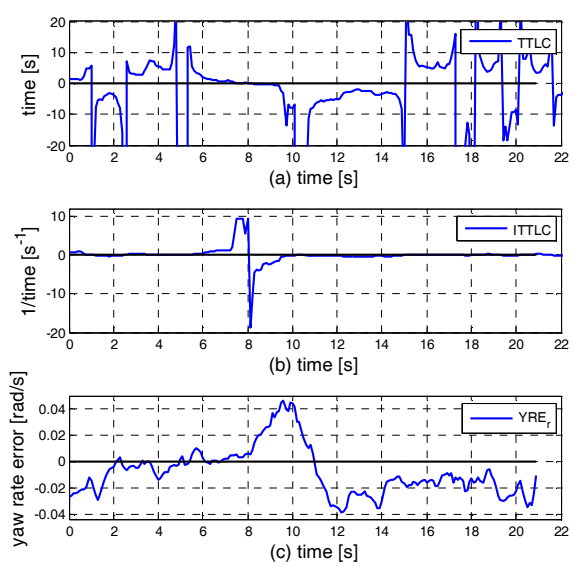

Figure 11. A comparison of the driver risk parameters for event 2; (a) the TTLC, (b) the ITTLC, and (c) the YRE.

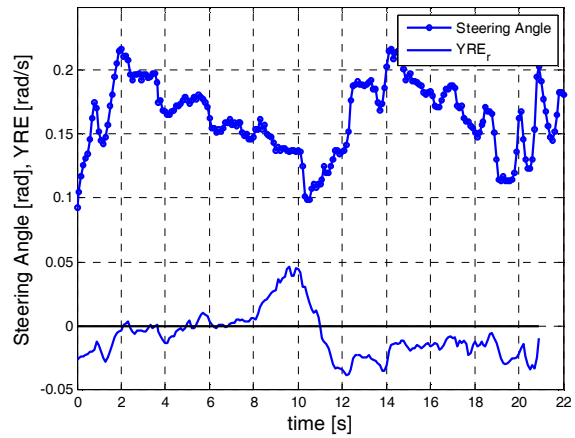

Figure 12. A comparison of the driver controlled steering angle and the calculated YRE for event 2

First however we consider a third example, also on a curved road section, but where there are no obvious lane boundary conflicts – see Figure 13 – which shows a nearly uniform distance from the car to the lane boundaries while negotiating the right-hand curve. Surely in this case the control loop is "inactive", meaning the driver has found a stable line and has no need to make multiple corrections to avoid boundary conflicts. Figure 14 appears to show otherwise. Again we are plotting YRE for the right boundary and steering control actions. Far from being random or disconnected from the boundary conflict, the driver appears to be making regular steering corrections (negative slope interventions) whenever YRE approaches a critical (zero or positive) value

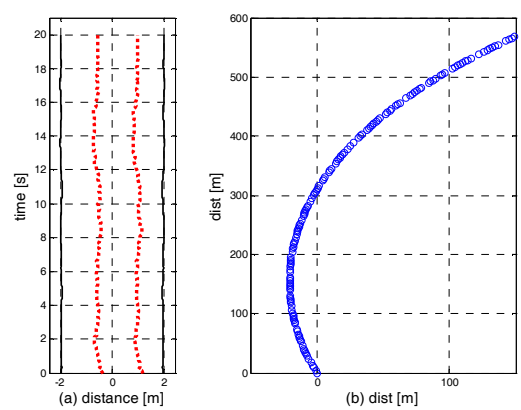

Figure 13. The vehicle path for event 3. (a) The dotted lines represent the left and right edges of the vehicle with respect to the center of the lane markings (solid lines). (b) The X-Y position of the vehicle in space.

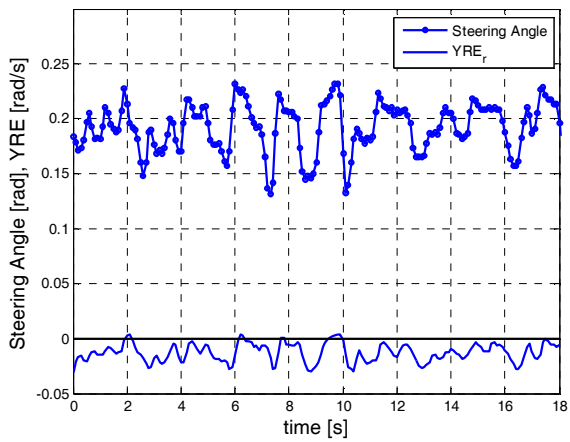

Figure 14. A comparison of the driver controlled steering angle and the calculated YRE for event 3.

Figure 15 now shows the yaw rate versus its two critical limits, where conflict avoidance takes the form

$$r_{c,left} < r < r_{c,right} \qquad (11).$$

All three events are shown, but the most striking is for event 3 in the lower plot: the vehicle appears to be controlled very precisely within the critical boundaries, with minimal overshoot but using the full range. Far from a stable "on center" steering control tracking the lane center, in "YRE space" the vehicle is "bouncing" quasi-periodically between its limits. If this interpretation is correct, the YRE provides a simple picture of lane-keeping control actions by the human driver. Turning to the center plot, where a single excursion event was seen, the degradation in control appears to be initiated as early as t=3 seconds when the more stable "bouncing between limits" is interrupted. After the lane excursion is corrected, normal effective control appears to be regained at around 14 seconds. Turning back to Figure 9(a) this same interpretation seems reasonable from the within lane drift – intuitively the driver is drifting right from about t=3, and only recovers full control at around 15 seconds. The point here is that YRE seems to provide a direct measure of lane keeping performance, and may even correlate with the error criterion active in the control loop of the human driver. In Figure 15(a) it appears that the driver does not regain effective control of the vehicle throughout the 15 seconds, and this is consistent with the distracted nature of the driving event. Finally in the upper two plots we see that left and right boundaries actually cross over, so no "solution" to (11) actually exists! We briefly consider this intriguing situation in the discussion below.

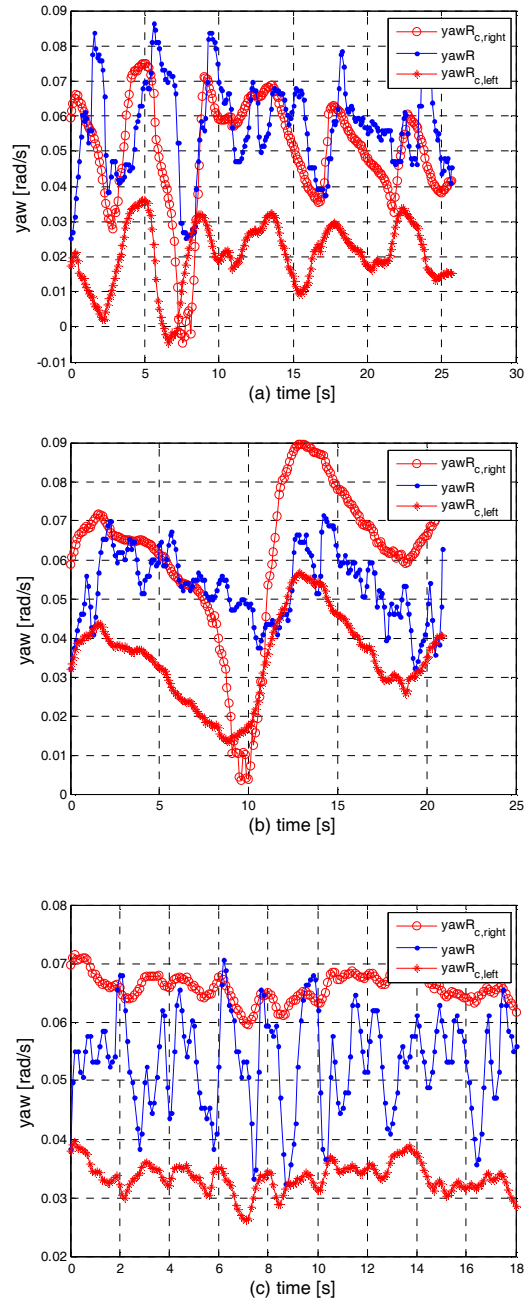

Figure 15. Comparison between the critical yaw rate for left and right boundary conflicts and the actual yaw rate for (a) event 1: riding the right boundary, (b) event 2: single boundary crossing with correction, and (c) event 3: good lane following.

DISCUSSION

In the above we have defined a yaw rate error (YRE) criterion that is motivated by the potential shortcomings of time to lane crossing (TTLC) as a measure of steering control performance during lane keeping. The main features have been seen above, but in summary:

- YRE behaves in a continuous way, even when lane boundary crossings take place, and this is not the case for TTLC and its reciprocal
- YRE excursions correlate strongly with rapid steering interventions by the driver, especially when the driver is providing effective control of lane position
- When left and right critical yaw rate boundaries are considered simultaneously, the normal effective control of lane position appears to operate to constrain between the crucial limits
- YRE may be a useful predictor of actual lane excursions, but more importantly it seems to provide a strong indicator of degraded or ineffective lane keeping

In events 1 and 2, the lane excursions appear to induce an "impossible" situation for the driver – the left and right limits cross over. This is most easily seen in Figure 15(b), where crossover takes place between approximately t=8 and t=12 seconds. From Figures 9(a) and 10(a) this corresponds to the vehicle being outside the lane boundary – clearly the steering task changes from lane keeping to lane recovery, though from Figure 12 the reaction seems to be consistent with a single sharp correction to "divert" the YRE to a correct linear rate of descent, followed by a second sharp correction in the opposite direction at around t=12 seconds. Thus it seems the crossover is not a major factor to the driver, who perhaps applies focus to one boundary at a time.

CONCLUSIONS

A simple yaw rate error criterion has been proposed for the analysis of steering control behavior. It can be used for the post-hoc analysis of naturalistic driving data, and with suitable development is likely to be feasible for real-time evaluation on the vehicle. It offers a number of simple advantages in terms of continuity and correlation to steering response, and offers a potential means of distinguishing between normal and degraded steering control while lane-keeping. In this paper there has been no attempt to analyze a large number of driving events, or establish a formal relationship between YRE and particular driving situations or other measures of control (e.g. eyes off the road, secondary tasking). The results above were based on randomly chosen events, and there was no selection procedure other than to find events from lane position typical of (1) an extended period of degraded lane control (2) a single event lane excursion error (3) well controlled lane keeping.

Further work will expand the number of events and attempt to more formally and accurately quantify the relationships hinted at in the three events presented. Also, further work is anticipated to evaluate YRE as a potential surrogate for crashes that happen due to disturbed control during lane-keeping. This particularly refers to lane-departure crashes and single-vehicle road departure crashes. Surrogate validation is to be based on factor analysis that link the statistical properties of both crash and surrogate.

ACKNOWLEDGEMENT

The authors are grateful to the SHRP 2 Safety Program [9] for funding and collaborative guidance in the conduct of this research.

REFERENCES

[1] Toffin, D., Reymond, G., Kemeny, A., and Droulez, J. 2007. "Role of steering wheel feedback on driver performance: driving simulator and modeling analysis." Vehicle System Dynamics. Vol. 45, No. 4, 375-388.

[2] Land, M., and Horwood, J. 1995. "Which parts of the road guide steering?" Nature. Vol. 377, 339-340.

[3] Chen, L-K. and Ulsoy, A. "Identification of a driver steering model and model uncertainty, from driving simulator data." J. Dyn. Sys. Meas., Control. Vol. 123, Is. 4, 623-629.

[4] Gordon, T.J. and Magnuski, N. 2006. "Modeling normal driving as a collision avoidance process." Proceedings of 8th International Symposium on Advanced Vehicle Control (AVEC), Taipai, Taiwan, August 2006.

[5] Chang, S and Gordon, T.J., 2008. "A Flexible Hierarchical Model-Based Control Methodology for Vehicle Active Safety Systems." Vehicle System Dynamics. Vol. 46, 63-75.

[6] Vogel, K. 2003. "A comparison of headway and time to collision as safety indicators." Accid. Anal. Prev. Vol 35. No. 3, 427-433.

[7] Trachtler, A. “Integrated vehicle dynamics control using active brake, steering and suspension systems.” 2004. International Journal of Vehicle Design. Vol. 36, No. 1, 1-12.

[8] Barnes, M., *et al*. “Development of analysis methods using recent data: a multivariate analysis of crash and naturalistic event data in relatin to highway factors using the GIS framework.” 2007. USDOT 7555-002565-01.

[9] Strategic Highway Research Program (SHRP 2) [Online]. Available: http://www.trb.org/SHRP2/

[10] Sayer, J., *et al.* “Road departure crash warning system field operational test: methodology and results. Volume 1: technical report” 2006. DTFH61-01-X-0053

METHODS AND PROCEDURES FOR TESTING THE E-CALL IN-VEHICLE UNIT FOR THE PURPOSE OF ITS PERFORMANCE ASSESSMENT AND CERTIFICATION

Rafal Grzeszczyk
Automex, Gdansk
Jerzy Merkisz
Poznań University of Technology
Piotr Bogus
Rail Vehicles Institute TABOR, Poznań
Tomasz Kaminski
Motor Transport Institute, Warsaw
Poland
Paper Number 09-0332

ABSTRACT

The main idea behind the pan-European eCall project is to automate the emergency call that is simultaneously extended by a message containing information such as current position and prior-to-crash speed, type of vehicle, VIN, VRN, number of passengers travelling, etc. The in-vehicle unit consists of measurement, communication, positioning and user-interface sub-systems, and all those sub-systems need to pass functional and performance type examinations before the device can be granted formal approval from the notified laboratory. The usual way of testing the module will be during the type approval of the car, as performance of the unit is strongly correlated to the dynamical parameters of the vehicle body and fitting procedures.

Technology of today makes it relatively easy and straightforward to measure linear and angular accelerations of the vehicle chassis to estimate its full state in the 6DOF space, however, the number of sensors required and resulting cost is mostly prohibitive, thus in practical solutions the crash detection is to be implemented based on signals acquired from a limited number of available sensors, preferably already present in the existing set-up, using also additional sources of data, such as longitudinal velocity from the speed sensor.

The purpose of the project is to design a testing methodology and set-up a testing bench for the type certification of the in-vehicle e-Call system units for the accredited laboratory. The test stand should allow the production of precise and repeated predefined testing conditions to excite the device-under-test sensors and to relate their logged data and results to those of reference set of sensors built-in to the test stand.

Another question we address during the study is the feasibility of data gathered in the in-vehicle e-Call unit for the purpose of reconstructing the crash.

INTRODUCTION

Within the framework of e-safety programme, a European Union initiative [3,9,15], eCall system is currently being implemented, which will decisively improve the process of road accident notification in the EU area. A few years ago, a need to introduce a uniformed emergency call number 112 across the EU territory was recognised by European legislation. The number is supposed to be operated with the same efficiency and effectiveness as the other traditional emergency numbers in each member state. Moreover, the personnel of the emergency call centre should be able to accept notifications in more than one language [1,4,16,18].

However, technical evolution has lead to further modifications of emergency call number 112, due to the development of new functionally extended version of the emergency call system named E112 (location-Enhanced 112), which will enable the emergency centre to automatically determine the location of the caller. This new feature of the technology is particularly important for people being abroad since the victims of the accidents often cannot precisely describe their current location and the time in emergency situations often means the difference between life and death.

The eCall system is another stage in the development of E112 technology. It assumes, the vehicles would be equipped during the production process with emergency sensors and communication modules, which, if the predefined emergency conditions are registered, will automatically dial the emergency centre and

convey exact information regarding place of the accident, vehicle identification (registration number and VIN), its type as well as initiate the voice connection allowing the call centre personnel to gather additional data on the accident details, therefore, reaching optimal decision as to the parameters of the rescue operation.

Organisation of the eCall system

The eCall system consists of three main subsystems, which should be adequately designed and compatible in order to allow their interoperability and functionality.

The first main element of the system consists of emergency sensors – devices installed in the vehicle – containing a set of inertial sensors which detect excessive linear and angular acceleration values (breaking deceleration, impact into the obstacle or another vehicle) which allow detection of the accident, GPS module determining geographical position of the vehicle, direction and speed of its movement shortly before the accident, and GSM module to automatically or manually initiate dialling sequence to Public Safety Answering Point (PSAP).

The other element of the eCall system is the ground telecommunication infrastructure of the GSM operator as well as the ground and space infrastructure of satellite navigation systems. The infrastructure of GSM operators should allow dialling of emergency module installed in the vehicle also outside native mobile operator. The roaming should be available not only outside country borders in which the vehicle is registered and where the SIM card was issued, but also in the territory of the country of the origin, especially when the accident took place outside the coverage of a native mobile operator or when the position of the vehicle after the accident does not allow connection to the native operator whose signal in the given location is weak and in particular conditions, i.e. when the vehicle is turned over and the GSM antenna is shielded by its body and/or local topographical conditions in which case, the propagation of radio waves is heavily limited and the use of another mobile network, that provides stronger signal is possible. At the current stage of works on the subject, the decision has not been reached yet, whether the SIM cards are to be installed in the vehicles or not. If the SIM cards were not to be used, a European wide harmonisation of regulations would be required in order to allow emergency notifications without the possibility of identification of the caller [4,16]

In order for the notifications generated automatically by eCall modules or those initiated manually to take effect, the PSAP centres must be equipped with appropriate technical means that would allow receiving emergency information, its efficient verification and processing as well as effective management of rescue resources.

Technical requirements – eCall car module

The device installed in the vehicles according to the specification in the working documents [1,2,5,18] of the expert bodies of European Commission, must perform the following functions:

- if the accident occurs, it should automatically decide (after predefined criteria of accident are satisfied) whether to initiate dialling sequence with emergency number 112,
- the system should provide possibility of manual initiation of dialling to PSAP centres with the use of easily accessible user interface; this implies the device should be equipped with button/keyboard to initiate dialling, its cancellation if activation is accidental as well as indicators of connection state (initiation, cancelling),
- the system should also allow sending the Minimum Set of Data required, which would identify the vehicle and circumstances of accident occurrence.
- initiation of the voice connection when dialling the emergency number 112 should be allowed.

At the current stage of works within the expert groups, a decision whether to install additional independent GSM modules with the emergency sensors in the vehicles or if to allow the use of mobile phones and SIM cards owned by driver/passengers has not been finally reached yet. From the technical point of view, the second choice is possible, from the economic perspective it seems even more plausible since it would decrease the general costs of the system introduction. However, there are also significant technical disadvantages of

this solution, which very likely will eventually cause its rejection.

The built-in GPS module allows the read out of current parameters of motion (geographical location, value and direction of speed) and it is required to transfer data on speed and direction of movement from the last three validly determined positions. In the communication protocol it was also agreed that the information on the quality of the determined position is to be transferred in order to estimate statistical uncertainty of the rescue calculated position.

Satellite navigation systems – GPS, Galileo, GLONASS

Currently, GPS (Global Positioning System) is the only fully functional system of satellite navigation, which was designed and constructed and is run by US Department of Defence in the framework of NAVSTAR programme.

Theoretically, as soon as in 1996, the full functionality of Russian system GLONOSS was announced, however, at the moment the number of working satellites in the orbit is less than the nominal 24, therefore, the system does not allow determination of position in any given time or area. In the worst period for the system (November 2001) due to the short life of the satellites, only six satellites were functional rendering the whole system useless. Now, the system consists of dozen or so of space vehicles located in two out of three planned orbits and there are plans to rebuilt the system to its full potential in the future.[18]

The third satellite navigation system, currently under development, is Galileo system. It is European project, financed by EU, being designed exclusively for civilian purposes (the other two systems depend on military structures, respectively of the US and Russia). The project also includes participants from outside EU, namely China, India, Israel, Morocco and Ukraine who have their share in co-financing. The future of the system as well as its completion date are still being hotly debated among its participants and regard mostly its financing and division of expected profits from its operation.

For the last few years there are plans to build a worldwide satellite navigation system GNSS (Global Navigation Satellite System), which would under the control of independent international organisation. Accession to the project was declared by the multitude of countries, including USA, Russia and EU member countries. During the first stage of GNSS development, the existing navigation systems are to be utilised, however, ultimately a completely new system of satellite navigation is to be constructed [9].

Every satellite navigation system consists of three segments: the ground segment, the orbitting vehicles and receivers which position is determined by receiver firmware. Currently, all of the systems in operation support passive receivers which means the user's receiver can calculate its own position, time as well as direction and velocity of the movement, based on the signals obtained from visible satellites only. In order to determine position it is vital to be able to receive navigational message from at least four satellites. The accuracy of positioning depends on many factors, among others, the number of visible satellites, their relative positions in the orbit and signal disruptions on the way from satellite to the receiver (these interferences are a result of refraction in the ionosphere, troposphere and multipath distortions of signal – receiving signals indirectly from satellites, reflected from various obstacles and object in the vicinity of the receiver).

Table 1.
Comparison of satellite navigation systems accuracy [7,9]

Parameter	Satellite Navigation Systems		
	GPS	GLONASS	Galileo
Accuracy of horizontal positioning (95%)	100m (with SA distortion) 13-36m (without SA distortion) 3,7m (after modernisation - GPSIII)	30-40 m (50-70m according to spec.)	15/4 m ≤0,8-7 m
Accuracy of vertical positioning (95%)	300m (with SA distortion) 22-77m (without SA distortion) 7m (after modernisation - GPSIII)	60-80 m (70m according to spec.)	35/8 m ≤1-15 m
Accuracy of determining speed (95%)	≤2m/s	-	20cm/s - 50cm/s
Time (95%)	340ns	1 µs	50/30 ns

All of the currently existing and planned satellite navigation systems provide free of charge and unlimited access to public services, on the assumption that determining of the position is done automatically by the navigation receiver. In case of the augmented navigation systems, when the calculation of the position of the given receiver is done externally and sent back to the user or corrective data indispensable for differential GPS is sent, such services may be payable.

The satellite navigation system enables its operators to selectively turn off public availability of the service (e.g. in the area of warfare), while providing unchanged accuracy of dedicated services to authorised users (i.e. military users). Due to the nature and importance of satellite navigation in the course of military activities, the systems are assessed as to their susceptibility to deliberate distortion of signals which is to disrupt the regular system use or to falsify its readings.

For the purpose of using satellite navigation in eCall system, the following features of the existing and planned systems seems vital: general accessibility of positioning services in the analysed area regarding both the geographical location and time (how often and for how long the service may be unavailable), accuracy of determining location, speed and time, sensitivity of the receivers regarding the strength of signal which translates into using the system in difficult conditions: in urban areas, in mountains and forests (e.g. between high buildings, in valleys, under trees the visibility of satellites is limited and so is the possibility of receiving the signal). Further technological development of the space segment of the navigation system (i.e. increase of strength of emitted navigation signals, more active satellites in the orbit, improved orbit models) as well as development of the receivers (new constructions of the antennas, increase of their sensitivity, improved algorithms for elimination of signal distortions) will allow in the near future to improve functional parameters of receivers, more accurate positioning also inside buildings, in the areas of intense vegetation or diverse topographical features.

In case of eCall system, the sensibility of the receiver may be of vital importance for determining the position of the vehicle after the accident, in particular, when the vehicle after the accident is turned over or under construction elements (bridge, flyover). However, the system assumes the constant work of the receiver and requires to send the three last correctly determined positions of the vehicle including the direction and speed. Therefore, in case of the unfavourable conditions it should be possible to send sufficient information regarding the place of the accident and position of the vehicle. Obviously this possibility depends on the GSM network signal availability.

In-vehicle unit eCall positioning sub-system testing

For the purpose of verification of the vehicle unit fitted into particular car under test set of procedures, devices and designated software has been developed. Two identical GPS sensors have been connected (fig.1) to the recorder (fig.2) which simultaneously records all the GPS data produced by the sensors. Using two independent sensors of known sensitivity, mounted on the top of the car is assumed to deliver reference level of possible signal reception in particular conditions during the test. If the signal is not available to branded GPS sensors fixed to the roof of the car, outside of its metal chassis, the technical feasibility of producing a high quality solution, i.e. characterised by low HDOP/VDOP/PDOP parameters, by in-vehicle unit shall not be overestimated. The prototype recorder capable of logging GPS and IMU (inertial measurement unit) data is depicted in figures 1 and 2. The data is recorded on a SD/MMC card, thus available capacity is sufficient and available memory space can be easily expanded if necessary.

Figure 1. The reference GPS sensors in set-up designed for verification of statistical robustness of the positioning subsystem of the in-vehicle eCall unit.

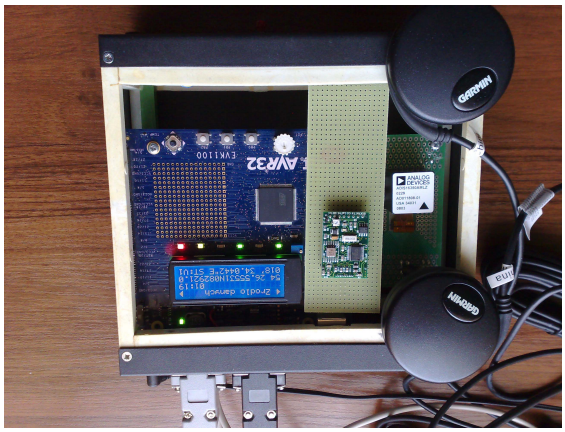

Figure 2. On-trip recorder designed for logging data from reference inertial measurement unit and two reference GPS sensors

To record the motion parameters of the vehicle output data stream of inertial measurement unit is used. In the prototype logger 6-DOF ADIS16350 has been utilised (fig.3) to produce reference stream of data to be compared with the eCall unit logged data. Data from the GPS sensors alone (both embedded in the eCall unit under test as well as in the reference sensor set) cannot be used for the purpose of attitude and trajectory determination for many different reasons, limited sample rate and continuity of signal availability among the most obvious ones, to list just two of them. In general raw data logged in in-vehicle eCall recorder cannot be easily used to retrace the vehicle trajectory. However combined information gathered from IMU and GPS can be seen as complete and sufficient to calculate the position and attitude, there are no legal requirements to facilitate in the eCall on-board unit algorithms to estimate the current parameters of the vehicle spatial attitude and heading, and without prior knowledge of used sensor parameters and performance it is generally impossible to reconstruct precisely the vehicle chassis trajectory, due to uncertain boundary conditions, unknown sensor stochastic noise parameters, and vehicle body dynamics. All the named information and noise characteristic of measurement channels and sensors is necessary to design a precise Kalman filter algorithm, the most commonly used family of algorithms to solve the problem of data fusion and processing of noisy, real-life data [6,7,8,14].

During the certification process it is to be manufacturer role to demonstrate how to use registered data to retrace the accident course, if claimed possible, or required by binding legal specification of minimal set of parameters and functional features of future eCall in-vehicle unit. The data registered by the reference tool is to verify the claim and to asses the precision of data and signals produced by eCall unit under test.

Figure 3. 6-DOF reference inertial measurement unit ADIS16350

The ADIS16350 inertial measurement unit is a 6-DOF sensor which consists of tri-axis (fig.3) accelerometers (+/-10g measurement range) and tri-axis gyroscopes (up to 300 deg/s digitally adjusted measurement range), producing data of 14-bit resolution in each measurement channel. The bandwidth of 350Hz, digitally controlled bias calibration, sample rate and filtering, with embedded temperature sensor sum up to a very convenient solution for motion control and analysis applications. If during the course of experiments the necessity of higher precision of measurement of accelerations emerge, there are compatible inertial measurement units available and tested in the set-up, featuring higher precision at the expense of a lower acceleration range.

GPS sensor sensitivity and performance assessment

In order to test statistical quality of the signals received by GPS sensors, data collected during the relatively long trip was evaluated statistically. In figure 4 there are showed short periods of precision parameters logged during the trip depicted in fig. 5. The VDOP, HDOP, PDOP (Vertical-, Horizontal-, Position Dilution of Precision) strongly correlate with the current number of satellites used in the fix.

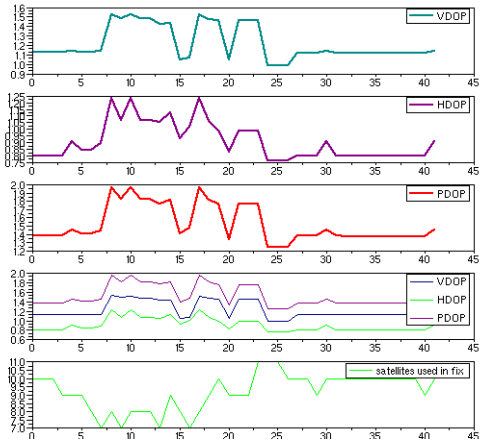

Figure 4. Quality of the GPS solution differs with current local conditions, with main factor being the number of available satellites used in the fix.

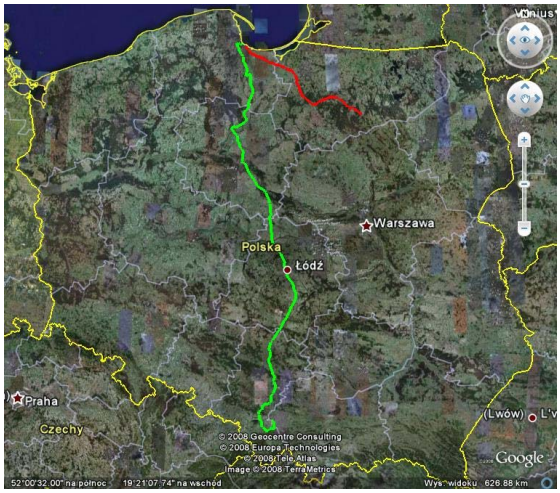

Figure 5. Two example registrations taken with the trip logger to gather data for statistical analysis referred to in the text and the following diagrams.

The higher the number, the more precise the navigational solution, however it depends also on the relative position of space vehicles used in the solution. In order to obtain good quality of the solution from minimal number of satellites, they had to be uniformly dispersed in the orbit, from the observer/receiver standpoint. Diagrams presented in fig. 6 depict histograms of satellite number used in solution during the test trip and related histograms of PDOP. Pairs of diagrams present data collected on the same route – upper two diagrams Southbound trip, and the lower two on the way back, Northbound. On the way Southwards most of the time eight or nine satellites were present and used in the fix, with considerable fraction of time when ten and eleven satellites available. On the way Northwards even better coverage of GPS signal has been registered, as for over 60% of time there were nine and more satellites available, frequency almost evenly spread for nine, ten and eleven satellites. That produced good PDOP distribution, of the value of 1.0 for most of the time, and negligible frequency for PDOP values above 2. In figure 7 the example of mapping the logged data is presented. It can be easily noticed that due to inadequacy of freely available Google map service, or GPS precision issues, or both the precision in mapping easily can be lower than a few meters, which agrees well with technical specification.

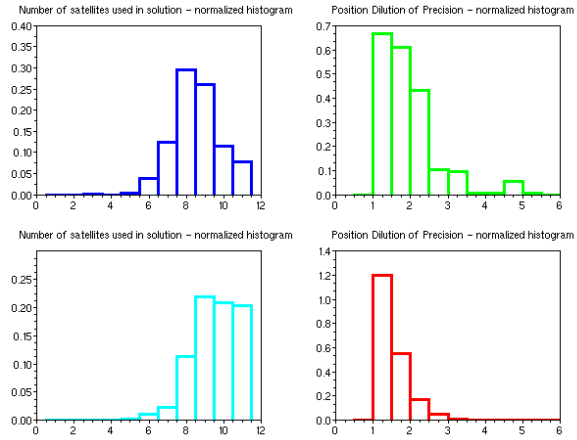

Figure 6. Histograms of satellite number and responding PDOP (Position Dilution of Precision).

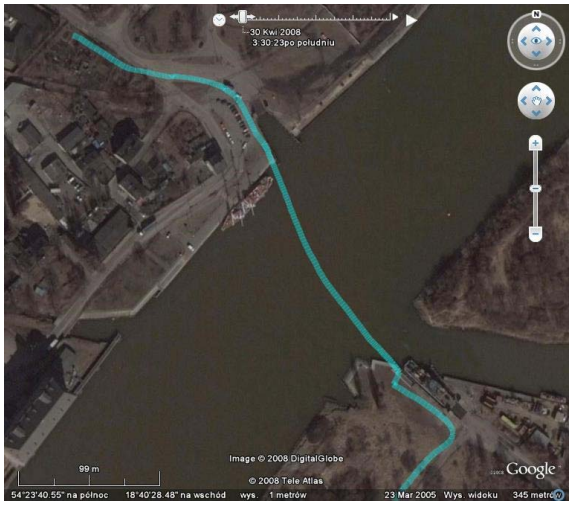

Figure 7. Example of inaccuracy of GPS mapping.

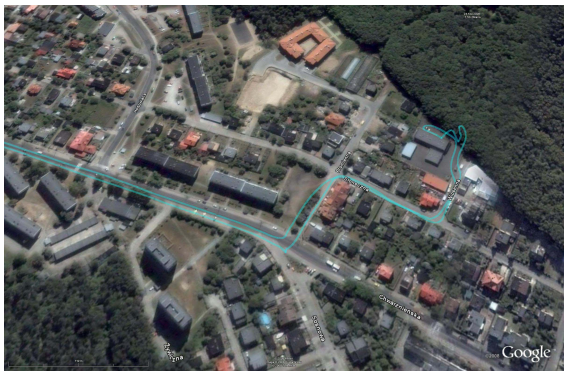

Figure 9. GPS logged data mapped in urban environment of low intensity

In figure 9 GPS signal was mapped on an aerial map, where again inaccuracy of a few meters is noticeable and repeatability of measurements far from ideal, even if the experiment was conducted in an urban area where no high buildings nor heavy vegetation were present. Additionally, there is tangible instability in GPS sensors read-out close to the final u-turn of the test ride, where bigger lost of precision has been observed. This demonstrates limit of potential trajectory reconstruction on the base of GPS output alone.

Data transmission

The basic difference between eCall system and E122 is the principle that the system should automatically detect the emergency event and send sufficient data to the PSAP centre. The data has to be transmitted on the main voice channel i.e. during the established connection with the operator. In the past, there were considered also other models of data transmission in GSM systems, such as GPRS or SMS. However, due to various reasons (reliability, limited accessibility, time required for connection different than voice connection in case of GPRS) these solutions were disqualified and currently the EU expert working groups consider the use of in-band modem technology or other similar systems of transmission at the beginning or during voice connection.

In the specification of the eCall car module there was defined the Minimum Set of Data (MSD) which the emergency sensor installed in the vehicle has to send in case of an accident. During the next development stage of eCall system it is expected the amount of data to be sent will increase and covey more information concerning the course and effects of the emergency event, which will influence the optimisation of the rescue operation. The additional data will concern number of passengers in the vehicle at the moment of the accident, the force of the impact, acceleration values, velocity change at the moment of the accident and thus it will allow estimation of the possible level of injuries. If these data and other will exceed 120 bites of MSD will be sent as Full Set of Data (FSD).

Certification of eCall system components

Certification of eCall system components is crucial, since their excessive sensibility (generation of false alarms) will cause the increase of the maintenance cost of the entire rescue system in EU. On the other hand, insufficient sensibility of the components will influence the whole system which will fail to meet the expectations as to diminishing the fatality rate of the road accidents.

Therefore, during the certification process, accuracy of sensor modules performance should be measured as well as their functionality in vehicles (do they meet the high technological criteria of the automotive industry). During these examinations it is necessary to measure the susceptibility of these devices to electromagnetic interferences, i.e. electromagnetic compatibility, as well as to measure their distortion emissions. What's more, the devices should undergo climatic research in order to determine their performance proprieties within the required temperature range i.e. -40 to +85°C.

The algorithms for emergency event detection should be assessed separately. In the first version of the documents announced to the public on EU web pages, the certification process was to be carried out by the producers of vehicles and realised based on the existing legislation regarding homologation of vehicles. However, currently, due to the recent arrangements, the independent suppliers may produce and install the sensors, therefore, a detailed technical specification is required, also test and research methods should be elaborated in order to be able to verify eCall modules.

Detection of the accident. Assessment of the potential injuries.

In order to detect accidents, there are used signals from available or specially installed linear acceleration sensors (accelerometers) and angular

acceleration sensors (gyroscopes), magnetometers (compasses) but also from conventionally installed acceleration sensors in the vehicles. In most vehicles that are equipped with airbags, two-axis acceleration sensors are used to activate the bag, which allow determining e.g. delta velocity, that is commonly regarded as an effective estimator of potential accidents results.

Regrettably, having at your disposal the two-axis acceleration sensor does not allow outlining the full trajectory of vehicle movement, moreover there are justified doubts whether it will be possible to even detect the turnover of the vehicle. In accordance with the EU statistics [14] only 0.2% of vehicle sold in Europe is equipped with sensors determining turnover of the vehicle. Due to the cost of the essential devices (gyroscopes) which would have to be installed in each eCall sensor, at the current stage of research, in order to determine the position of the vehicle after the accident, only acceleration sensors are being considered when developing eCall system since they are already installed in the vehicles to initiate airbags.

Among potential applications of eCall, which directly result from the fact of registration and data collection regarding the accident, there is the attempt to use these data to reconstruct the course of the accident, identify its main causes and the guilt of the accident participants both in minor events and in case serious road catastrophe. The usefulness and reliability of collected data regarding reconstruction of the events should be the subject of further research and analysis. Other important issue is legislative aspects of the collected data use, who is their owner, who is allowed and in what way should access and analyse the data, can the vehicle owner reject data availability, what procedures should be used when the data is purposely destroyed, etc. Law enforcement bodies as well as insurers should definitely be interested in these data.

Testing the eCall module using vehicle model

To produce motion to excite both reference measurement system and the device under test a remotely controlled vehicle model has been adopted. The model (fig.10) previously used by authors for testing the “black-box” recorder [10] has been upgraded and equipped with new sensors and new control system to facilitate extensive tests of eCall in-vehicle module.

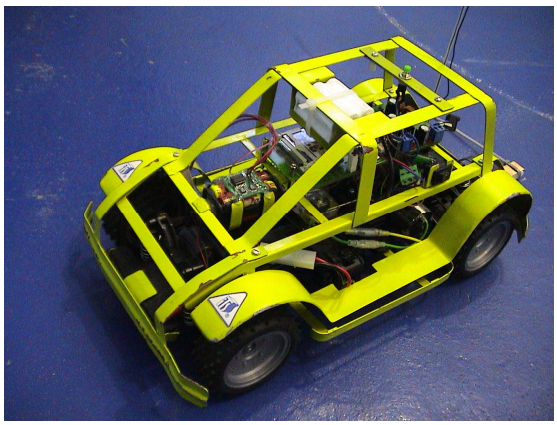

Figure 10 . Vehicle model

Previously the model was controlled by “classical” remote controller equipped with two potentiometric manipulators (one for speed and one for direction control), now the control on-board the model is effectuated by 32-bit Freescale micro-controller receiving commands via wireless Zigbee link from the PC based application. This allows to produce repeatable, pre-programmed control sequences, for instance designed as Scilab scripts, allowing for visualisation of data gathered during the tests. Optionally it is possible to use game console connected to the PC USB port to allow controlling of the model with the use of steering wheel, and accelerator and brake pedals. The model on-board controller is responsible for maintaining precise control over the model vehicle, i.e. close-loop algorithms ensure following precisely pre-programmed trajectory at pre-programmed vehicle velocity. All the motion parameters are logged in the model controller memory.

To produce higher velocities and to allow of testing of bigger and heavier eCall modules more robust and more powerful model driven by combustion engine also has been equipped with similar set of equipment, remote controller link and actuators.

The first couple of tests have been carried out without any eCall in-vehicle unit as there weren't any available for tests at the time of writing. Data was only registered in the reference data acquisition system. The electric-motor-driven car model was directed towards concave ramp to force a roll-over accident (fig.11). Only data from model IMU has been logged, no GPS sensor data was collected nor analysed, due to the fact that the

experiment was conducted inside the building, the ride duration was considerably shorter and the reached velocities was tangibly lower than anticipated in the real-life conditions preceding an accident. However, the IMU registered data is expected to be relevant to real-life conditions, even at lower velocities, due to smaller dimensions and lower weight and moments of inertia of the model. Some data have been also logged on the real passenger cars, commercial good vehicles and coaches, to verify dynamics of registered signals, both on the models and real vehicles.

In following experiment the model has also been driven with marking its trace piece of chalk (fig.12), to allow to assess the reliability of collected data for the purpose of accident course reconstruction.

Figure 11. Selected consecutive video frames featuring a rollover

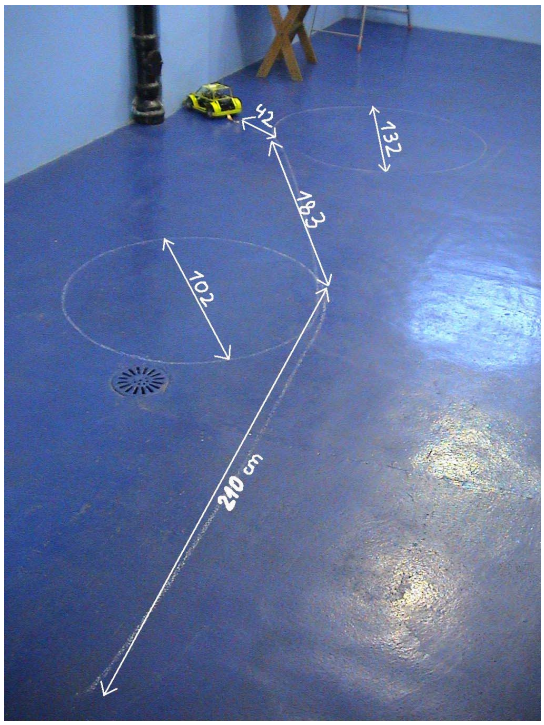

Figure 12. A trajectory reconstruction test

CONCLUSIONS

Many publications express the necessity of further research on accident detection and severity estimation algorithms, as deep understanding and wide availability of complete and robust solutions is far from satisfactory. In order to fully explore all possible benefits that can be brought by eCall implementation within the EU territory, not only well designed algorithms to detect the accident and estimate its severity are required, but also legal framework, methods and technical means to allow the formal authorisation of all the devices and systems (in-vehicle units, telecommunication and GNSS infrastructure and the public, emergency answering point network, both equipment and organisation performance). Without verification and certification before the legal approval is granted to introduce such devices to operation, if it leads to approval of devices producing false alarms or failing to recognise the actual accident, the chaos sparked by the eCall implementation could jeopardise all the hopes and expectations in reducing severity of injuries and number of fatalities.

REFERENCES

[1] Bouler Y., et. al., Clarification Paper EG1-eCall Performance Criteria, Draft V14, 11 April 2006.

[2] Clarification Paper – EG.2. High level requirements for eCall In-vehicle system. Supplier perspective. Ver. 1.0.

[3] COMMISSION RECOMMENDATION of 25 July 2003 on the processing of caller location information in electronic communication networks for the purpose of location-enhanced emergency call services, C(2003) 2657, 2003/558/EC

[4] eCall – saving lives through in-vehicle communication technology, European Commission, Information Society and Media leaflet, czerwiec 2007.

[5] European e-Call functional specifications In Vehicle System, Working Document ver. 1.1., Vehicle Functionality Working Group (ECIV).

[6] Grewal M. H., Andrews A.P., Kalman Filtering, Wiley 2001.

[7] Grewal M. H., Weill L. R., Andrews A.P., Global Positioning Systems, Inertial Navigation, and Integration, Wiley 2007.

[8] Huang M., Vehicle Crash Mechanics, SAE International CRC Press 2002.

[9] Januszewski J., Systemy satelitarne GPS, Galileo i inne, Wydawnictwo Naukowe PWN 2006.

[10] Merkisz J., Boguś P., Wrona A.: Using Signals of Registered Linear and Angular Acceleration to Reconstruct the Trajectory of Vehicle's Movement. European Automobile Engineers Cooperation 2003, 9th EAEC International Congress "European Automotive Industry Driving Global Changes", Paris 16-18.06.2003.

[11] P. Boguś, J. Merkisz, S. Mazurek, R. Grzeszczyk. Application of GPS and other ORD sensors to detection of the vehicle state. CD Proceedings of FISITA 2008 World Automotive Congress, 14-19 September, Munich, Germany, p. 1-8 (Book o Abstract, World Atomotive Congress 2008, str. 247).

[12] P. Boguś, J. Merkisz, S. Mazurek, R. Grzeszczyk. Detection Of Critical Situations In Rail Transport Using Ord Motion Parameters. CD Proceedings of the 10th International Conference on Application of Advanced Technologies in Transportation, Athens, Greece, May 28th 30st, 2008, p. 1-10.

[13] P. Boguś, J. Merkisz, S. Mazurek. The Proscpect of Artificial Intelligence Methods in Identification and Prevention of Criticial Railway Accidents. In: L. Rutkowski, R. Tadeusiewicz, L. Zadeh, J. Zurada (eds.). Computational Intelligence: Methods and Applications. EXIT, Warsaw 2008, p. 445-453.

[14] Simon D., Optimal State Estimation, Wiley 2006.

[15] The 2nd eSafety Communication: Bringing eCall to Citizens C(2005) 431

[16] The Communication on ICT for safe and intelligent vehicles C(2003) 542

[17] The Council Decision on the introduction of a single European emergency call number (91/396/EEC)

[18] www.esafetysupport.org

A COMPARISON OF COMPUTER MODELING TO ACTUAL DATA AND VIDEO OF A STAGED ROLLOVER COLLISION

Stanley B. Andrews MS,
Phillip Mark Partain MS,
David A. Renfroe Ph.D. PE
The Engineering Institute
Michael Gilbert PE
Gilbert Engineering LLC
USA
Paper Number 09-0346

ABSTRACT

Vehicle accidents in which the automobile "rolls over" or overturns are among the most difficult accidents to reconstruct. Vehicles typically overturn about their longitudinal axis and in highway speed rollovers can overturn multiple complete revolutions. The accident reconstruction specialist is left to piece together the incident from physical evidence produced both on the vehicle and at the accident site. A number of works have been published by various authors detailing the methods for calculating many aspects of the accident. Using these methods the reconstruction professional is obliged to illustrate and present the accident using two-dimensional or three-dimensional drawings to illustrate the accident. One can also use such a diagram to produce an animation of the accident. These animations are based on one's own conceptualization of the accident as physical evidence reveals, but they are not the result of the extensive time step calculations of vehicle dynamics that can be done with computer reconstruction software.

As the computer has become more powerful and faster, physics based modeling programs have been developed to aid the reconstruction professional with the analysis of automobile accidents. For the most part, accident reconstruction software packages do not contain detailed component/suspension modeling capability. However, for the purposes of accident reconstruction, the models in these software packages are more than sufficient to model an accident scenario such as a vehicle tumbling or rolling over.

In this paper, a reconstruction of a staged rollover accident involving an SUV type vehicle will be presented. The subject rollover is a staged un-tripped rollover. The test vehicle overturns because of frictional forces at the tires imparted by steering inputs. This rollover is modeled using PC Crash™. The test site was well documented after the event and pertinent physical data was recorded. Damage produced on the vehicle as a result of the rollover is also well documented. Numerous video cameras were used to record the rollover from a variety of vantage points. All of this information is used in conjunction with the software to demonstrate how properly used software can effectively model a rollover accident. If rollover accidents can be accurately modeled, then the data may be used in developing vehicle safety and occupant protection systems.

INTRODUCTION

In recent years rollover accidents have become more significant in number. Computer modeling is becoming more widely used for the reconstruction of rollover accidents. PC-Crash is a modeling program which is able to simulate the vehicle motion during rollover events. The accuracy of any accident reconstruction depends heavily on the available evidence used in analyzing the event. The accident reconstruction professional is obliged to ascertain whether sufficient information is available to draw whatever level of conclusions are desired.

Over the past years modeling programs have become powerful tools to aid in determining vehicle and occupant motions. PC-Crash is just one of the programs which have gained popularity over the past few years. PC-Crash has been validated in many studies and has proven its accuracy and capability (1-3). Studies have even shown that occupant motion can be determined by coupling PC-Crash and MADYMO (4). The majority of these studies have not necessarily included rollovers.

Although rollover accidents are among some of the most difficult to accurately reconstruct, PC-Crash has been found capable of determining vehicle paths, timing, number of rolls and most relevant rollover parameters (5). In this study, the vehicle motion prior

to and during the rollover event is determined using PC-Crash, version 7.3.

Rollover simulations to model occupant kinematics have been published in peer reviewed publications as early as 1984 (6). Shortly thereafter three-dimensional rollover modeling of occupant kinematics using ATB and MADYMO begin to appear in publication (7-9). Next, complete vehicle and occupant kinematics were modeled within MADYMO and demonstrated a good match to FMVSS 208 test data.(10,11). The combined use of MADYMO and a separate vehicle dynamics prediction program approach appeared in publication in 1999 (12) Direct simulation by extracting vehicle motion and accelerations from NTSHA crash data has been limited due to the unreliable data rendered by the rollover crash sensing for these tests (13). This difficulty in rollover crash sensing was acknowledged and addressed by Viano, et. al. in a research program aimed at defining rollover sensing requirements to activate belt pretensioners, roof-rail airbags and convertible pop-up rollbars. (14) Here is an interesting excerpt:

Throughout the [research] program, mathematical simulation was used to assure robust testing, sensing and algorithms. The mathematical models were applied to each specific test condition, validated and used for evaluation of parameters influencing rollover sensing requirements. The simulations were found to be robust representations of a vehicle rollover. Two simulations tools were used: PC-Crash, which simulates vehicle dynamics and the rollovers, and Madymo, which simulates occupant kinematics in the vehicle. Madymo allows the quick study of various safety systems to prevent ejection and interior impact injury. **Excellent comparability was demonstrated between the tests and simulation.** [Bold Emphasis Added]

In this study, a staged rollover collision is reconstructed using a computer simulation program known as PC-Crash. The results of the PC-Crash reconstruction were compared to results from a conventional hand reconstruction and data collected from the staged rollover collision. The hand reconstruction has been published in Collision magazine. (15)

PC-CRASH MODEL

PC-Crash utilizes physical vehicle data that can be obtained through several databases or data that can be actual measurements. Once the vehicle data has been entered, *sequences* are used to define braking/acceleration, steering, friction parameters, or vehicle geometry changes. These sequences are used to model the vehicle as it moves over the intended path.

The test vehicle for this event is a 1991 Ford Explorer XLT, 4-door, 4X2. The VIN is 1FMDU32X5MUD76298. The vehicle is equipped with a 4.0 L V-6 and an automatic transmission. The vehicle is loaded with sandbag ballast of 150 lbs for each seating position for a total of 750 lbs. The tires are Goodyear Wrangler RT/S P235/75R15. The vehicle data used in the PC-Crash model are shown in table 1 found in Appendix A.

The model has been overlaid onto a very detailed survey of the rollover site. This survey was performed with a Total Station type laser device and documents tire marks, scrapes, gouges, location of broken glass, and other pertinent information. The survey data was imported directly into PC-Crash.

SEQUENCES

PC-Crash uses sequences in order to provide inputs to the model and re-create the accident scenario. These sequences specify the vehicle steering, drag factors, timing, and other parameters, such as geometry changes to be input for the simulation.

- Sequence 1: Starts the model at 50 mph and last for 0.6 seconds. No braking or steering is applied during the first sequence. This sequence allows the vehicle to approach the first set of yaw marks.
- Sequence 2: Applies left steer to match the first set of documented yaw marks. No braking is applied during the yaw marks. The sequence last for 0.38 secs.
- Sequence 3: This sequence last for 4.5 secs and applies right steer to match the final yaw marks leading up to the point of roll. Steering was applied at the same rate and magnitude as the steering input in the staged rollover. (note: steering remains constant throughout the rest of the rollover sequences.)
- Sequence 4: At the end of sequence 3, sequences 4 and 5 are activated. The left rear tire breaks off of the vehicle and the friction is increased to 1 at the left rear tire location in order to account for any axle gouging.
- Sequence 5: Is a geometry change at the left rear tire position that is used to simulate the left rear wheel breaking from the axle.

- Sequence 6: Is a time sequence used to separate sequence 5 and sequence 7. At the left rear tire position the brake force is set to 500% to simulate the broken off wheel. Steering remains unchanged.
- Sequence 7: Is a second friction change used to simulate the right front wheel breaking from the vehicle and at the same time, sequence 8 is activated.
- Sequence 8: Is a second geometry change used to simulate the right front wheel breaking off.
- Sequence 9: Is used to finish out the simulation. The time is set for 15 sec, the steering is constant and the same as sequence 3, and the braking force for the two broken wheel are set at 500% to prevent any possibility of rolling.

The data for the sequences are presented in table 2 in Appendix B.

The results of the simulation show the vehicle approaching the first set of yaw marks at approximately 50 mph. The vehicle is traveling approximately 43 mph at the point of roll. The vehicle then rolls 4 complete revolutions and comes to rest in an upright position. Figure 1 shows the motion of the vehicle as indicated by the PC-Crash simulation.

COMPARISON OF SIMULATION TO ACTUAL DATA

The results of the simulation were compared to the prior reconstruction and the actual data collected at the time of staged rollover. The data from each of the four rolls are compared in table 3 located in Appendix C. As can be seen in the table, the results of the PC-Crash simulation very closely correlate to the data and manual reconstruction results.

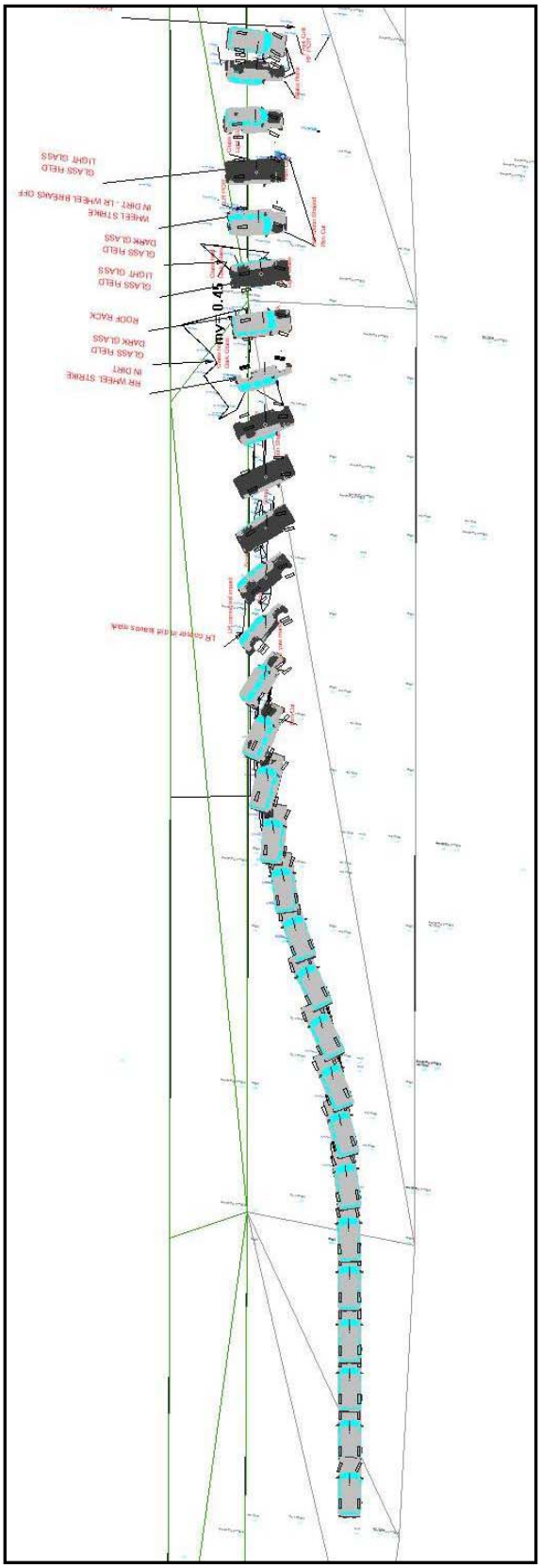

Figure 1: PC-Crash vehicle motion diagram.

PC-Crash was able to model the vehicle passing over the surveyed yaw marks. In figure 2 the heavy yaw marks are surveyed marks and the thin/light marks are yaw marks from the PC-Crash model. As can be seen in figure 2, the PC-Crash yaw marks very closely correlate to the surveyed yaw marks.

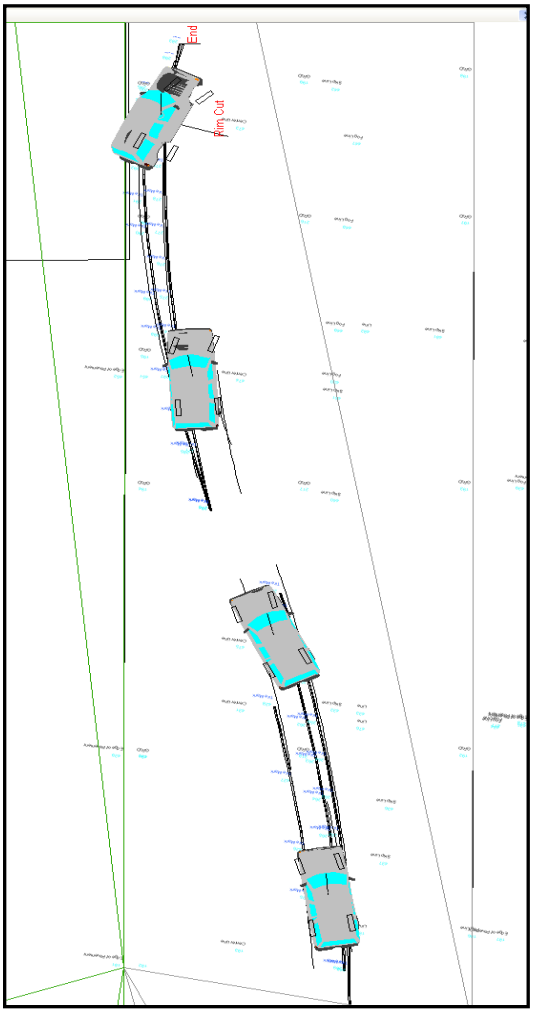

Figure 2: Vehicle positions during pre-roll yaw from PC-Crash. The heavy yaw

The following figures (*figures 3 through 6)* compare the position of each roll from the simulation to that of the hand reconstruction diagrams. The image on the top of each figure is the layout according to the hand reconstruction and the image on the bottom of each figure is from the PC-Crash output. In general, the positions during the rollover sequences are consistent. However, as can be seen, the angle of the vehicle varies in agreement between the two.

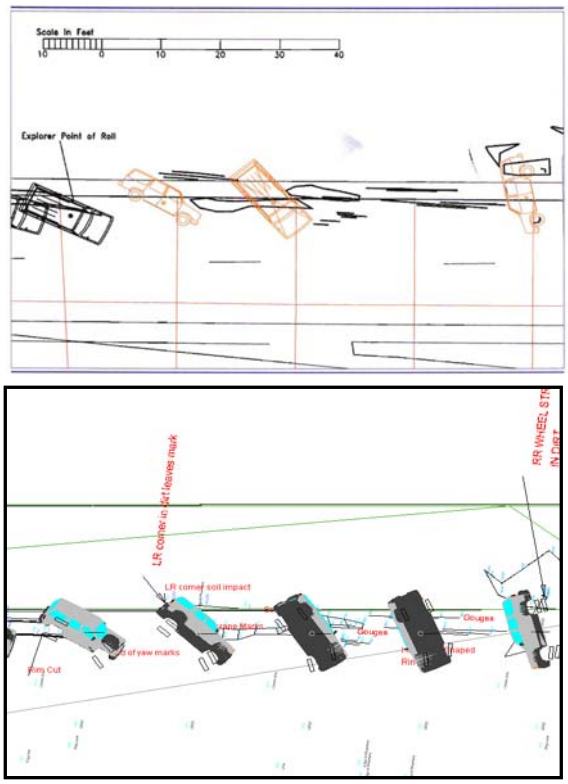

Figure 3: Roll 1 of the rollover sequence. Hand reconstruction results above and PC-Crash output below.

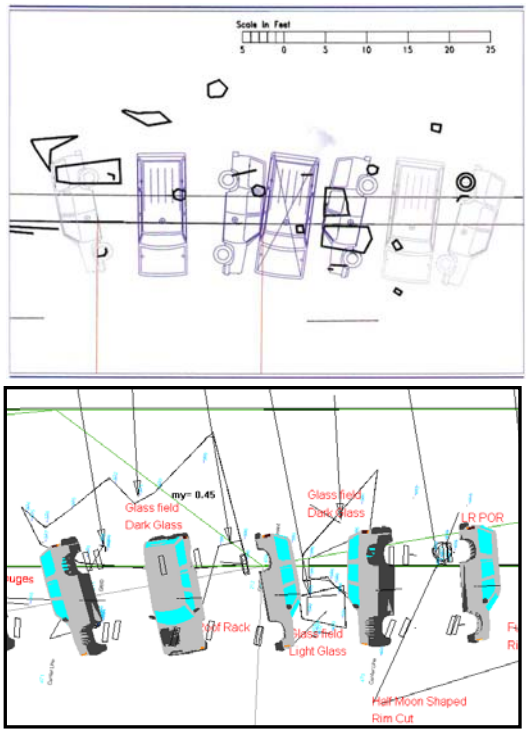

Figure 4: Roll 2 of the rollover sequence. Hand reconstruction results above and PC-Crash output below.

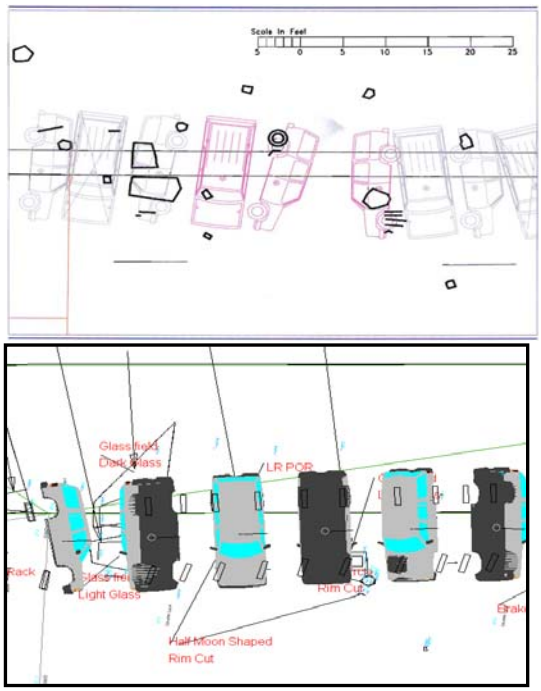

Figure 5: Roll 3 of the rollover sequence. Hand reconstruction results above and PC-Crash output below.

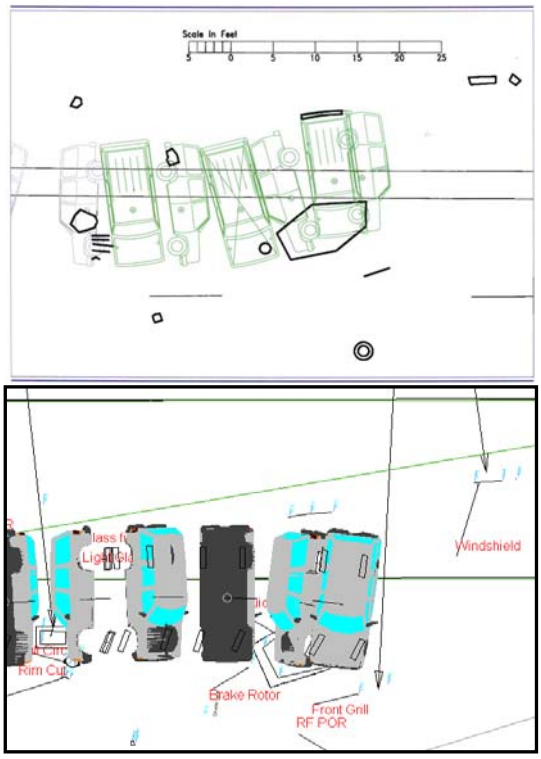

Figure 6: Roll 4 and the final rest position of the rollover sequence. Hand reconstruction results above and PC-Crash output below.

PC-Crash generates data and graphs of pertinent reconstruction results such as yaw rate, roll rate, acceleration, and other information. Yaw rate and roll rate were compared to actual data collected during the staged rollover. The figures below show the comparison of the data presented in the form of graphs.

As can be seen in figure 7 the yaw rate during the first yaw (left hand yaw) from PC-Crash very closely matches the data collected during the staged rollover. The data comparison of the second yaw (right hand yaw) shows that PC-Crash produced a slightly higher yaw rate than the actual data suggested. This is also shown in figure 2 with the left rear wheel of the model tracking just outside the surveyed yaw marks.

Figure 8 compares the roll rate from recorded data and PC-Crash. It should be noted that the roll rate exceeded the capability of the instrumentation at 350 deg/sec. PC-Crash indicates that the peak roll rate was approximately 520 deg/sec., and occurred during the time when the instrumentation clipped data at the maximum. The graph shows that PC-Crash data

closely matched the actual data before and after the truncation at 350 deg/sec.

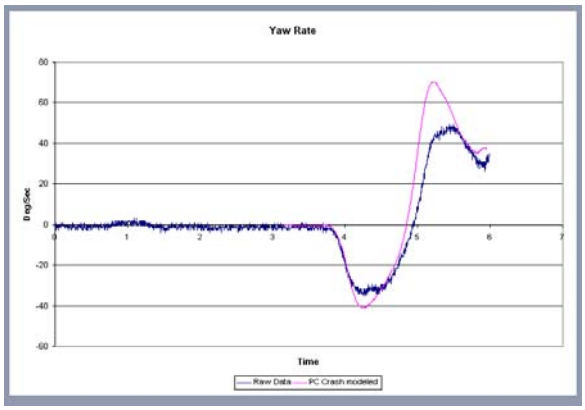

Figure 7: Yaw rate comparison of data from staged rollover and PC-Crash model.

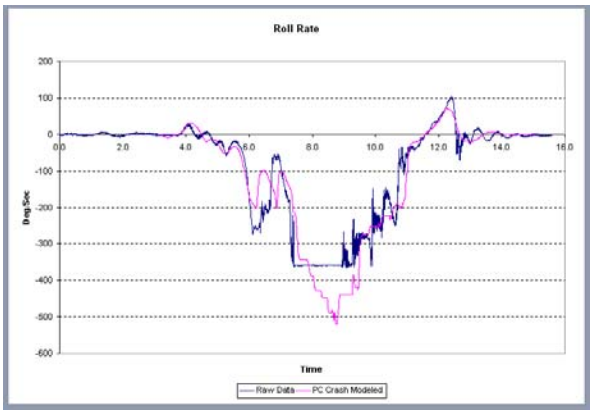

Figure 8: Roll rate comparison of data from staged rollover and PC-Crash model.

An additional feature of PC-Crash is the ability to produce real time videos of the simulation. Figures 9 and 10 compare the video frames of the PC-Crash simulation to videos of the actual staged rollover.

Figures 9 and 10 illustrate the comparison of the vehicle positions at the Point of Roll and the Point of Rest, respectively. In the PC-Crash model, the vehicle comes to rest at the documented Point of Rest. However, the final rest position in PC-Crash is approximately 15 deg clockwise of the documented Point of Rest for the staged rollover.

Figure 9: Compares the Point of Roll form PC-Crash (upper image) to an actual video frame of the rollover (lower image).

Figure 10: Compares the Point of Rest form PC-Crash (upper image) to an actual video frame of the rollover (lower image).

CONCLUSIONS

PC-Crash was successfully utilized to reconstruct the staged rollover collision. The PC-Crash reconstruction showed the speed of the vehicle at the point of roll to be within 2.1 mph of the actual data. The number of rolls and the vehicle path during the yaw phase and the rollover phase were consistent between PC-Crash and the collected data.

There were slight deviations in the vehicle position angles throughout the rollover sequences. However the vehicle locations were consistent with the hand reconstruction and evidence documented in the survey.

The yaw rate recorded in PC-Crash was slightly higher than data suggested but followed similar trends. Roll rates calculated by PC-Crash also followed similar trends as the actual data collected during the rollover.

Although the final point of rest in the PC-Crash model was consistent with the surveyed data, PC-Crash showed the vehicle point of rest rotated approximately 15 deg clockwise of the documented point of rest.

In general, PC-Crash was able to accurately reconstruct the staged rollover collision based on the surveyed data. When compared to actual data, PC-Crash data followed similar trends and was consistent with data collected during the staged rollover collision.

ACKNOWLEDGMENTS

The authors would like to acknowledge the following for participating in the testing, collection of data, and analysis of the staged rollover test: Accident Reconstruction Services, Inc., Mechanical Forensics Engineering Services, LLC, Mechanical Systems Analysis, Inc., Ponderosa Associates Limited, and Wilson Consulting, LLC.

References

1. Cliff, William, and Andreas Moser. *Reconstruction of Twenty Staged Collisions with PC-Crash's Optimizer.* Maclnnis Engineering Associates. SAE 2001-01-0507. 2001.

2. Cliff, William, Darcy Montgomery. *Validation of PCCrash-A Momentum- Based Accident Reconstruction Program*. Maclnnis Engineering Associates. SAE 960885. 1996

3. Moser, Andreas, et al. *Validation of the PC-Crash Pedestrian Model*. DSD Linz. 2000.

4. Steffan, Hermann, Andreas Moser and B. C.Geigl, *A New Approach to Occupant Simulation Through the Coupling of PC-Crash and MADYMO," Graz University of Technology*. SAE 1999-01-0444. 1999.

5. Steffan, Hermann, Andreas Moser, *How to Use PCCrash to Simulate Rollover Crashes.* SAE 2004-01-0341. 2004.

6. Robbins, D.H. and D.C. Viano. *MVMA 2-D Modeling of Occupant Kinematics in Rollovers.* SAE 840860, 1984.

7. Obergefell, L.A., I. Kaleps, and A.K. Johnson. *Prediction of Occupants Motion During Rollover.* SAE 861876, 1986.

8. Ma, D., A.L. Rizer, and L.A. Obergefell. *Dynamic Modeling and Rollover Simulations for Evaluation of Vehicle Glazing Materials.* SAE 950050. 1995.

9. Cheng, H., A.L. Rizer, and L.A. Obergefell. *ATB Model Simulations of a Rollover Accident With Occupant Ejection.* SAE 950134. 1995.

10. Renfroe, D.A., J.F. Partain, J.F. and J. Lafferty. *Modeling of Vehicle Rollover and Evaluation of Occupant Injury Potential Using MADYMO. S*AE 980021. 1998.

11. Renfroe, D.A. and J.F. Partain. *Modeling of Occupant Impacts During Rollover Conditions.* SAE 2000-01-0854. 2000.

12. Bardini, R. and M. Hiller. *The Contribution of Occupant and Vehicle Dynamics Simulation to Testing Occupant Safety in Passenger Cars During Rollover.* SAE 1999-01-0431. 1999.

13. Martin, Mark R. and Kerry Allen. *A Comprehensive Evaluation of NHTSA Rollover Test Data For Use In Computational Model Validation.* ASME IMECE 2004-60809. 2004.

14. Viano, David C. and Chantal S. Parenteau. *Rollover Crash Sensing and Safety Overview.* SAE 2004-01- 0342. 2004

15. Wilson, Lawrence A., Gilbert, Michael, Godrick, Daniel A. *Reconstruction and Analysis of Steering-Induced, On-road, untripped SUV Rollover Test*, Collision, Vol 2, Issue 1, 2007

APPENDIX A

Table 1:
PC-Crash input data

Length [in] :	184
Width [in] :	70
Height [in] :	67
Number of axles :	2
Wheelbase [in] :	112
Front overhang [in] :	30
Front track width [in] :	59
Rear track width [in] :	59
Mass (empty) [lb] :	4142
Mass of front occupants [lb] :	303
Mass of rear occupants [lb] :	457
Mass of cargo in trunk [lb] :	0
Mass of roof cargo [lb] :	0
Distance C.G. - front axle [in] :	55.91
C.G. height above ground [in] :	28.75
Roll moment of inertia [lbfts^2] :	513.2
Pitch moment of inertia [lbfts^2] :	2875.5
Yaw moment of inertia [lbfts^2] :	2732.5
Stiffness, axle 1, left [lb/in] :	175.7
Stiffness, axle 1, right [lb/in] :	175.7
Stiffness, axle 2, left [lb/in] :	175.11
Stiffness, axle 2, right [lb/in] :	175.11
Damping, axle 1, left [lb-s/ft] :	237.19
Damping, axle 1, right [lb-s/ft] :	237.19
Damping, axle 2, left [lb-s/ft] :	236.4
Damping, axle 2, right [lb-s/ft] :	236.4
Max. slip angle,axle 1, left [deg]:	10
Max. slip angle,axle 1, right [deg]:	10
Max. slip angle,axle 2, left [deg]:	10
Max. slip angle,axle 2, right [deg]:	10

APPENDIX B

Table 2:
PC-Crash sequences

Sequence 1	
Velocity [mph] :	50.5
Time [s]	0.6
Brake force [%]	0
Sequence 2	
Time	0.38
Brake force [%]	0
STEERING	
Steering time [s] :	0.4
New steering angle [deg]	
Axle 1 :	13.34
Axle 2 :	0
Sequence 3	
Time [s]	4.5
Brake force [%]	0
STEERING	
Steering time [s] :	0.99
New steering angle [deg]	
Axle 1 :	-19
Axle 2 :	0
Sequence 4	
Friction change	
Friction coefficient (mu)	
Axle 1, left :	0.8
Axle 1, right :	0.8
Axle 2, left :	1
Axle 2, right :	0.45
Sequence 5	
GEOMETRY CHANGE	
Sequence 6	
Time [s]	0.95
Brake force [%]	
Axle 1, left :	0
Axle 1, right :	0
Axle 2, left :	500
Axle 2, right :	0
mean brake acceleration [g] :	-0.1
STEERING	
Steering time [s] :	0.99
New steering angle [deg]	
Axle 1 :	-19
Axle 2 :	0
Sequence 7	
Friction change	
Friction coefficient (mu)	
Axle 1, left :	0.8
Axle 1, right :	1
Axle 2, left :	1
Axle 2, right :	0.45
Sequence 8	
GEOMETRY CHANGE	
Sequence 9	
Time [s]	15
Brake force [%]	
Axle 1, left :	0
Axle 1, right :	500
Axle 2, left :	500
Axle 2, right :	0
mean brake acceleration [g] :	-0.2
STEERING	
Steering time [s] :	0.99
New steering angle [deg]	
Axle 1 :	-19
Axle 2 :	0

APPENDIX C

Table 3:
Comparison of manual accident reconstruction to PC-Crash

		Manual Reconstruction Results	PC-Crash Results
Roll 1	Speed at Point of Roll [mph]	44.8	42.7
	Distance [ft]	84	91
	Ave Speed [mph]	41	36
	Time [sec]	1.4	1.8
	Ave Roll Rate [deg/sec]	250	173
Roll 2	Distance [ft]	34	31
	Ave Speed [mph]	29	24
	Time [sec]	0.8	0.9
	Ave Roll Rate [deg/sec]	450	417
Roll 3	Distance [ft]	23	22
	Ave Speed [mph]	18	18
	Time [sec]	0.9	0.8
	Ave Roll Rate [deg/sec]	400	451
Roll 4	Distance [ft]	23	22
	Ave Speed [mph]	11	11
	Time [sec]	1.5	1.5
	Ave Roll Rate [deg/sec]	250	248

COMPUTERIZED CRASH RECONSTRUCTION OF REAL WORLD CRASHES USING OPTIMIZATION METHODOLOGY

Vikas Hasija
GESAC, Inc
Erik G. Takhounts
Stephen A. Ridella
NHTSA
United States
Paper Number: 09-0415

ABSTRACT

Computerized crash reconstruction of real world crashes involves dealing with a lot of unknown parameters and as such the reconstruction problem cannot be solved deterministically as was shown using a parametric methodology presented in our previous ESV paper titled "Computational Analysis of Real World Crashes: A Basis for Accident Reconstruction Methodology." This paper introduces a modified version of the parametric methodology, which involves using an optimization scheme to derive an optimal solution for the reconstruction problem in a given range of unknown parameters. Real world crashes were selected from the CIREN database and were solved using the proposed methodology. Human-Vehicle-Environment (HVE) software was used to generate the crash pulse where EDR data were missing. The problem was set up in MADYMO. During the set up, the unknown parameters were identified. ModeFRONTIER software was used for optimization. The identified unknown parameters were treated as design variables. The objective function and the constraints were defined such that they minimize the differences in injuries and occupant-vehicle contacts between the real world data and the model prediction. Since the objective function has a great effect on the final solution, a normalized form of the objective function, weighted based on the AIS level of the injuries sustained by the occupant, was formed in this study. A genetic algorithm with Sobol DOE (Design of Experiments) was used for optimization. Results of the simulations showed that the optimal solution correctly predicted both the occupant-vehicle contacts and the injuries sustained by the occupant. By viewing the occupant motion inside the vehicle during the crash, better occupant protection systems can be devised. Correlation studies were also carried out to find the critical parameters affecting the solution. In addition, a best case scenario study was carried out to find, using optimization, the design changes that could help mitigate all or some of the injuries sustained by the occupant.

INTRODUCTION

Computerized crash reconstruction is carried out to investigate crash sequences and to study occupant kinematics during crashes. Occupant kinematics can then be used to design better and more efficient safety systems for occupant protection. There are a lot of parameters that affect an occupant's kinematics and injury risk. Due to lack of information on these parameters, the reconstruction cannot be carried out accurately. Since assumptions have to be made for these unknown parameters, it is imperative not to predict the model outcome using just one set of parameter values as different sets of parameter values within the range can lead to quite different injury predictions for the same case, as was shown in Hasija et al [1]. In the past, injury evaluation based on reconstruction has been carried out using just one set of parameters. For example, Mardoux et al [2] and Franklyn et al [3] presented papers where computational models used to predict injuries were driven using data obtained from physical tests. The experiments can have errors associated with them that can lead to errors in the model's injury predictions. The effect of these uncertainties was not analyzed.

Optimization, which refers to the study of problems in which one seeks to minimize or maximize a function by systematically choosing the values of variables from within an allowed set, while satisfying the constraints, is becoming more popular for carrying out crash reconstruction analysis. For example, Untaroiu et al [4] presented a paper that was used to investigate the application of optimization techniques to the field of crash reconstructions of pedestrian accidents. In their papers, it was shown, using a mock or "ideal" crash reconstruction problem, that optimization algorithms combined with an appropriate objective function have the capability to identify accurately the pre-impact conditions of the pedestrian and vehicle. The pre-impact parameters of pedestrian and vehicle models were treated as unknown design variables. In

addition, optimization methodology was successfully applied to reconstruction of a real-world pedestrian crash. Also, Shen et al [5] presented a paper evaluating optimization-based method for reconstructing pedestrian-vehicle accident and testing its performance. By reconstructing two real-world pedestrian collisions, they concluded that optimization is very effective in finding a optimum solution, which not only reduces the number of cycles, but also saves manual operation.

The objective of this paper is to present a methodology that utilizes an optimization scheme to come up with the best possible solution to a reconstruction problem, which has a lot of unknown variables that cannot be fixed to a particular value but are defined by a range. The best possible solution helps provide the occupant kinematics during crash. The methodology is shown by reconstructing two real world crash cases selected from the CIREN database [6]. These cases include: a) a "moderate brain injury" case, and b) a "severe brain injury" case. The unknown parameters are treated as design variables. The occupant-vehicle contacts and the injuries sustained by the occupant as listed in CIREN are used to set up the objective function and constraints for optimization. The best solution obtained for the reconstruction problem from optimization is one that matches all the occupant-vehicle contacts and injuries sustained by the occupant. The paper also shows how crirtical parameters are identified and how a best case scenario (minimum injury or no-injury) for a given case can be obtained.

METHODOLOGY

The methodology introduced in this paper (Figure 1) for reconstructing real world crashes uses an optimization technique to find the best possible solution to the reconstruction problem.

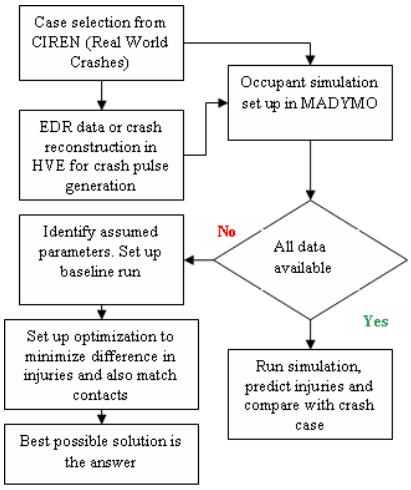

Figure 1. Optimization Methodology.

The methodology starts with the selection of a real world crash case from CIREN. Following the case selection, the Event Data Recorder (EDR) information available for the case is searched in CIREN to get the crash pulse. If the selected case has an EDR pulse available, the pulse is directly used for occupant simulation. If EDR pulse is not available, the crash details available from the case are used in HVE [7] to generate the crash pulse. Next, the occupant simulation is set up in MADYMO [8] based on the case information available from CIREN such as occupant information, restraints information etc. The EDR crash pulse or the HVE-generated crash pulse is used to drive the MADYMO model. During this set up, the data availability is checked to see if all parameters required for reconstruction are available. If all data is available, the occupant simulation set up in MADYMO can be run and the results can be compared with the real world data. But most of the time, all data required for reconstruction is not available. These unknown parameters are identified during the MADYMO set up stage and assumptions are made for these unknown parameters. Once the MADYMO model is set up, a baseline run is obtained by matching the occupant-vehicle contacts listed in CIREN for the particular crash case. Using these assumed parameters as design variables, the optimization is set up around the baseline run in modeFrontier software [9]. The range for these selected design variables is defined, the objective function is set up, and the constraints are defined. Two types of constraints are defined i.e. contacts based constraints and injury based constraints. The constraints and objective functions are defined such that they minimize the differences in injuries and occupant-vehicle contacts between the real world data and the model prediction. The solution obtained from optimization takes into account the variation in the assumed parameters, and thus gives the best possible answer to the reconstruction problem. The methodology is demonstrated by reconstructing two real world CIREN cases.

Case Selection

The real world crash cases were selected from CIREN. Only cases with single event, frontal impact with PDOF of 0 ± 10° and no rollover were considered. Cases were selected that provided enough information for reconstruction in HVE (vehicle type, collision partner involved, Collision Deformation Classification(CDC), Principal Direction of Force (PDOF), Crush and DeltaV) and also enough information for occupant simulation in MADYMO (age, height, weight of the occupant, occupant role (driver or passenger), restraints used, air bag information, seat performance information, etc). One

important criterion for case selection was good occupant-vehicle contacts that could be simulated. All cases with air bag failure, seat performance failure and seat belt failure were ignored. Cases where the occupant was asleep or in an out-of-position (OOP) states were ignored. In this study, only cases where the occupant had brain injury were considered. Only brain injury cases were selected so that these cases, in future, can be evaluated using NHTSA-developed finite element head model (FEHM). The cases were not filtered based on vehicle model year as the idea was to select cases and study the use of optimization as a reconstruction tool. Based on these criteria, two brain injury cases were selected.

"**Moderate Brain Injury" Case:** Details of the "moderate brain injury" case are provided below.

The crash occurred during the hours of daylight. The weather at the time of the crash was clear and dry. The posted speed limit was 45 mph. The crash occurred on a two lane roadway (Figure 2). Case Vehicle (V1, in red), a 1999 four-door Chevrolet Cavalier, was traveling eastbound. Vehicle two (V2), a 1997 four-door Oldsmobile Achieva, was traveling westbound. V1 crossed into the westbound lane. V1's front struck the front of V2. The impact caused V1 to rotate counterclockwise, coming to rest in the eastbound lane. V2 was forced to the right and rearward coming to rest off the shoulder of the westbound lane. The case vehicle had a delta-V of 35 mph.

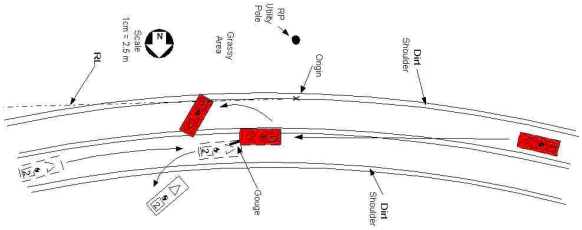

Figure 2. Crash Scene for "moderate brain injury" case

The case occupant was the driver of the vehicle (V1). The case occupant was a 61 year old male, 175cm in height and 86 kg in weight. He was wearing the available lap and shoulder belt and had frontal air bag deployment. The occupant sustained moderate brain injury (Table 1). The occupant also sustained AIS 1 injuries not listed in Table 1.

Table 1.
Occupant Injuries

AIS Code	Description
1610002	Cerebral concussion
5408243	Colon laceration, perforation
5420222	Mesentery laceration
8516143	Fibula Fx, bimalleolar

Occupant-vehicle contacts were taken from CIREN (Table 2).

Table 2.
Occupant-Vehicle Contacts

Contact	Component	Body Region
1	Air bag-driver side	Head
2	Steering wheel rim	Chest
3	Knee bolster	Knee-Left
4	Knee bolster	Knee-Right

"**Severe Brain Injury" Case:** Details of the "severe brain injury" case are provided below.

This crash occurred at night (with street lights) on the southbound lanes of a six lane divided freeway with dry conditions with a slight downgrade in the location (Figure 3). The posted speed limit was 60 mph. The case vehicle (in red), a 2006 Scion TC 2-door hatchback, was southbound in lane two of the three lanes and attempted to change lanes to the right and pass an unknown vehicle in lane two. Another unknown vehicle was traveling at a slower speed in lane one. V1 then swerved left and began braking as it crossed over lanes two and three before impacting the left side concrete barrier with the front of V1. V1 rotated slightly counterclockwise and came to final rest in lane three facing east. The case vehicle had a delta-V of 29 mph.

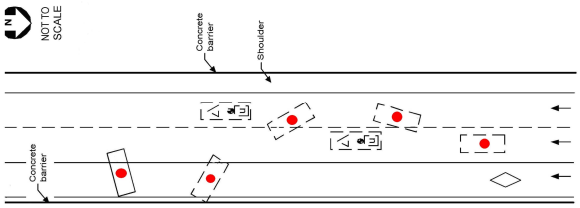

Figure 3. Crash Scene for "Severe Brain Injury" case

The case occupant was the driver of vehicle V1. The case occupant, a 27 year old male (178 cm in height and 69 kg in weight) was wearing the lap and shoulder belt with the seat belt pretensioners firing. The frontal steering wheel air bag as well as the knee bolster air bag deployed. The occupant rode down the deploying steering wheel air bag, causing the head to hit the steering wheel rim/hub. The occupant suffered severe brain injuries (Table 3). The occupant also suffered facial injuries and other AIS 1 injuries that are not listed in Table 3 as these were not considered in the analysis.

Table 3.
Occupant Injuries

AIS Code	Description
1406285	Cerebrum diffuse axonal injury (DAI)
1406843	Cerebrum subarachnoid hemorrhage
1504043	Vault skull fracture
8526043	Pelvis Fx
6506202	Lumbar Spine Fx, transverse process

The occupant-vehicle contacts were taken from CIREN (Table 4). Only contacts listed as "Certain" in CIREN were considered. "Probable" and "Possible" contacts were not considered in this study. This case was chosen particularly because the occupant sustained "diffuse axonal injury (DAI)", an injury which will be evaluated further using NHTSA developed FEHM and it was also the best-described case among all others.

Table 4.
Occupant-Vehicle Contacts

Contact	Component	Body Region
1	Steering wheel hub	Face
2	Steering wheel rim	Face
3	Knee air bag	Knee-Left
4	Knee air bag	Knee-Right
5	Knee bolster	Knee-Left
6	Foot controls	Right Foot

Crash Pulse Generation

The crash pulse generation for the two selected cases is described below:

"Moderate Brain Injury" case: For this case, the deceleration pulse of the case vehicle was available from the EDR. Since the selected case had a PDOF of 350°, there were both longitudinal and lateral components of the crash pulse. Since the EDR did not record any lateral component, it was estimated from HVE. The case was reconstructed in HVE. Not only the crash quantities were matched but also a consistent post impact motion, as given in CIREN crash analysis, was ensured. Generic vehicle models were selected for both vehicles. Both vehicle models were updated with respect to the exterior vehicle specifications: front overhang, rear overhang, overall length and width, wheelbase and weight. The exterior specifications for both vehicles were obtained from the CIREN case information. The total weight used was the sum of the "Curb weight," "Weight of the Occupants," and "Cargo weight." Vehicle stiffness plays an important role in correct crash pulse generation. Hence, the front, side, rear, top and bottom stiffnesses and the inertias of these generic vehicle models were updated based on the values available from actual vehicle models available in the HVE vehicle database. After the vehicle set up was completed in the vehicle mode, the crash event was set up in the event mode (Figure 4).

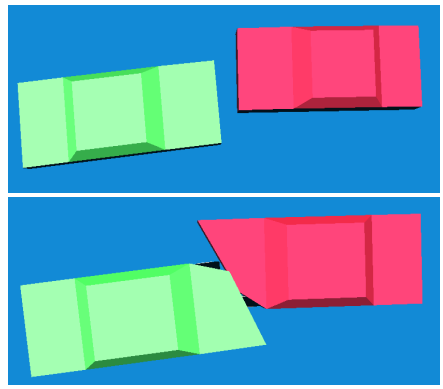

Figure 4. Crash Event.

The vehicles were positioned with respect to the global coordinate system. An estimated initial velocity was then assigned to each vehicle as their velocities were unknown. To generate a valid crash pulse for the selected CIREN case, various crash quantities (i.e. Principal Direction of Force (PDOF), Collision Deformation Classification (CDC), Crush and Delta-V) were matched between CIREN and the HVE simulation by carrying out parametric variations with respect to the impact location, vehicle velocities, inter-vehicle friction, etc. Since CIREN does not report all these quantities for the non-case vehicle, only Delta-V was matched for the non-case vehicle. A good match between CIREN and HVE was obtained for both the case and non-case vehicle (Table 5 and Table 6). The EDSMAC4 module [10], which is a 2D physics program in HVE, was used to generate the crash pulse.

Table 5.
Case vehicle match

Chevrolet	CIREN	HVE
DeltaV, mph	35	35.5
Crush, in	32.6	31.49
CDC	12FYEW5	12FYEW6
PDOF(deg)	350	349.3

Table 6.
Non-case vehicle match

Oldsmobile	CIREN	HVE
DeltaV, mph	33.5	34.5

After the crash quantities were matched between HVE and CIREN, the longitudinal component of crash pulse obtained from HVE was compared with the EDR pulse. Since the longitudinal component obtained from HVE showed good match with that obtained from EDR (Figure 5a), it was decided to use the corresponding lateral component of crash pulse obtained from HVE for reconstruction. The final crash pulse used for this case included the longitudinal component from EDR and lateral component from HVE (Figure 5b).

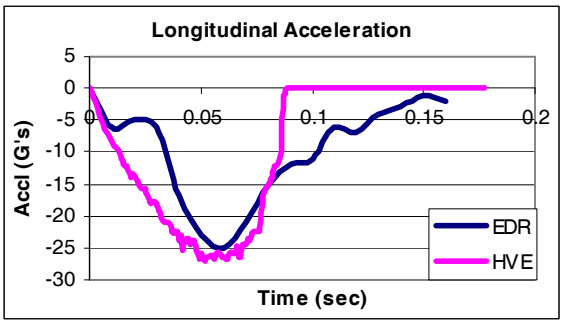

(a)

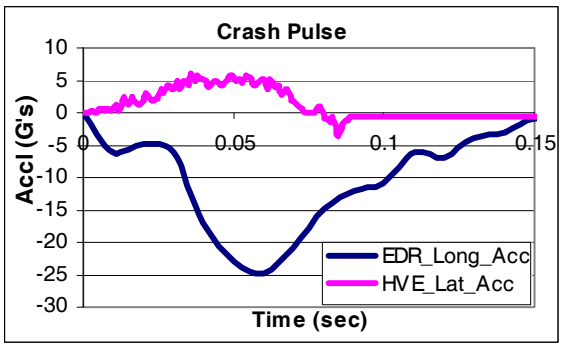

(b)

Figure 5. (a) Longitudinal component of crash pulse. (b)Crash pulse used for "Moderate Brain Injury" case.

<u>"Severe Brain Injury" case:</u> For this case, no EDR data was available. HVE was used to generate the crash pulse. Similar to the "moderate brain injury" case, a generic vehicle model was used for the case vehicle. The vehicle model was updated with respect to the vehicle parameters. Since no stiffness and inertia information were available for the case vehicle, the stiffness and inertia information from 2006 Toyota Corolla model available in HVE database was used to update the case vehicle. The crash event was set up in HVE (Figure 6) and crash quantities were matched between HVE and CIREN to generate the crash pulse.

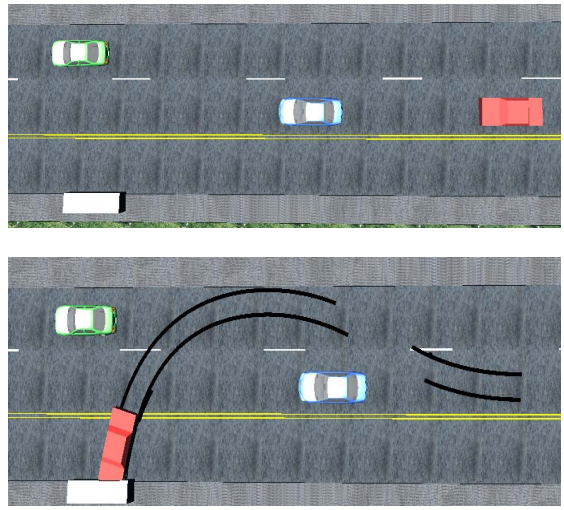

Figure 6. Crash Event

A good match between CIREN and HVE was obtained with respect to the crash quantities for the case vehicle (Table 7).

Table 7.
Case vehicle match

Scion TC	CIREN	HVE
DeltaV, mph	29.2	28.7
Crush, in	18.89	18.92
CDC	12FDEW3	12FDEW3
PDOF(deg)	350	351.4

The EDSMAC4 module in HVE was used to generate the crash pulse (Figure 7).

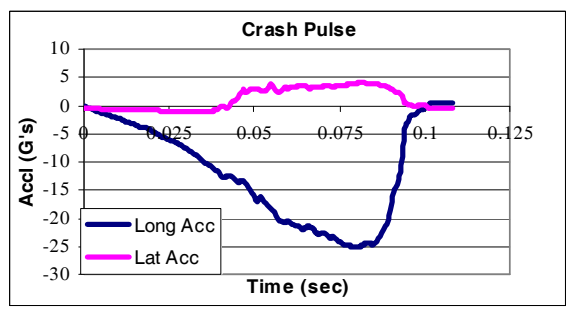

Figure 7. Crash Pulse for "Severe Brain Injury" case.

Occupant Simulation Set Up

<u>"Moderate Brain Injury" case:</u> The occupant simulation was set up in MADYMO, which is a widely used occupant safety analysis tool that can be used to simulate the response of an occupant in a dynamic environment. The occupant size for this "moderate brain injury" case was close to a 50th percentile size, and hence the Hybrid-III (H-III) 50th ellipsoid model was used as occupant model in MADYMO. The case vehicle interior surfaces were

created in MADYMO. The location of these surfaces was obtained from HVE, which had the actual vehicle model of a Chevrolet Cavalier available in its vehicle database. The contact surfaces were first created in HVE (Figure 8) and only the necessary contact surfaces were created based on the contacts listed in CIREN between the occupant and the vehicle interior. This information was then used to create the case vehicle in MADYMO (Figure 9).

(a)

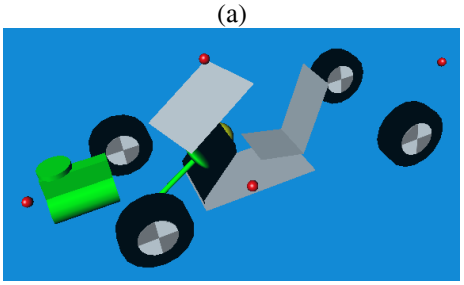

(b)

Figure 8. Contact surfaces generated in HVE (a) Full View, and (b) No Body View.

The properties for the seat structure, seat back, seat cushion, knee bolster, steering column and the contact characteristics between the occupant model and the vehicle interior were taken from the frontal impact application file available in MADYMO [11], which has generic but realistic properties. Since the occupant (driver) had an air bag deployment during the crash, a generic air bag model was added to the steering wheel hub. The generic driver air bag model was selected from MADYMO applications. Since the occupant was wearing the lap/shoulder belt during the event, a finite element lap and shoulder belt was created and wrapped around the occupant (Figure 9). The properties for the belts were taken from MADYMO application file to be close to the realistic properties. This run was further set up according to the case information given in CIREN. The dummy was positioned in a normal posture with the right foot on the brake and the left foot on the floor.

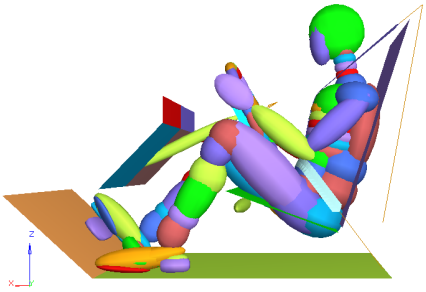

Figure 9. Impact Simulation model for "moderate brain injury" case.

The EDR-HVE combination crash pulse (Figure 5b) was used to drive the simulation. The baseline run was obtained once the occupant-vehicle contacts in simulation were matched with those listed in CIREN.

<u>"Severe Brain Injury" case:</u>

A similar set up as explained for "moderate brain injury" case was followed for the "severe brain injury "case with a few additions. According to the case information given in CIREN, a seat belt pretensioner and a knee bolster air bag were installed in the vehicle. The pretensioner fired and the knee-bolster air bag deployed during the crash. A pretensioner and knee bolster air bag were added to the MADYMO model. Since no generic knee air bag model was available in MADYMO, one was created by scaling and shaping the generic steering wheel (SW) driver air bag model. The case vehicle's actual knee air bag model was 18 liters in volume and had tethers 50 mm in length. To create a knee air bag model close to the actual air bag, the following was done:

- The reference geometry of the SW driver air bag (which was circular) was scaled non-uniformly in X and Y direction to form an elliptical shape, which is a better approximation to the actual knee air bag (Figure 10a).
- Tethers were added (Figure 10b) each with a length of 50 mm. Since the location of the tethers was not known, eight tethers were added to control the shape of the deploying air bag.
- The air bag was scaled until inflated volume was close to 18 liters. The volume of the modeled air bag was 17.67 liters (Figure 11).

(a)

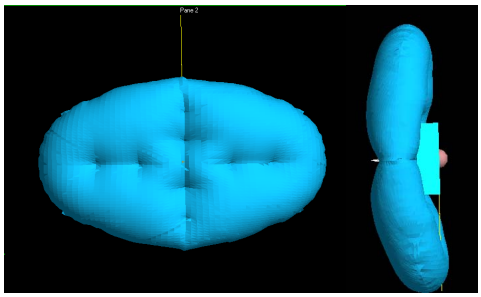

(b)

Figure 10. (a) Actual, and (b) modeled knee bolster air bag

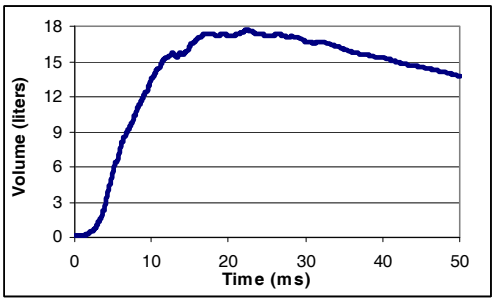

Figure 11. Volume vs. Time for knee air bag.

The crash pulse obtained from HVE (Figure 7) was used to drive the model. The baseline run (Figure 12) was obtained for this case by matching the occupant-vehicle contacts with those listed in CIREN.

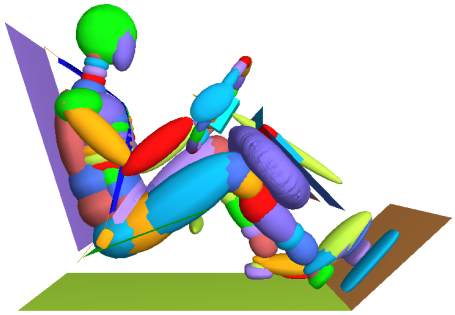

Figure 12. Impact Simulation model for "Severe Brain Injury" case.

The unknown variables were identified for both the cases during their respective baseline set up.

Injury Thresholds

The injury threshold values for the injuries sustained by the occupant were established from literature review. Injury thresholds were also found for the uninjured body regions. These injury thresholds were established for use in the optimization study. It is important to note that the point of the paper was to study the optimization methodology as a reconstruction tool. The injury threshold values were established from the best available data set, and are not intended as definitive transformation to the reported occupant injuries. Since any chosen injury threshold value would represent a certain probability of injury and there was an uncertainty in choosing a value, the injury threshold values given in reports and papers were selected. The injury thresholds for the two cases are described below:

"Moderate Brain Injury" case: The occupant sustained AIS 1 and AIS 2+ injuries. AIS 1 injuries were not incorporated into this analysis as these were minor injuries such as skin abrasion/laceration. The occupant sustained:

- Abdominal Injury (AIS 2 & AIS 3): Since the occupant had two abdominal injuries (AIS 2 and AIS 3), only the AIS3 injury was considered. It was mentioned in the CIREN injury analysis that the "Belt Restraint webbing/buckle" was the injury source for both the abdominal injuries. The Hybrid III 50th dummy model does not have any force output or any injury metric output for the abdomen. Therefore, the lap belt –abdomen contact force was related to abdominal injury. The force corresponding to 30% probability of injury was obtained as the injury threshold. Since there was no test data available for frontal impact, the threshold force was obtained from the experimental results obtained from lateral impacts [12].
- Lower Extremity Injury (AIS 3): The occupant suffered a bimalleolar fibula fracture on the right foot because of inversion-eversion. The inversion-eversion moment corresponding to 30% probability of injury was obtained as the threshold value [13]. The lower tibia moment was compared with this threshold value for predicting this injury.
- Head Injury (AIS 2): For cerebral concussion sustained by the occupant, the HIC value corresponding to mild traumatic brain injury (MTBI) given by Pellman et al [14] was used. This value is based on national football league (NFL) reconstruction data. This was the only published human volunteer data available that correlated HIC with concussion. Since concussion occurred because of soft contact, HIC_{36}, which is calculated over an extended time period of the acceleration pulse, was thought to be better predictor than HIC_{15} and hence HIC_{36} was used.

The threshold values for the uninjured body regions were also obtained from literature [15]. The established threshold values (Table 8) were used for optimization.

Table 8.
Established injury threshold values for "Moderate Brain Injury" case

Body Region	Injury Criteria	Threshold from Literature
Head	HIC_{36}	250
Neck	Nij	1.0
Thorax	Acceleration & Deflection	60g & 63mm
Abdomen	Abdominal Force	3200N
Femur	Resultant Force	10KN
Lx-Injury (Tibia Injury)	Tibia Index	1.3
Lx-Injury (Fibula-Injury)	Eversion-Inversion Moment	35Nm

"Severe Brain Injury" case: Similar to the "Moderate Brain Injury" case, the AIS 1 injuries were ignored for this case as well. The occupant in this case sustained:

- Cerebrum diffuse axonal injury (AIS 5): The injury threshold was obtained from Takhounts et al [16]. Angular acceleration was used as injury criteria. In [16] the relationship between DAI & maximum principal strain and that between angular acceleration & maximum principal strain was used to establish injury risk as a function of angular acceleration. The angular acceleration corresponding to 50% probability of injury was used as the threshold value.
- Cerebrum subarachnoid hemorrhage (AIS 3): The injury threshold was obtained from Takhounts et al [16]. Angular acceleration was used as injury criteria. The angular acceleration corresponding to 30% probability of injury was used as the threshold value. Data was not available to form AIS 3 and AIS 5 injury risk curves in [16]. Hence, assumptions were made for DAI and hemorrhage threshold from the injury risk curve available.
- Vault skull fracture comminuted (AIS 3): This was a depressed left, frontal skull fracture associated with overlying laceration. Since the Skull Fracture Criteria (SFC) is only applicable for linear skull fractures, HIC was used as the injury criteria for this depressed skull fracture. Since this was a contact-type injury, HIC_{15} was used to properly capture the short time period of the contact that causes the injury. The HIC_{15} value corresponding to 30% probability of AIS3+ injury was used as the threshold value [17].
- Pelvis fracture (AIS 3): According to CIREN injury analysis, this fracture was sustained by loading onto the lap belt. The Hybrid III 50th percentile dummy model does not have any force output or any injury metric output for the pelvis. Therefore, the lap belt–abdomen contact force was related to pelvis injury. The injury threshold was obtained from Salzar et al [18].
- Lumbar spine fracture transverse process (AIS2): Since no injury risk curves are available for lumbar spine, the lumbar spine load cell output from H-III 50th dummy model was simply monitored and was not used in the optimization analysis.
- Facial Injuries (AIS 3-Orbit fracture, AIS 2-Nose fracture): Since the H-III 50th dummy model does not have any load cell output from the face region, facial injuries were ignored in this analysis.

The established injury thresholds (Table 9) were used for optimization.

Table 9.
Established injury threshold values for "Severe Brain Injury" case

Body Region	Injury Criteria	Threshold from Literature
Head-DAI	Angular Acceleration	8000 rad/s^2
Head-Hemorrhage	Angular Acceleration	6250 rad/s^2
Head-Skull Fracture	HIC_{15}	1177
Neck	Nij	1.0
Thorax	Acceleration & Deflection	60g & 63mm
Pelvis	Force	5470N
Femur	Resultant Force	10KN
Lx-Injury	Tibia Index	1.3

Optimization Set up

After setting up the baseline run and obtaining the injury thresholds, optimization was set up for the two cases using modeFrontier software. The assumed parameters identified earlier were used as design variable and their ranges were defined (Table 10).

Table 10.
Design Variables

	Parameters	Range [Ref]
SEAT	Seat Friction	0.2-0.4
KNEE BOLSTER	Knee Bolster Properties	± 20% [1]
	Knee Bolster Friction	0.1-0.4
BELT SYSTEM	Belt Segment Properties	± 20% [1]
	FE Lap/Shoulder Belt Properties	± 20% [1]
	Belt Friction	0.1-0.3
	Retractor Properties (film spool effect)	± 20% [1]
	Retractor Locking Time	1ms -30ms
DRIVER AIR BAG	Air bag Firing Time	5ms-55ms
	Air bag Friction	0.1- 0.3
	Steering Column Angle (Air bag Deployment Angle)	± 5° around baseline
	Air bag Mass Flow Rate (MFR)	± 20% [1]
	Steering Col. Position (translation –X-dir i.e. Air bag Position)	± 15% around baseline
CRASH PULSE	Crash Pulse-Y component	Scaling 0.5-1.5
OTHER PARAMETERS	Thorax-SW Loading	Scaling 0.8-1.2
	Friction Shoes –Toe board/Floor	0.5-0.7
	Friction Brake-Right Shoe	0.5-0.7
ADDITONAL PARAMETERS FOR "SEVERE BRAIN INJURY" CASE	Knee Air bag (KAB) MFR	± 20% [1]
	KAB Firing Time	5ms-40ms
	Pretensioner Firing Time	10ms-40ms
	Load Limiting Force	3.5KN-5.5KN
	Crash Pulse-X component	Scaling 0.85-1.4

Objective function and constraints were set up. Since the objective function has a great effect on the final solution, a normalized form of the objective function (Equation 1 & Equation 2) weighted based on the AIS score of the injuries sustained by the occupant, was formed in this study. This form of objective function can be generalized to other cases. For "moderate brain injury" case we had:

$$\left(1-\left(\frac{2\times HIC\times AbF_{cr}\times M_{cr}+3\times HIC_{cr}\times AbF\times M_{cr}+3\times HIC_{cr}\times AbF_{cr}\times M}{8\times HIC_{cr}\times AbF_{cr}\times M_{cr}}\right)\right)^2 \quad (1)$$

where,

(2, 3, 3)= AIS score of the respective injuries used as weights, HIC=HIC value from simulation, HIC_{cr}=Critical HIC value (250), AbF=Abdomen force value from simulation, AbF_{cr}=Critical abdomen force value (3200N) M=Inversion-Eversion moment from simulation, M_{cr}=Critical inversion-eversion moment value (35 N-m).

For "severe brain injury" case we had:

$$\left(1-\left(\frac{5\times DAI\times H_{cr}\times P_{cr}\times SFC_{cr}+3\times DAI_{cr}\times H\times P_{cr}\times SFC_{cr}+3\times DAI_{cr}\times H_{cr}\times P_{cr}\times SFC+3\times DAI_{cr}\times H_{cr}\times P\times SFC_{cr}}{14\times DAI_{cr}\times H_{cr}\times P_{cr}\times SFC_{cr}}\right)\right)^2 \quad (2)$$

where,

(5, 3, 3, 3)= AIS score of the respective injuries used as weights, DAI=Head angular acceleration from simulation, H = Head angular acceleration from simulation, SFC= HIC from simulation, P=Pelvis force from simulation, DAI_{cr}=Critical head angular acceleration value for diffuse axonal injury (8000 rad/s^2), H_{cr} = Critical head angular acceleration value for hemorrhage (6250 rad/s^2), SFC_{cr}= Critical HIC value for skull fracture (1177), P_{cr}=Critical pelvis force value for pelvis injury (5470N)

Two types of constraints were defined i.e. contact constraints and injury constraints (Table 11 & Table 12).

Table 11.
Constraints for "moderate brain injury" case

Contact Constraints	Injury Constraints
Head-Air bag $_{\text{contact-force}}$>0	HIC_{36} > 250
Thorax-SW $_{\text{contact-force}}$>0	Abdomen_Force>3200 N
KneeL-Bolster $_{\text{Contact-force}}$>0	RF_IE_Moment>35Nm
KneeR-Bolster $_{\text{Contact-force}}$>0	RF_DF_moment <52Nm
Head-Hub $_{\text{contact-force}}$=0	Nij<1
Head-SW $_{\text{contact-force}}$=0	Thorax_acc <60g's
Thorax-Hub $_{\text{contact-force}}$=0	Thorax_deflection<63mm
	Femur_force<10KN
	TI <1.3

where *RF_IE-Moment* is the right foot inversion-eversion moment and *RF_DF_moment* is the right foot dorsi-flexion moment. Right foot dorsi-flexion moment was used to make sure that the right foot fracture was because of inversion-eversion and not because of dorsi-flexion moment.

Table 12.
Constraints for "Severe Brain Injury" case

Contact Constraints	Injury Constraints
Head-Air bag $_{contact\text{-}force}$>0	HIC_{15} > 1177
Head-Hub $_{contact\text{-}force}$>0	Ang_Acc>8000 rad/s^2
Head-SW $_{contact\text{-}force}$>0	Pelvis_force>5470 N
KneeL-Bolster $_{Contact\text{-}force}$>0	Nij<1
KneeR-Bolster $_{Contact\text{-}force}$=0	Thorax_acc <60g's
Thorax-Hub $_{contact\text{-}force}$=0	Thorax_deflection<63mm
Thorax-SW $_{contact\text{-}force}$=0	Femur_force<10KN
KneeR-Knee Air bag>0	TI <1.3
KneeL-Knee Air bag>0	

The objective function and the constraints were defined such that they minimize the differences in injuries and occupant-vehicle contacts between the real world data and the model prediction. A multi objective genetic algorithm (MOGA) with Sobol DOE was used for optimization. Convergence for the "moderate brain injury" case was obtained after 571 simulations and convergence for the "severe brain injury" case was obtained after 452 simulations. A correlation study and a best case scenario study were also carried out.

RESULTS

Optimization Results

"Moderate Brain Injury" case: Of the 571 simulations (Figure 13), 388 were feasible i.e. matched CIREN listed occupant-vehicle contacts and injuries. From these feasible solutions, the one with the minimum value of objective function was selected as the solution.

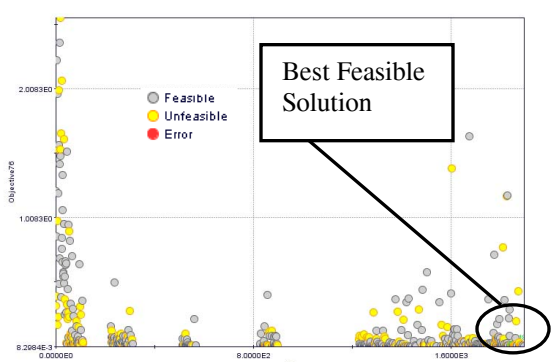

Figure 13. Design ID vs. Objective Function.

The optimized solution obtained was checked for injuries and contacts. The optimized solution matched all the CIREN listed contacts (Table 13, Figure 14).

Table 13.
Contact Match

CIREN listed Contacts	Matched by Simulation
1. Head –Air bag	√
2. KneeL-Bolster	√
3. KneeR-Bolster	√
4. Thorax-SW	√

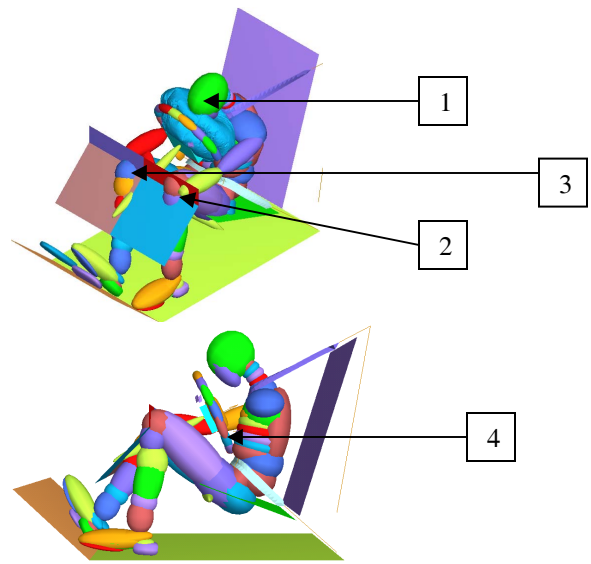

Figure14. Occupant-Vehicle contacts.

The occupant injuries predicted by the optimized solution were also matched with those listed in CIREN. The optimized solution predicted all the injuries listed in CIREN correctly (Table14).

Table 14.
Injury Match

Body Region	CIREN listed Outcome	Injury Criteria	Threshold from Literature	Opt-Solution Prediction	Predicted Correctly
Head (AIS 2)	Injured (Concussion)	HIC_{36}	250	251.3	√
Neck	Not Injured	Nij	1.0	<1.0	√
Thorax	Not Injured	Acceleration & Deflection	60g & 63mm	<60 g & <63mm	√
Abdomen (AIS 3)	Injured	Lapbelt-abdomen contact force	3200N	3464.6 N	√
Femur	Not Injured	Resultant Force	10KN	<10 KN	√
Lx-Injury (Tibia Injury)	Not Injured	TI	1.3	<1.3	√
Lx Injury (Fibula Injury) (AIS 3)	Injured (Fx) Right Foot	Eversion-Inversion Moment	35Nm	42.7 Nm	√
Lx Injury	Right Foot	Dorsi-Flexion Moment	52 Nm	<52Nm	√
Lx Injury (Fibula Injury)	Uninjured Left Foot	Eversion-Inversion Moment	35Nm	<35Nm	√

"Severe Brain Injury" case: This case converged after 452 simulations of which 119 were feasible (Figure 15). The solution with minimum objective function value was selected as the solution to the problem.

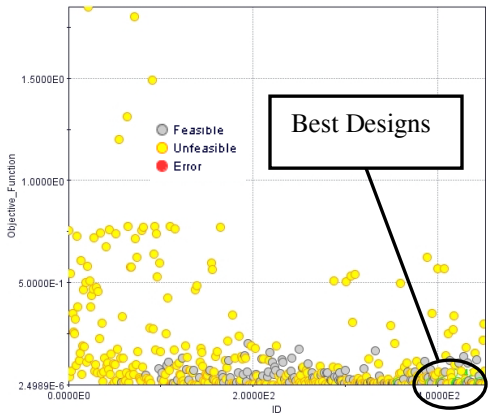

Figure 15. Design ID vs. Objective Function.

The optimal solution was checked for both injuries and occupant-vehicle contacts. The occupant-vehicle contacts (Table 15, Figure 16) and injuries (Table 16) predicted by the optimal solution matched with those listed in CIREN.

Table15.
Contact Match

CIREN Listed Contacts	Matched by Simulation
1. Face- SW Hub	√
2. Face-SW Rim	√
3. KneeL-Knee Air bag	√
4. KneeR-Knee Air bag	√
5. KneeL-Knee Bolster	√
6. Right Foot-Foot Controls	√

According to the case information, the occupant rode down the SW driver-air bag causing the head to hit the steering wheel rim and hub. The SW driver-air bag bottom-out was captured by the optimal solution (Figure 16a).

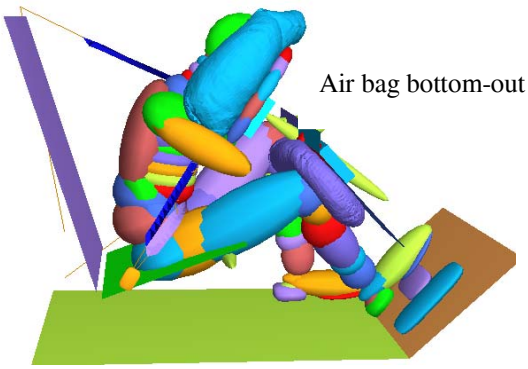

(a)

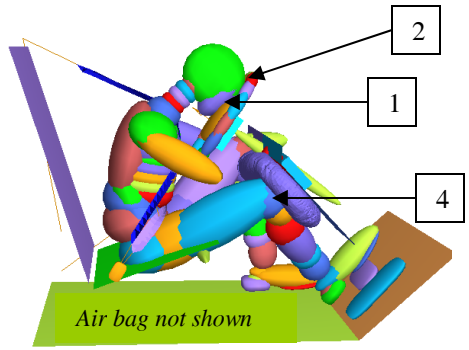

(b)

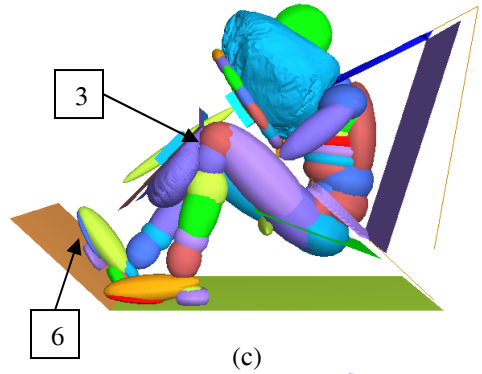

(c)

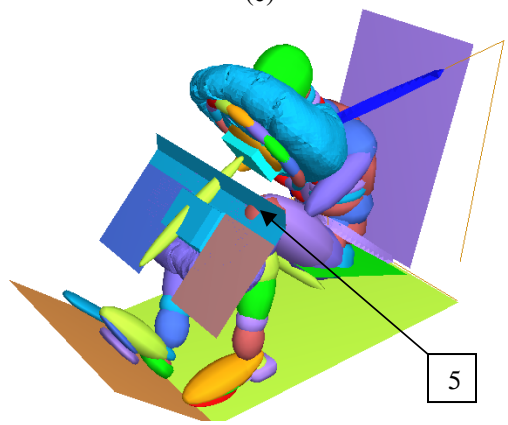

(d)

Figure 16. (a) Air bag bottom-out, (b, c, d) Occupant-Vehicle contacts.

Table16.
Injury Match

Body Region	CIREN listed Outcome	Injury Criteria	Threshold from Literature	Opt Solution Prediction	Predicted Correctly
Head	Diffuse Axonal Injury	Angular Acceleration	8000 rad/s^2	8011.6 rad/s^2	√
	Hemorrhage	Angular Acceleration	6250 rad/s^2	8011.6 rad/s^2	√
	Skull Fracture	HIC_{15}	1177	1183.3	√
Neck	Not Injured	N_{ij}	1.0	< 1.0	√
Thorax	Not Injured	Acceleration & Deflection	60g & 63mm	< 60g & < 63mm	√
Pelvis	Injured	Lapbelt-Abdomen Force	5470 N	6283.6	√
Lumbar Spine	Injured	Only Monitored	------	------	------
Femur	Not Injured	Force	10KN	< 10KN	√
Lx Injury	Not Injured	Tibia Index	1.3	< 1.3	√

Correlation Study and Best Case Scenario Study Results

A Correlations study and a best case scenario study were carried out to find critical parameters and to find a minimal or no injury scenario for the given case. These studies are only presented for the "moderate brain injury" case due to space limitations.

Correlation Study: This study was carried out to find critical parameters. The critical parameters were identified by analyzing the correlation coefficients obtained from the optimization study. Apart from the design space explored by the optimizer (571 design points), the design space was explored further by adding 150 Sobol DOE points and 100 random DOE points (Figure 17) in the design space to make sure the design space was properly explored to generate good correlations. This "physically possible" design space with 821 design points was then used to generate the correlation coefficients.

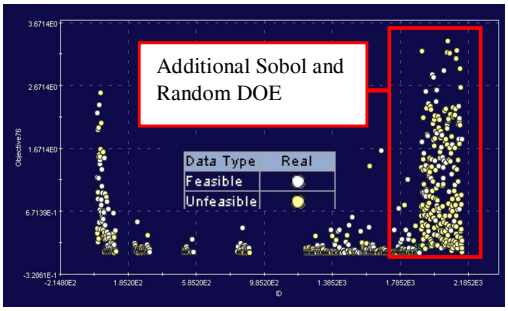

Figure 17. Correlation Study

The software modeFrontier provides correlation coefficients between all the input variables and the output variables. The correlation coefficients range from -1 (strong negative correlation) to 1 (strong positive correlation). Using the correlation coefficients, the critical parameters were identified for each of the injuries sustained by the occupant (Figure18). No particular threshold was used to separate out the critical parameters. Only a ranking from most-critical to least-critical was obtained. Absolute values were used for the correlations plots (Figure 18).

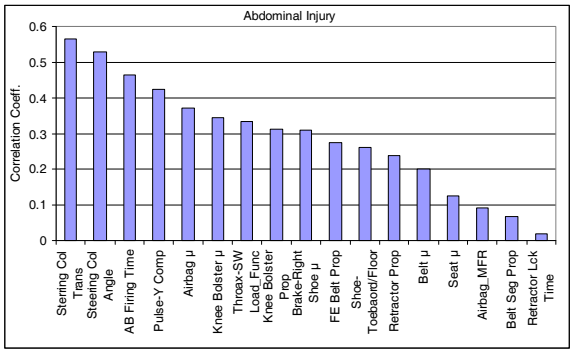

(a)

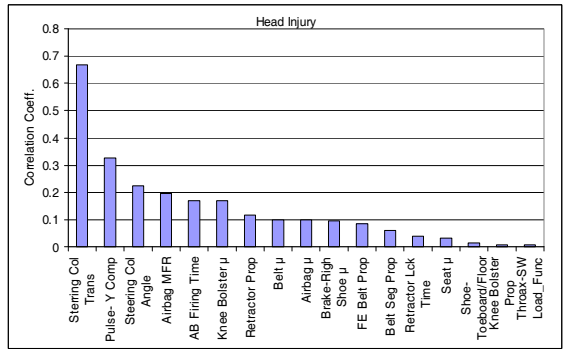

(b)

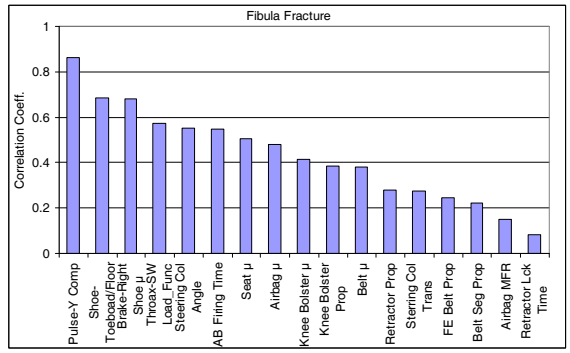

(c)

Figure 18. Critical parameters for (a) abdominal injury (b) head injury, and (c) fibula fracture

If more detailed information can be obtained on some of the critical parameters, a more accurate reconstruction analysis may be carried out.

Best Case Scenario Study: For identifying the best case scenario for the "moderate brain injury" case, the pulse was fixed to the optimized pulse obtained previously. For this given pulse, seat position and seat track position, an optimization attempt was made to see if a scenario with no-injury or minimum injuries could be obtained. A few changes as listed below were made to the problem set up.

- After fixing the pulse to the optimized one, the Sobol DOE was re-generated.
- The injury constraints on HIC, abdomen force and fibula fracture were modified with respect to the threshold. Lower non-injurious thresholds were selected. For HIC a threshold value of 100, for abdomen force a value of 1000N and for Fibula fracture a value of 10N-m was selected. The constraints and objective function were modified accordingly.

The problem converged after 602 simulations (Figure 19).

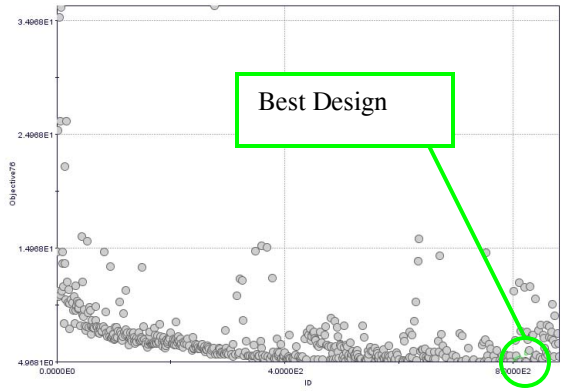

Figure 19. Best Case Scenario

After the convergence was obtained, the injuries were compared between the best case scenario solution and the optimized solution obtained before (Table 17).

Table 17.
Best case scenario: Injury comparison

Body Region	CIREN listed Outcome	Injury Criteria	Threshold Value	Injury Value	Best Case Scenario Injury Prediction	Optimal Solution Injury Prediction
Head (AIS2)	Injured (Concussion)	HIC36	250	175.4	**Not Injured**	**Injured**
Neck	Not Injured	Nij	1.0	<1.0	**Not Injured**	**Not Injured**
Thorax	Not Injured	Acceleration & Deflection	60g & 63mm	<60 g & <63mm	**Not Injured**	**Not Injured**
Abdomen (AIS3)	Injured	Lapbelt-abdomen contact force	3200N	3256 N	**Injured**	**Injured**
Femur	Not Injured	Resultant Force	10.6KN	<10.6KN	**Not Injured**	**Not Injured**
Lx-Injury (Tibia Injury)	Not Injured	TI	1.3	<1.3	**Not Injured**	**Not Injured**
Lx Injury (Fibula Injury) (AIS3)	Injured (Fx) Right Foot	Eversion-Inversion Moment	35Nm	41.8 Nm	**Injured**	**Injured**
Lx Injury	Right Foot	Dorsi-Flexion Moment	52 Nm	<52Nm	**Not Injured**	**Not Injured**
Lx Injury (Fibula Injury)	Uninjured Left Foot	Eversion-Inversion Moment	35Nm	<35Nm	**Not Injured**	**Not Injured**

It was found that for the given crash pulse, seat position and seat track position, the optimizer was able to find a scenario without head injury. The abdominal injury and fibula fracture were still present. The abdominal force and fibula inversion-eversion moment did come down to lower values as compared to the optimized solution, but did not go below the injury threshold for the given range of design variables.

DISCUSSION

This paper presents an optimization methodology for reconstructing real world crashes. Optimization was selected as it can give the best possible solution to a problem where instead of a specific value; a range is available for the input parameters. Even though crash reconstruction engineers collect a lot of details from the crash site, computerized crash reconstruction utilizes much more information than reported and, as such, specific values for a lot of parameters are not available and one has to work with a range of the parameters. Since even within a given range of input parameters the injury predictions can be quite different for the same case [1], it is imperative to take into account all the variability and come up with the best possible solution to the reconstruction problem. Optimization is one way to accomplish this and hence was used.

Crash pulse plays a very vital role when predicting occupant injuries. The crash pulse for "moderate brain injury" case was available from the EDR data with part of it, i.e. the lateral component, generated using HVE. Also HVE was used to generate the crash pulse for "severe brain injury" case. HVE has its own limitations, insofar as the stiffness of the vehicle, which plays an important role in generating the right crash pulse, can only be defined as linear and homogenous for any given side of the vehicle. Additionally, hard spots cannot be defined. As a result, the crash pulse obtained from HVE is not precise, but approximate. Hence the Y-component of crash pulse for the "moderate brain injury" case and the entire crash pulse (X &Y components) for the "severe brain injury" case were used as design variables during optimization. An EDR pulse, if available, should be used to reduce the design variables in the optimization process.

Genetic algorithms (GA) are categorized as global search heuristics and can help find global minima as compared to gradient based methods that have a tendency of converge to local minima. Also genetic algorithms can provide solutions for highly complex search spaces. For these reasons, a GA was used for the optimization. Sobol DOE was used to generate starting population for the GA as it uniformly distributes starting points in the design space.

For the "severe brain injury" case, the retractor locking time was not used as a design variable. This case had a pretensioner and varying the retractor locking time was creating belt problems and thus it was fixed to 1ms. Also for the "severe brain injury" case, the knee air bag, created from the driver air bag, had the same mass flow rate characteristics as the driver air bag. During optimization, both the abscissa and the ordinate of the mass flow rate curve (for driver air bag and knee air bag) were used as design variables. They were varied by $\pm 20\%$ around the baseline. The "Thorax-SW loading" design variable as used in the "moderate brain injury case" was not

used as a design variable in the "severe brain injury" case as CIREN did not list any contact between the thorax and the steering wheel for this case.

The optimal solution obtained for both the "moderate brain injury" case and "severe brain injury" case correctly predicted the occupant-vehicle contacts and the injuries sustained by the occupant. Since these are the two most important things that can be matched with the real world data, the kinematics predicted by the optimal solution are believed to be reliable. The accuracy of the solution strongly depends on the quality of the crash data reported. It is reasonable to assume that further improvement in field investigation and amount of data collected can help improve reconstruction analysis.

The optimized solution for the "severe brain injury" and "moderate brain injury" cases did match the injury thresholds obtained from literature. Since injury risk curves were not available for some of the injuries sustained by the occupant, threshold were obtained from the best available data set, for example for the abdominal injury sustained by the occupant in the "moderate brain injury" case, injury threshold for frontal impact was obtained from lateral impact experiments. So it is possible for some of the optimized force levels not to match the reported injury severities. A more accurate analysis may be carried out if injury risk curves are available for all body regions under different impact conditions.

The correlation study conducted helped identify critical parameters. Figure 18a shows that for abdominal injury, air bag parameters (air bag position, air bag deployment angle, air bag firing time) and Y-component of the crash pulse were most critical. For head injury, air bag parameters (air bag position, air bag deployment angle, air bag firing time, air bag mass flow rate) and Y-component of the crash pulse were most critical (Figure 18b) and for fibula injury, Y component of crash pulse and shoe related friction parameters were most critical (Figure 18c). These critical parameters can help understand how different body regions are affected by the vehicle environment and what design changes can be made to mitigate these injuries. If more detailed information can be obtained on some of the critical parameters, a more accurate reconstruction may be carried out. The correlation coefficients in this paper were generated using all the design points i.e. around 821 simulations. A few hundred more simulations exploring the design space and further division of the step size defined for the design variables might help further improve the correlation coefficients.

A best case scenario study was done to find, using optimization, the design changes that could help mitigate all or some of the injuries sustained by the occupant for the given crash pulse, seating position and seat track position. The no-head injury outcome predicted by the optimizer was achieved by making changes to the belt system and air bag system. Compared to the optimal solution, the optimizer, for the best case scenario, predicted scaling down the belt properties i.e. reducing the stiffness of the seatbelts, increasing the air bag mass-flow rate and late firing of the air bag as design changes that can help mitigate head injury. These three design variables converged to values within the feasible range of variability. The correlation study results and best case scenario results predicted are only for this particular "moderate brain injury" case and should not be generalized. The results may be different for other cases.

In this study, neither full finite element nor human facet models that better define human geometry and material properties were used because of the prohibitive run times. For better reconstruction, human models should be preferred if the run time can be reduced. This study was done only for frontal impacts but an analysis such as the one presented in this paper can easily be extended to other types of impacts.

Future work may involve, among other things, reconstructing more real world crashes with different kinds of impacts, using human FE or facet models for better occupant simulations.

CONCLUSION

The optimization methodology presented in this paper and demonstrated by successfully reconstructing two real world crash cases introduces a method that can be applied for finding solutions to crash reconstruction problems, which due to unavailability of data, cannot be solved deterministically. The kinematics predicted by the optimal solution can give insight on how the occupant moved inside the vehicle during the crash, which can help provide better understanding of the crash. The paper also showed how critical parameters can be identified using the correlation coefficients calculated during the optimization process.

ACKNOWLEDGEMENT

The authors would like to thank Mr. Mark Scarboro for help with the selected CIREN cases, ESTECO technical support for providing help with

modeFrontier and Toyota for providing details on the Scion airbags.

REFERENCES

[1] Hasija, V., Takhounts, E.G., Ridella, S.A, 2007. "Computational Analysis of Real World Crashes: A Basis for Accident Reconstruction Methodology." The 20th International Technical Conference on the Enhanced Safety of Vehicles Conference (ESV) in Lyon, France, June 18-21.

[2] Mardoux, D., Baumgartner, D., Deck, C., Willinger, R. 2006. "Head Injury Prediction Capability of the HIC, HIP, SIMon and ULP Criteria" IRCOBI conference, September: 143-157.

[3] Franklyn, M., Fildes, B., Zhang, L., Yang, K. and Sparke, L. 2005. "Analysis of Finite Element Models for Head Injury Investigation: Reconstruction of Four Real-world Impacts." Stapp Car Crash Journal, Vol.49, November: 1-32

[4] Untaroiu, C.D., Mark U. Meissner, M.U., Crandall, J.R., Takahashi ,Y., Okamoto, M., Ito,O., 2008 "Crash reconstruction of pedestrian accidents using optimization techniques". International Journal of Impact Engineering.

[5] Shen, J., Jin, X-L., 2007 "Reconstruction of pedestrian-vehicle accidents using sequential linear programming optimizer." International Journal of crashworthiness, Vol 12, Issue 6, pp 653-661.

[6] Crash Injury Research and Engineering Network (CIREN), National Highway Traffic Safety Administration, Department of Transportation Washington, D.C., United States.

[7] Human-Vehicle-Environment (HVE), Version 5.2, March 2006, Engineering Dynamics Corp.

[8] MADYMO, Version 6.2, 2004, TNO, Delft, The Netherlands.

[9] modeFrontier, Version 4.0, 2008, ESTECO, Italy.

[10] Day, T.D., 1999, ''An Overview of the EDSMAC4 Collision Simulation Model", SAE 1999-01-0102, Engineering Dynamics Corp.

[11] MADYMO Application manual, Version 6.2, 2004, TNO, Delft, The Netherlands.

[12] Viano, D.C., Lau, I.V., Asbury, C., King, A.I., Begeman, P., 1989 "Biomechanics of the human chest, abdomen and pelvis in lateral impacts". Accident Analysis and Prevention, Vol 21, No 6, pp553-574.

[13] Kuppa, S., Wang, J., Haffner, M., Eppinger, R. 2001, "Lower Extremity Injuries and Associated Injury Criteria" The 17th International Technical Conference on the Enhanced Safety of Vehicles (ESV) - Amsterdam, The Netherlands, June 4 – 7.

[14] Pellman, E.J., Viano .D.C., Tucker, A.M., et al., 2003. "Concussion in Professional Football: Reconstruction of Game Impacts and Injuries," *Neurosurgery*, 53(4): 799 – 814.

[15] Eppinger, E., Sun, E., Bandak, F., Haffner, M., Khaewpong, N., Maltese, M., Nguyen, T., Erik Takhounts, E.G., Tannous, R., Zhang, A., Saul, R., 1999 "Development of Improved Injury Criteria for the Assessment of Advanced Automotive Restraint Systems – II." National Highway Traffic Safety Administration Report.

[16] Takhounts, E.G., Hasija, V., Ridella, S.A., Tannous, R.E., Campbell, J.Q., Malone, D., Danelson, K., Stitzel, J., Rowson, S., Duma, S, 2008, "Investigation of Traumatic Brain Injuries Using the Next Generation of Simulated Injury Monitor (SIMon) Finite Element Head Model." 52nd Stapp Car Crash Conference.

[17] The U.S. Department of Transportation's FMVSS No. 208 Final Economic Assessment.

[18] Salzar, R.S., Bass, C.R., Kent, R.,Millington, S., Davis, M., Lucas, S., Rudd, R., Folk, B., Donnellan, L., Murakami, D., Kobayashi, S., 2006. "Development of Injury Criteria for Pelvic Fracture in Frontal Crashes." Traffic Injury Prevention, 7:299–305.

CRUSH VS ENERGY RELATIONSHIP FOR YUGO GV – CASE STUDY

Krsto Lipovac
Faculty of Transport and Traffic Engineering,
University of Belgrade
Milan Vujanic
Faculty of Transport and Traffic Engineering,
University of Belgrade
Miladin Nesic
Criminalistic-police Academy
Republic of Serbia
Paper Number 09-0424

ABSTRACT

Due to extremly different vehicle structural performanse it is required to individualy analyze vehicle stiffness in any situation where acurate results of calculating crash speed are needed. From the begginings of vehicle stiffness modeling, by Emori, Campbell or any of there successors, methods of establishing equations are constantly improved. Nowdays, it is well known that normalized crush energy (known as EAF-Energy of Approach Factor) vs deformation can be succesfuly approximated with linear relationship using results from NHTSA 30 m/h frontal crash test speed. For higher speeds, bi-linear appeared to be accurate enough in most cases. But, there are certain cases where different relationship could give better results. Some researchers showed that nonlinear relationships could be also succesfuly used.

In this work, all known attempt from previous researchers where exercized on a YUGO GV vehicle. For this vehicle there are three NHTSA full frontal tests available. Using those results, it was concluded that, altough bi-linar relationship could be succesfuly used, best performanse was achived by combined approximation. Linear up to speed of 30 m/h and quadratic above that speed. This approximation gives best results in upper register of speeds, thus it is usefull for very deep crash deformations. Using computer for analysis eliminate complicated calculations, so establishing such relationships is no more hard job. It is important to notice that this kind of approximation can't be aplied in situation where only one crash test point is known. So, field of application is very limited.

УВОД

For a long period YUGO GV has been a national car in republic of Serbia (SE Europe). It's been widely used as a common vehicle for transportation and thus very often participant in crashes. That's why this case study is conducted for YUGO GV. This vehicle was selled in USA during 80s and it was subject to NHTSA Compliance and NCAP tests. Results of these tests are freely available and for the purpose of this analysis they were downloaded from internet adress: http://www-nrd.nhtsa.dot.gov/database/nrd-11/veh_db.html. In this analysis NHTSA database and detailed reports in PDF format were used to analyse and select appropriate dataset from YUGO GV frontal test.

METHOD OF ANALYSIS

Many researches about establishing equation between depth of deformation (deflection) and vehicle speed during crashes, or some other physical measure which is speed dependent, based upon crash test data, has been published.

Erliest pioneer work of Emori from 1968. [1] has brought into relationship depth of deformation and speed during crash testing, but it's been improved and Campbell (1974) [1] has established relationship between depth of deformation and force, and also analyzed crush energy per vehicle weight.

It's appear to be that it is useful, in order to take into account difference between masses of different vehicles or different test for same vehicle and various width of deformations, to analyze some sort of normalized energy. An appropriate measure for analysis would be Energy of Approach Factor (EAF) which was given by Strother [5] and which was extensively used after [5]. In fact, EAF take into account energy calculated from crash speed during testing, so it doesn't include energy of restitution, but only energy absorbed by the residual deformation. Thus, Energy of Crush Factor (ECF), which also takes into account energy of residual deformation, would be better for analysis, since it calculates energy in more comprehensive way, but it is more demanding for data that are often not available [2].

Strother [5] defined EAF as:

$$EAF = \sqrt{\frac{2E}{L}}$$

where

L -length of deformation

E -absorbed energy (J)

This equation can be written as

$$EAF = \sqrt{B} \cdot C$$

C -depth (amount) of deflection (m)

B -represents coefficient of stiffness, per width unit

B is defined as

$$B = \frac{k}{L_C}$$

Adding initial energy before residual deformations occure, described as EAF_0 (known also as Onset Energy Factor), tipicaly comprehended as speed of starting deformations, in EAF equation, we have

$$EAF = EAF_0 + \sqrt{B} \cdot C$$

Since Δv data from tests are not available for all tests of YUGO GV, EAF will be used in this case study.

SOME PREVIOUS RESEARCHES

Using least squares method, Strother [5] approximated EAF and crush depth using linear (and bi-linear) and nonlinear (quadratic) relationships. They have found that, for GM Citation 1980-1982, bi-linear relationship is more appropriate (Figure 1) while for Plymouth Satellite 1974 (Figure 2), data shows quadratic trend.

Jiang [1] called upon Sakurias work which describes that "two-stage constant force-crush relationship with a transition as the deformation reaches the engine, could be used to represent vehicles' frontal crush characteristics", and which was confirmed by Futamata and Toyama.

Kerkhoff [2] showed, based on repeated crash tests data for Ford Escort, that relationship between ECF or EAF and deflection, can be considered as linear between 15 and 40 m/h.

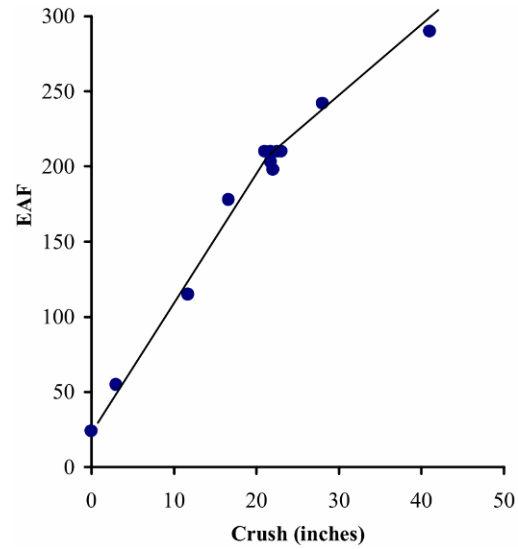

Figure 1. EAF **vs crush for Citation 1980-1982.**

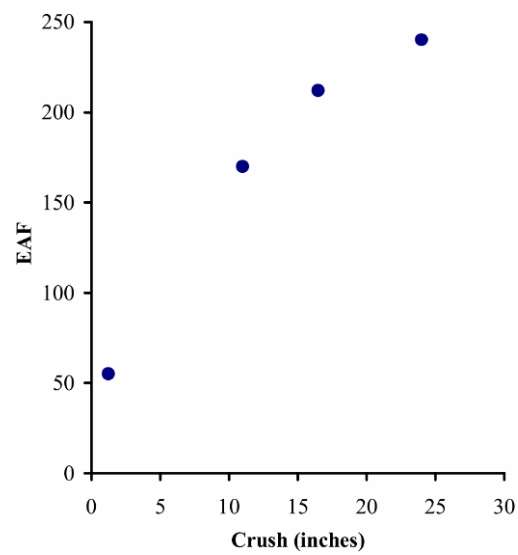

Figure 2. EAF **vs crush for Plymouth Satellites 1974.**

Varat [5] analyzed EAF and found that there two trends of frontal stiffness (relationship between EAF and deflection): linear and non-linear. Non-linear takes into account some softening of vehicle structure with deeper deflections. Some vehicles, as Ford Anglia, showed linear trend (Figure 3) up to 35 m/h and non-linear (Figure 4) for higher speeds (up to 50 m/h). They have also analyzed application to accident reconstruction using available tests data, for speeds of 30 and 35 m/h, and not knowing whether appropriate relationship between EAF and crush would be linear or non-linear.

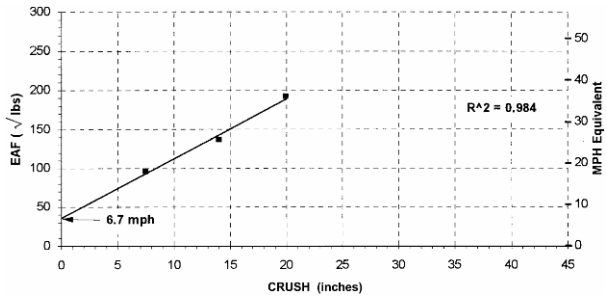

Figure 3. Anglia up to 35 m/h.

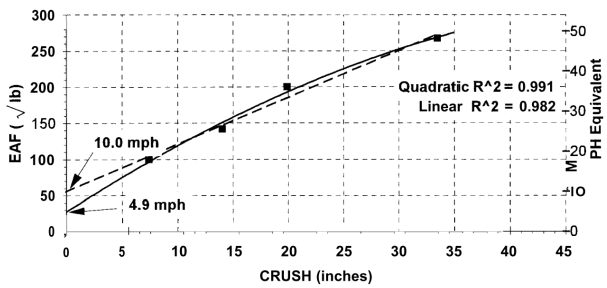

Figure 4. Anglia up to 50 m/h.

Bi-linear relationship by Strother [1] was used to describe EAF vs crush. Bi-linear relationship is presented as one linear relation for speeds up to 30 m/h and second linear for speeds from 30 to 50 m/h (Figure 5). They share the common 30 m/h data point.

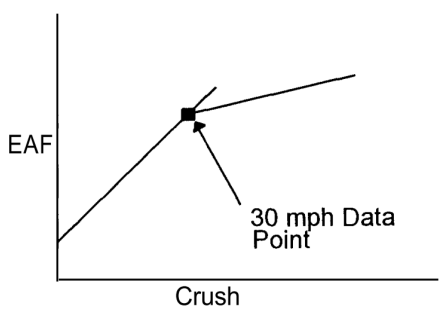

Figure 5. Bi-linear approximation.

In general case, bi-linear relationship is mathematicaly defined by next equations:

$$f(C) = \begin{Bmatrix} A_1 + B_1 C, & 0 \le C \le C_{30} \\ A_2 + B_2 C, & C_{30} \le C \end{Bmatrix}$$

where

C_{30} -crossover point, crush depth for 30 m/h test speed

For establishing relationship in first range (up to 30 m/h) datapoint for 30 m/h was used and EAF_0 was estimated for speed of 7.5 m/h (because they have found that average onset speed was 7.7 m/h for analyzed data).

For fitting in second range of bi-linear relationship (30 to 50 m/h), datapoint for 30 m/h was used and EAF_0 was estimated for speed of 15.2 m/h.

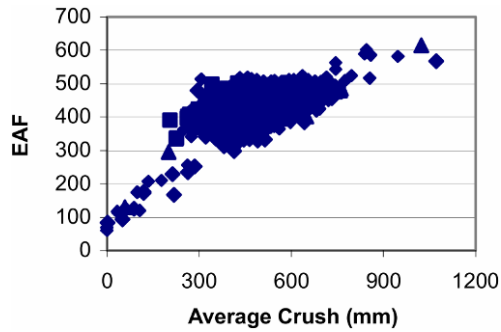

Figure 6. EAF **vs crush for passenger cars.**

Neptune [1999] also concluded that, in general, crush response characteristics of vehicle can be divided into two regions. First related to engine compartment deformation and second to passenger cage. Thus, vehicle can be modeled as bi-linear dissipator with second one not being compressed until first one "bottoms out". Both regions can be approximated with different linear functions.

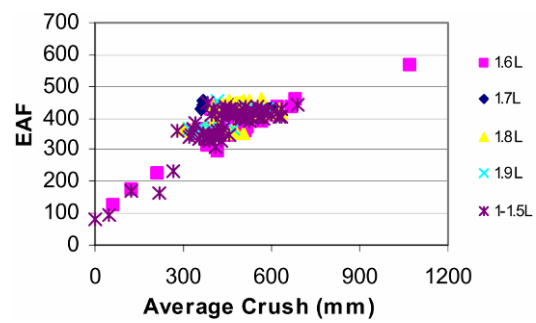

Figure 7. EAF **vs crush for cars with a 4cylinder transverse engine (1,0-1,9L).**

Jiang [1] analyzed EAF vs average crush depth for over 1000 vehicles tests from 1960. to 2002. Average crush depth was calculated based on at least 3, but mostly six (according to NHTSA vehicle test protocol) crush measurements. Figure 6 shows the results with bi-linear trend for analyzed passenger cars. They were further grouped according to engine configurations and for 4-cylinder transverse engine from 1000 ccm to 1900 ccm, and also showed bi-linear trend (Figure 7). For engines 1000 to 1500 ccm, bi-linear trend is also observed. Jiang also proposed a strategy for fitting. It is proposed that ECF should be used, unless rebound velocities are not available, when EAF should be used.

If only one test point is available, bi-linear relationship is recommended. The first stage for speeds up to 35 m/h

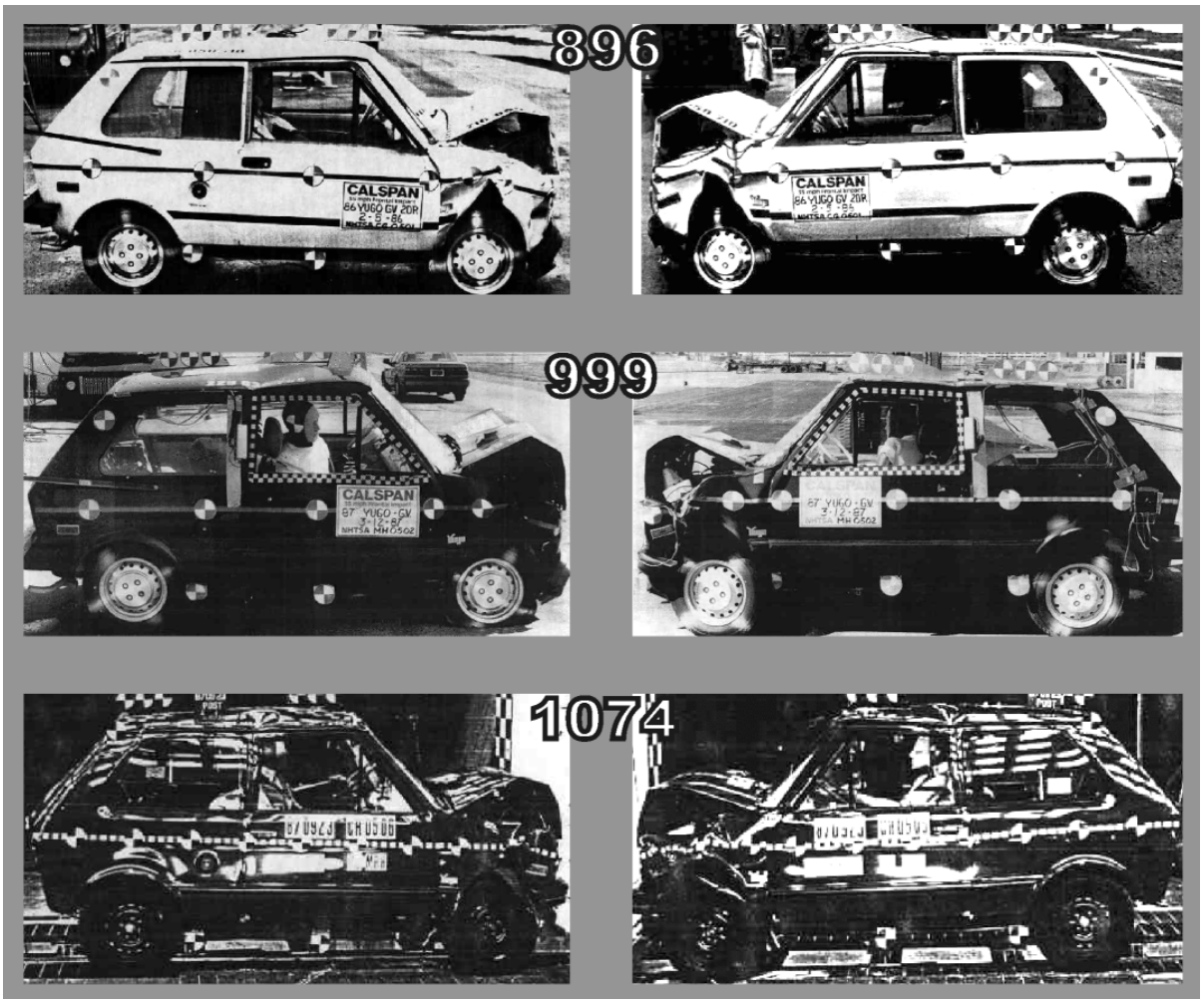

Figure 8. YUGO GV after testing.

(56 km/h) and with onset estimated at 5 m/h (2.2 m/s or 8 km/h). The second stage, for speeds 56-80 km/h, and with onset estimated at 15 m/h (6,7 m/s 24 km/h), as Varat [5] recommended.

DATA FOR CASE STUDY ANALYSIS

Four NHTSA crash tests has been conducted with YUGO GV. Three frontal and one side test. Results are available in NHTSA database, as separate detailed reports (in pdf form), and also as files containing digital data from accelerometers. Main data source for this analysis were NHTSA database and reports.

Three frontal crash tests are available for YUGO GV: no. 896, no. 999 and no. 1074. Considering recommendations about the test data from previous researchers (adjusting the gap during measuring from Neptune [3]) and fact that test reports present crush data in different manner, and that data from reports and database are sometimes different, all used data are logicaly checked and, if needed, corrected.

Relevant data

All crash test data for case study were summarized and shown in table 1. Vehicle photographs are shown in Figure 8. Vehicle width was corrected from obviously misspelled 1346 mm to 1546 mm.

Onset speed is estimated as 8 km/h (5 m/h), in accordance with recommendations from Jiang [1].

Тбл. 1. Data for YUGO GV case study.

Test No.	Vc [km/h] ±0,8 km/h	Vc [m/s]	Test mass [kg]	Model Year	DPD1 [mm]	DPD2 [mm]	DPD3 [mm]	DPD4 [mm]	DPD5 [mm]	DPD6 [mm]	C_{ave} [mm]	Max Deflection [mm]	Lc* [mm]	Vehicle Width [mm]	Δv [m/h]
0896	56,5	15,69	1052	1986	462	472	480	480	475	467	0,474	480	1387	1542	39,1
0999	56,2	15,61	1052	1987	381	414	434	445	447	450	0,431	450	1384	1546	/
1074	47,2	13,11	1035	1988	302	320	325	335	330	320	0,324	348	1410	1529	/
estimated	8	2,22	1035-1052		0	0	0	0	0	0	0	0	1410	1529	

***Lc** (означено као LENCNT у NHTSA бази података) је укупна дужина контакта на возилу, односно ширина чеоне стране возила захваћена оштећењем. Ова дужина обухвата директно и индуковано оштећење.

Equivalent uniform deformation ($Cave$) for six measured distances of deformation profile was calculated according to recommendation from Neptune [3]. Same equation is used in German traffic accident analysis software, PC CRASH.

$$Cave = \frac{C_1 + 2\times\left(C_2 + C_3 + C_4 + C_5\right) + C_6}{10}$$

ESTABLISHING RELATIONSHIPS-APROXIMATION

Linear relationship

Since only one test has rebound velocity (896), EAF vs deflection was analyzed.

According to recommendations, for linear approximation EAF vs deflection through three crash test points, and estimated onset speed of 5 m/h (8 km/h or 2,2 m/s), EAF was calculated using next equation:

$$EAF = \sqrt{\frac{2E}{L_C}} = \sqrt{\frac{2\frac{m\cdot v^2}{2}}{L_C}} \qquad (\sqrt{N})$$

Using MS Excel, linear approximation was conducted with equation that is defined as:

$$EAF = EAF_0 + \sqrt{B}\cdot C = 61 + \sqrt{697058}\cdot C$$

EAF_0 was calculated with 1052 kg mass (like for tests 896 and 999) and 1410 mm crush lenght (like test no. 1074).

From established equation B, which represent individual characteristic of vehicle crash performance, here is 697058 $\sqrt{N}$.

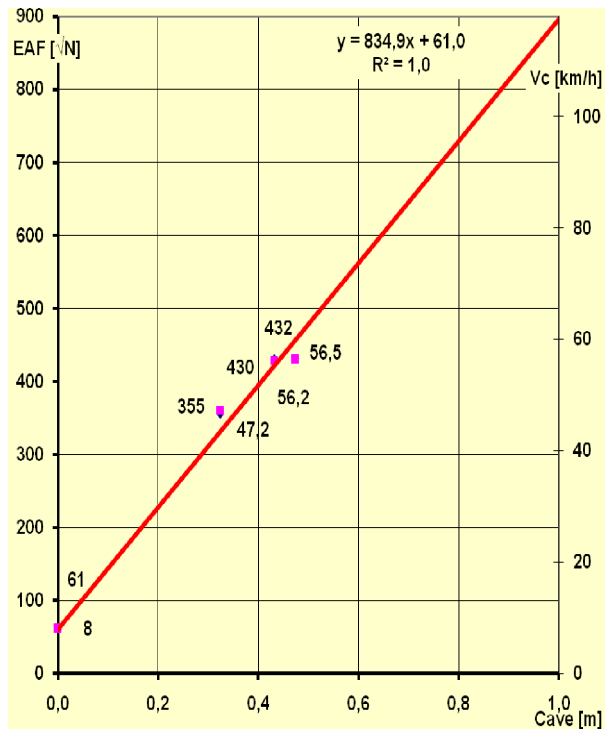

Figure 9. Linear EAF vs crush YUGO GV relationship.

For comparison, Figure 10 shows FORD Escort 1981-1985. linear approximation [5] for speed up to 35 m/h, where EAF is presented in $\sqrt{lb}$ and crush in inches.

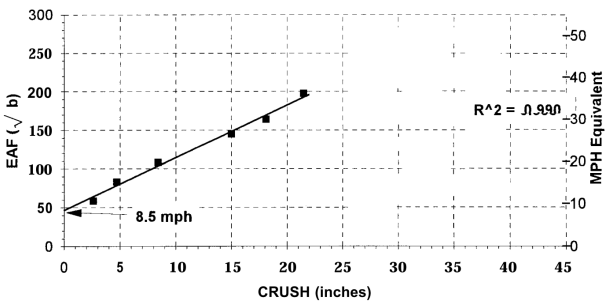

Figure 10. Ford Escort 1981-85, linear up to 35 m/h.

Bi-linear relationship

Varat [5], Jiang [1] and many others recommended that bi-linear approximation should be done with one linear relationship up to 30 m/h and second for 30 to 50 m/h.

Since for YUGO GV exists points for 35 m/h (35,1 and 34,9 m/h) and 30 m/h (29,3 m/h), and onset is estimated at 5 m/h, first part of bi-linear relationship is approximated for 5 and 30 m/h and second for 30 and 35 m/h.

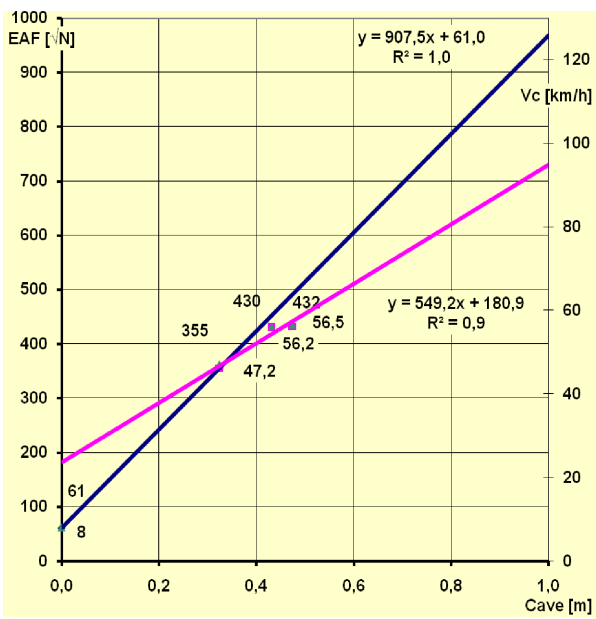

Figure 11. Bi-linear EAF vs deflection approximation.

Two linear relationships are defined as:

$$EAF_1 = EAF_{01} + \sqrt{B} \cdot C = 61 + \sqrt{823556} \cdot C$$

$$EAF_2 = EAF_{02} + \sqrt{B} \cdot C = 180,9 + \sqrt{301621} \cdot C$$

This bi-linear relationship is mathematicaly defined with next equations:

$$f(C) = EAF = \begin{Bmatrix} 61 + \sqrt{823556} \cdot C, & 0 \le C \le C_{30} \\ 180.9 + \sqrt{301621} \cdot C, & C_{30} \le C \end{Bmatrix}$$

$$C_{30} = 0.324\ m$$

In second part of bi-linear approximation EAF_0 would be 180.9 $\sqrt{N}$. Using equation for EAF and expressing v:

$$v = \sqrt{\frac{L_C \cdot EAF^2}{m}}$$

we can calculate corresponding onset velocity:

$$v = \sqrt{\frac{1.41 \cdot 180.9^2}{1052}}$$
$$= 6.62\ m/s = 23.8\ km/h = 14.8\ m/h$$

This velocity is equal to one recommended by researchers [1, 3, 5] for second part of bi-linear fitting.

The representer of frontal stiffness (B) for the first part of bi-linear would be 823556$\sqrt{N}$ and for the second part, 301621$\sqrt{N}$. This means that stiffness is about 2.7 times lesser in second phase, than in the first (about 37%).

Nonlinear (2nd order polynomial) relationship

It should be beard in mind that all nonlinear approximation has been done only for max test speeds, so there is no exact recommendations for fitting above that speed.

Fitting 2nd order polynomial relationship through YUGO GV test data yield us to (Figure 12)

$$EAF = 60.4 + 1188.6 \cdot C - 822.8 \cdot C^2$$

Relationship shows great amount of softening for speeds above max tested, and for speeds over 65 km/h is unuseable, because graph starts to fall down.

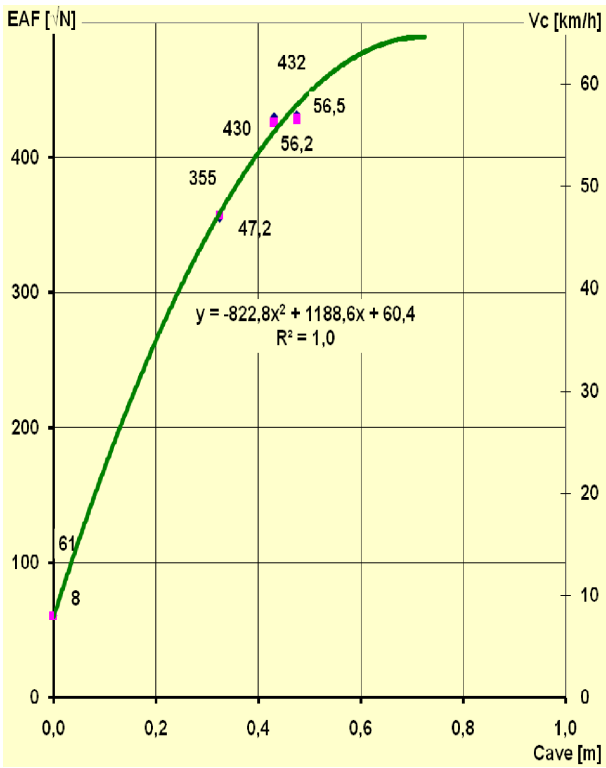

Figure 12. 2nd order polynomial EAF vs deflection approximation.

2nd order polynomial fitting using only one 56 km/h and rest data points has been done also. This yield to two relationships: softer and stiffer 2nd order polynomial. It could be said that these lines are boundary and, based on analyzed data set, represent marginal values.

Both of these lines shows some softening with speed, but the "stiffer" one (blue line on Figure 13) could be usefull for speeds over 80 km/h while "softer" one is unusable for speeds over 62 km/h.

Relationship were expressed as:

$$EAF_H = 60.7 + 1062.8 \cdot C - 475.98 \cdot C^2$$

$$EAF_S = 60.7 + 1178.7 \cdot C - 833.67 \cdot C^2$$

As a comparison, Figure 14 shows nonlinear approximation for Ford Escort 1981-85 [5]. It can be seen that this one is very similar to "stiffer" one for YUGO GV, but is a bit "softer".

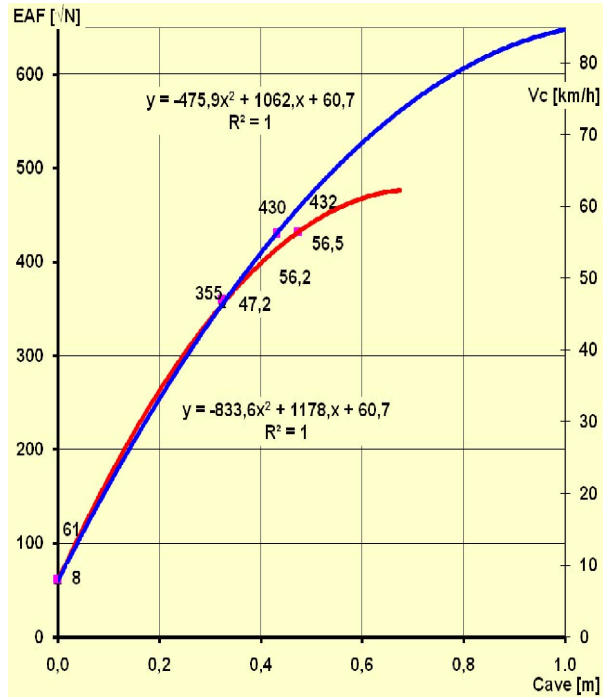

Figure 13. Two 2nd order polynomial EAF vs deflection approximations.

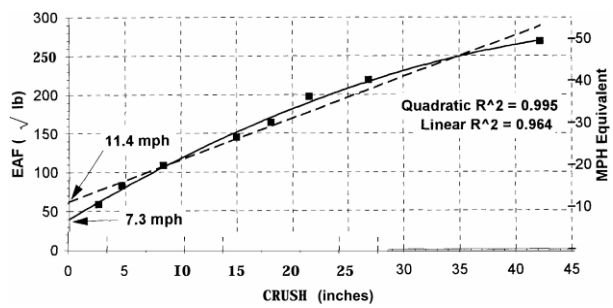

Figure 14. Ford Escort 1981-85, up to 50 m/h.

Combined relationship

In order to provide best fitting, and inspired by Varat's foundings [5] that quadratic equation is more suitable for upper speed register (over 30 m/h), Nesic [4] approximated EAF vs deflection with linear relationship for speeds up to 30 m/h and non-linear (quadratic) for higher speeds.

Equations that describes combined approximation are:

$$EAF_1 = EAF_{01} + \sqrt{B} \cdot C = 61 + \sqrt{823556} \cdot C$$

$$EAF_2 = \sqrt{B} \cdot C = \sqrt{443699} \cdot C^{0,552}$$

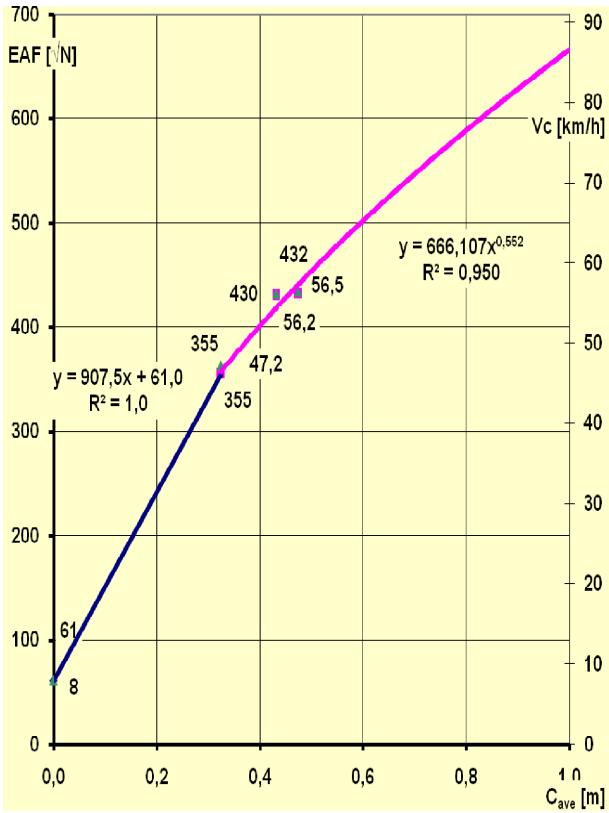

Figure 15. Combined EAF **vs deflection**

relationship.

First equation describes linear relationship for speeds up to 30 m/h, and second for speeds over 30 m/h. Equivalent uniform deformation for "crossover" speed of combined relationship (30 m/h), would be $C_{ave} = 0,324\ m$.

Combined relationship would be fully mathematicaly defined as:

$$f(C) = EAF = \begin{cases} 61 + \sqrt{823556} \cdot C, & 0 \le C \le C_{30} \\ \sqrt{443699} \cdot C^{0,552}, & C_{30} \le C \end{cases}$$

$$C_{30} = 0.324$$

Combined relationship demonstrate softening with higher speeds, and at the top of the researched range (for the average deflection of 1 m), speeds are slightly higher than demonstrated by quadratic approximation for Ford Escort (Figure 14).

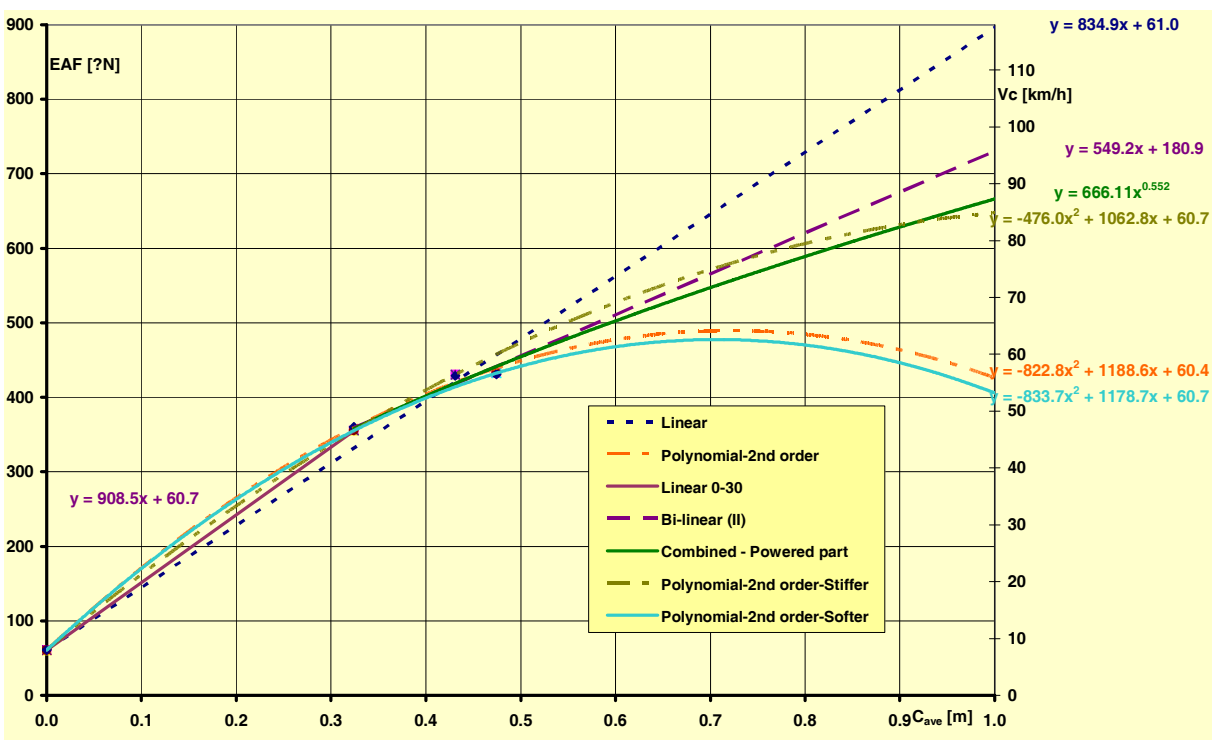

Figure 16. Summarium of YUGO GV case study.

Table 2. Known errors of YUGO GV case study approximations.

		Linear	Bi-linear	Quadratic	Quadratic-softer	Quadratic-stiffer	Combined
[m]	[m/s]	[%]	[%]	[%]	[%]	[%]	[%]
C_{ave}	V	∈	∈	∈	∈	∈	∈
0,474	56,50	**5,7**	**2,1**	**1,6**	**0,0**	**5,9**	**2,1**
0,431	56,20	**-2,3**	**-3,0**	**-2,4**	**-3,8**	**0**	**-2,7**

DISCUSSION

All showed approximation were conducted based on the available NHTSA crash test results for YUGO GV.

Results from previous researches, that shows that it is acceptable solution to estimate speed that start to cause residual deformation (onset speed) as 5 m/h, have been used. They have also showed that it is acceptable to approximate *EAF* vs deflection with linear relationship up to speed of 30 m/h, although in extreme condition it can be expected substantial error in lower range of speeds (or deflections) as, for instance, up to -19% for VW Rabbit and 9.3% for Ford Escort, according to Varat [5].

However, error is more significant if a vehicle that shows nonlinear relationship is approximated with linear relationship, because errors in lower register are then even higher, and goes up to 40%.

On the other side, Jiang [1] estimated that, if linear approximation is conducted with only one data point, error goes up to 26%, and could be even 50% if relationship placed on the higher data margin for certain vehicle category was established.

In this case study linear approximation (Figure 16), known errors vary but are acceptable in any case, even for the worst scenario.

According to known errors in table 2, it could be seen that any relationship is good enough for all known data points. However, there are substantial differencies in higher range of speeds and deflections. Quadratic and "softer" quadratic are completely unusable and linear is "too stiff". "Stiffer" quadratic, bilinear and combined are pretty close. Between those three, quadratic shows highest maximal error (5.9%), so it is least recommendable. Combined showed two errors same as bi-linear, but slightly better for one error (0,3% better). Thereat, for maximal average deflection of 1 m, combined gives speed of about 85 km/h, while bi-linear gives higher speeds (for about 10 km/h). Frontal performance of YUGO GV in this region is not known, but it is for FORD ESCORT (Figure 14) [5], where it can be seen that, for 1 m average deflection, speed is about 80 km/h. This can be considered as slightly advantage toward combined approximation over the researched region (0 to 1 m of deflection).

However, it should be recognized that, least error over 47 to 56.5 km/h region, is achieved by quadratic relationship. This make it appropriate for approximation in that region of speeds and corresponding deflections.

LITERATURE

[1] Jiang T., R. H. Grzebieta, G. Rechnitzer, S. Richardson, X. L. Zhao (2003) REVIEW OF CAR FRONTAL STIFFNESS EQUATIONS FOR ESTIMATING VEHICLE IMPACT VELOCITIES, The 18th International Technical Conference on the Enhanced Safety of Vehicles (ESV), Nagoya, Japan.

[2] Kerkhoff, J. F., S. E. Husher, M. S. Varat, A. M. Busenga, K. Hamilton (1993) AN INVESTIGATION INTO VEHICLE FRONTAL IMPACT STIFFNESS, BEV AND REPEATED TESTING FOR RECONSTRUCTION, SAE Technical Paper 930899.

[3] Neptune, J. A. (1999) A COMPARISON OF CRUSH STIFFNESS CHARACTERISTICS FROM PARTIAL-OVERLAP AND FULL-OVERLAP FRONTAL CRASH TESTS, SAE Technical Paper 1999-01-0105, http://www.neptuneeng.com.

[4] Nesic, M (2007) FRONTAL IMPACT VEHICLE SPEED ANALYSIS, Magister thesis, Faculty of Transport and Traffic Engineering, University of Belgrade, Republic of Serbia, Europe.

[5] Varat, M. S., S. E. Husher, J. F. Kerkhoff (1994) AN ANALYSIS OF TRENDS OF VEHICLE FRONTAL IMPACT STIFFNESS, SAE Technical Paper 940914, http://www.kevaeng.com.